3D GROUND MOTION SIMULATIONS FOR SITE EFFECTS ASSESSMENT:
LEARNINGS FROM EUROSEISTEST VERIFICATION AND VALIDATION PROJECT

Emeline MAUFROY, Emmanuel CHALJUB, Fabrice HOLLENDER Pierre-Yves BARD, Florent DE MARTIN, Zafeiria ROUMELIOTI, Nikos THEODOULIDIS, Cédric GUYONNET-BENAIZE, Olga KTENIDOU, Vincent PERRON

(23, October 2014 – Version 1)

AUTHORS			REVIEW			APPROVAL		
NOM	DATE	VISA	NOM	DATE	VISA	NOM	DATE	VISA
E. Maufroy (ISTerre)			M. Mucciarelli (Università della Basilicata)			F. Hollender		
			R. Paolucci (Politecnico Milano)			G. Senfaute		

DISSEMINATION: *Authors; Steering Committee; Work Package leaders, Scientific Committee, Archiving.*

EXECUTIVE SUMMARY

The use of numerical-simulation tools for prediction of seismic ground motion is often considered a valid option especially for poorly instrumented or moderate-seismicity countries lacking representative earthquake recordings, mostly due to the rapid development of the simulation codes and computational facilities. Such a use of 3D ground-motion simulation codes for design purposes requires a careful evaluation of their actual performance. This issue was the topic of only a few international studies, including international blind prediction tests or comparative exercises, focused on various sites.

This report is intended to present an overview of the work accomplished since the launching of the E2VP project. This project has been organized in two phases, E2VP1 (2007-2010) and E2VP2 (2012-2014). In short, the basic ideas of the project were, on the example of the Euroseistest site, to (1) quantify the "distance" between results of independent models and numerical schemes, and as much as possible to reduce them to the lowest possible level through a careful understanding of the differences; and (2) to compare this "cross-computation distance" to their "distance" to actual measured data for as many as possible real events. The first phase led to a number of lessons and recommendations on the use of the numerical-simulation approach, but it also led to the identifications of a few further issues that needed to be addressed in a second phase. The second phase of E2VP was thus designed to answer some of these identified issues, all related with 3D linear modelling.

First, the main findings of E2VP1 were confirmed in E2VP2, for both verification and validation aspects:

• The use of numerical simulation codes, even after extremely careful testing and even with the most sophisticated and up-to-date numerical schemes, can still be subject to errors (especially related to the "human factor"): careful use and cross-checking still proves to be mandatory.

• Our new results also confirm that there is no single numerical-modelling method that can be considered the best in terms of accuracy and computational efficiency for all structure-wavefield configurations.

• In addition, the very detailed investigations on canonical models, allowed identifying the origin of inaccuracies and relating them to the involved type of seismic waves and to the smoothness of the velocity model. We thus go on with recommending that any numerical method and code that is intended to be applied for numerical prediction of earthquake ground motion should be verified through stringent models that would make it possible to test the most important aspects of accuracy. The canonical cases developed within E2VP, and made freely available to the seismological community (http://www.sismowine.org), can serve this purpose.

Most of the new work achieved during E2VP2 is related to validation. The feasibility of such a validation up to the frequency limit considered here (4 Hz) is still a real challenge, which is in the front edge of applications of numerical simulation to deterministic ground-motion prediction, for several reasons that are listed below and clearly outlined by our new results:

• The site response proves to be very sensitive to the exact position of the source – especially its depth and back azimuth – for very close events and for local, shallow events: as it is unrealistic to obtain a precision on localization smaller than 2 km (especially for the depth), it is not recommended to select such events for validation.

• The distance between observations and numerical predictions remain significantly larger than the distance between carefully selected, up-to-date, and carefully implemented numerical simulation codes. However, a significant part of the uncertainties come from uncertainties in the source parameters. Therefore, for the prediction of ground motion for future, expected events with a priori defined source characteristics, the numerical-simulation approach is fully legitimate in the toolbox for site-specific ground-motion estimation.

• In addition, the predictions-to-observations differences are significantly lower when considering only the site amplification, especially when the reference is at depth within a vertical array. The main characteristics of site amplification at TST site could be satisfactorily reproduced, in terms of spectral contents and signal duration. This emphasizes the added value of "hybrid" approaches made possible by the availability of down-hole recordings

The comprehensive sensitivity study also showed also that, beyond the deterministic prediction of ground motion for a given earthquake scenario, numerical simulation proves also to be a useful tool for investigating the structure of the aleatory variability.

Finally, the lessons of this verification and validation exercise have already been partially taken into account in the present version of the "operational guide to account for site effects" (Deliverable SIGMA-2014-D3-136), and will definitely be fully accounted for in the final version. One of the most important lessons is the invaluable usefulness of in-situ recordings: it seems today very difficult to predict site effects in complex geometry context with only geological, geophysical and geotechnical information. Such instrumentation should include sensors on rock and as much as possible a vertical array to allow both a control of the crustal model and hybrid modelling. In addition, another very valuable side outcome of the comprehensive numerical simulations is the insight into the structure of the aleatory variability, with special emphasis on the single-site sigma.

TABLE OF CONTENTS

1 <u>INTRODUCTION AND OBJECTIVE</u>

The use of numerical-simulation tools for prediction of seismic ground motion is often considered a valid option especially for poorly instrumented or moderate-seismicity countries lacking representative earthquake recordings, mostly due to the rapid development of the simulation codes and computational facilities. This was indeed the option officially chosen by the French Nuclear Authority in the early 2000s when the CEA Cadarache center was officially asked to launch a process in view of performing a 3D, non-linear modeling of the Cadarache site to assess the characteristics of site amplification.

Such a use of 3D ground-motion simulation codes for design purposes requires a careful evaluation of their actual performance. This issue was the topic of only a few international studies, including international blind prediction tests or comparative exercises, focused on various sites.

It started with the Turkey Flat, California (Cramer 1995), and Ashigara Valley, Japan (e.g., Bard 1992), blind tests focusing on effects of surface sediments, the results of which were presented during the first ESG conference in Odawara (1992). It was followed by the more comprehensive comparison exercises on the Osaka/Kobe basin area in Japan (Kawase and Iwata 1998), and on the Southern California area within the SCEC framework (Day et al. 2001, 2003, 2005; Bielak et al. 2010), which also included the effects of extended sources and regional propagation in the low frequency range (f < 1 Hz). Each of these cases had its own specificities (for instance, very low frequencies with respect to nuclear engineering applications for the Osaka and SCEC exercise), and included indeed only few French or even European teams. The above mentioned ASN request (late 2003) was thus the initial impetus for a R&D program funded by CEA Cadarache and the ILL (Laue-Langevin Institute), which started by an international benchmarking exercise on the Grenoble basin (ESG2006; Chaljub et al., 2006, 2010), and was further deepened through the Euroseistest Verification and Validation Project (E2VP): Considering the lessons of the ESG2006 Grenoble benchmark, the E2VP project was launched in 2007 with two main objectives: (a) a quantitative analysis of accuracy of the current, most-advanced numerical methods applied to realistic 3D models of sedimentary basins (verification); (b) a quantitative comparison of the recorded and numerically-simulated ground motions (validation). The target was selected as the Euroseistest site located within the Mygdonian basin near Thessaloniki, Greece: a detailed, realistic 3D model of the medium had already been derived from a comprehensive set of geological, geophysical and geotechnical investigations, and the site instrumentation installed for about two decades provided a significant number of surface and borehole recordings.

This report is intended to present an overview of the work accomplished since the launching of the E2VP project. This project has been organized in two phases, E2VP1 (2007-2010) and E2VP2 (2012 – 2014). As the main results of the first phase have already been presented in deliverable D3-38 (Rome, May 2012), the present report will focus more on the latest results, while reminding the overall process.

In short, the basic ideas of the project were, on the example of the Euroseistest site, to (1) quantify the "distance" between results of independent models and numerical schemes, and as much as possible to reduce them to the lowest possible level through a careful understanding of the differences; and (2) to compare this "cross-computation distance" to their "distance" to actual measured data for as many as possible real events. As mentioned in deliverable SIGMA-2012-D3-38 (Maufroy et al., 2012), the first phase led to a number of lessons and recommendations on the use of the numerical-simulation approach, but it also led to the identifications of a few further issues that needed to be addressed in a second phase. These lessons, recommendations and issues are summarized in Table 1 and Table 2.

Table 1: Summary of main learnings from E2VP Phase 1

Main lessons about verification and validation studies	• Careful verification requires time and often to "go back to basics", while careful validation requires high quality data, i.e., including rich and high quality metadata. • No ground-motion simulation code accounting for wave propagation in complex media can be considered as press-button, neither in the linear, 3D domain, nor in the non-linear 2D case (nor probably in the 1D, NL case). The most common case is that, without iterations and cross-checking, different codes provide significantly different results when applied to the same case study. • Too fast applications of existing codes may yield VERY wrong ground-motion estimates, potentially resulting in raising mistrust in end-users. • Some codes currently used in engineering applications would deserve some significant improvements, or strong warnings on stringent validity limits, while even state-of-the-art codes (predominantly in the "academic" field) deserve constant upgrading.
Main recommendations for a wise use of such numerical simulation codes	• One should never be satisfied with only one computation from one single team, but should request several teams (at least two) with different numerical schemes to perform parallel computations of the same case. Results shoud be considered as reliable only if they agree beyond some quantitative goodness-of-fit threshold. • These goodness-of-fit criteria should definitely be agreed upon by the engineering community in order to reach an objective of transparent quantitative comparison, which should replace sentences such as "one can see the very good agreement on the figure"… • In the long run, it would be very valuable to assign a specific "quality label" to numerical codes and teams that did accept to run some of the now existing "canonical" cases with their own numerical code, which are freely available on web pages such as http://www.sismowine.org/. Maintaining this kind of internet facility in the long run will be beneficial for the whole community. • External peer reviews are always useful in assessing the quality of results derived from highly sophisticated numerical codes. • Comparison with actual data (in-situ earthquake recordings), whenever possible, are always useful. Having sensitive in-situ instrumentation (continuously recording broad-band velocimeters or sensitive accelerometers) proves to be invaluable for checking the reliability of numerical-simulation results.

Table 2: Remaining issues identified at the end of E2VP Phase 1

Remaining high-pritority issues	A – Non-linear (NL) modelling Similar efforts are still to be done as to the verification of the NL simulation codes especially as they are much more often used in engineering practice than 3D, linear simulation codes: • NL verification should be performed on the simplest possible cases (1D soil columns); • it should be performed on already instrumented sites having recorded large acceleration levels; • it should be associated with careful in-situ surveys and lab tests designed in tight connection with the needs of the rheological models implemented in the various NL codes. B - 3D linear modelling: • The small number of "candidate events" for validation is a typical situation of moderate/weak seismicity areas. Future validation events would however benefit from the possibility to include more events, and particularly more distant events (which would imply the use and/or the development of some "hybrid" numerical schemes coupling computations at different scales); • How do uncertainties and/or variability of source parameters (x-y coordinates, depth and focal mechanism) map on the variability of site-specific ground motion from local earthquakes? • To which extent can the apparent robustness of site amplification (surface to downhole Spectral ratios) observed at TST be extrapolated/generalized to other sites and other sources, including in particular extended sources? • What is the engineering importance of the local surface waves (time domain NL analyses, broadening effects on amplification spectra)? In other words, what is the engineering added value of more reliable 3D predictions compared to 1D common practice? Up to which levels of accuracy should they be modeled/accounted for by 2D and 3D models?

The second phase of E2VP was thus designed to answer some of these identified issues, all related with 3D linear modelling *(those related to NL modelling were considered for the design of the "Prenolin" verification and validation exercise, co-funded by the SIGMA/CASHIMA and SINAPS@ projects).* The main addressed questions are the following:

- Estimation of the impact of geological and source parameters uncertainties on the accuracy of numerical predictions:
  - o This component implies an update on the localization, magnitude and focal mechanism of each of the available recorded events, together with an update on the geological / geophysical model of the Mygdonian basin and of the underlying crust. It also includes an investigation of the sensitivity of numerical results to typical errors in source parameters.
- Estimation of the amount of ground-motion variability using simulations
  - o The comparison between simulation and real data can be done typically on a limited number of earthquakes. The estimation of the whole variability/uncertainty requires a much wider dataset spanning a broader range of source parameters (magnitude, hypocenter depth, incidence angle, back azimuth…). This wider set of results will be used (among other analyzes) to estimate the "single-station sigma" from a numerical point of view.
- Estimating "single-station sigma" with real accelerometric data
  - o Complementarily, a work on the real accelerometric database has been launched in order to determine a local GMPE, estimate the associated uncertainties and the "single-station sigma" from an empirical point of view. This is a common WP2-WP3 work, presented in the deliverable SIGMA-2012-D2/D3-132 (Ktenidou et al., 2014).

The present report, while presenting an overview of all the E2VP activities since the launching of the project in 2007, will therefore focus more on the results corresponding to these three fields. It includes: (1) a first section devoted to the presentation of the site, of the corresponding models and events; (2) an overview of the verification work accomplished throughout Phase 1 and finalized recently through the submission of a journal article (see Appendix 1); and (3) three sections on the validation work: the main outcomes from E2VP1 are briefly reminded in the main text (similarly, a copy of another recently submitted paper can be found in Appendix 2), while the new results corresponding to new computations on the new, extended model and including a larger number of seismic events are detailed in chapter 4. This "validation" is performed not only in a deterministic way (up to a frequency of 4 Hz) on a set of 19 events, but also in a statistical way: a database of realistic synthetics was built (up to now for a limited set of receivers) for a broad-enough range of (small to moderate) distances and back-azimuths, allowing the performance of statistical comparisons between observed and synthetic variabilities, with a special emphasis on the structure of the aleatory uncertainty and the correspondence between the variability of SSR and single site sigma (chapters 5 and 6). The conclusions emphasize the new findings of the second phase.

2   DESCRIPTION OF SITE

The first step of the early E2VP phase 1 project was to identify a test site. The ideal site should have:

- a good preexisting geological, geophysical and geotechnical characterization in order to produce a realistic model of the medium;

- availability of many seismic event recordings from many different stations (for the validation process);

- a global framework in which all of these information could be used without restriction in a large collaborative project.

After an international investigation, where thirty sites were mentioned, the site "Euroseistest", located a few tens of kilometers east of Thessaloniki, Greece, was chosen. This site have the advantage of a velocity model already available in both 2D (7-layers model derived from Raptakis *et al.*, 2000) and 3D (3-layers model derived from Manakou *et al.*, 2007) that we used in phase 1 (this 3D structure has been updated for phase 2 as we will describe in Section 4.2). In addition, numerous accelerograms are available.

The target of the project is the Mygdonian basin located in North-Eastern Greece, 30 km ENE of Thessaloniki (see *Figure 1*), in the epicentral area of a magnitude 6.5 event that occurred in 1978.

Figure 1: Location of the Euroseistest and the Mygdonian basin in the NE Greece.

The Mygdonian basin is the place of the so-called "Euroseistest" test site which has been extensively investigated within the framework of various European projects (Euroseistest, Euroseismod, Euroseisrisk, Ismod) and is now maintained by ITSAK and AUTH (Pitilakis *et al.*, 2009). The basin has been shaped by NS extensive tectonics with EW trending normal faults on each side. It is now densely instrumented with surface accelerometers, including a vertical array with 6 sensors over 200 m depth at the central TST site.

3   VERIFICATION OF NUMERICAL SIMULATION

A huge effort was devoted during E2VP to verify a set of numerical methods and codes representative of the state-of-the-art for 3D modeling of earthquake ground motion in sedimentary basins. A large part of this work was presented in the deliverable SIGMA-2012-D3-38 (Maufroy et al., 2012), in which the results of the methods and codes were extensively compared in realistic models of the Mygdonian basin and for a set of stringent canonical cases.

The analysis of the results of the canonical cases was completed between the writing of the last deliverable (April 2012) and July 2014, when a joint article was submitted to Geophysical Journal International. Here we summarize the new results of the article that were not presented in the deliverable SIGMA-2012-D3-38 (Maufroy et al., 2012). The reader is referred to the Appendix 1 to access the submitted manuscript.

The main objective of the article was to understand the origin of differences between numerical predictions of the seismic response of the Mygdonian basin for frequencies up to 4 Hz. Those differences were mainly seen in basin models with internal discontinuities within the sediments and were associated with local surface waves (i.e. generated at the basin edges from the conversion of body waves, due to lateral velocity contrasts). The article clearly evidences that those differences are related to the incorrect representation of the small-scale variations of the material properties at the discrete level.

A new method to design anisotropic effective media has been developed by the Bratislava group and its performance has been tested in the article. More generally, the article suggests that in order to decrease the epistemic uncertainty in 3D numerical ground motion prediction, a proper strategy should be used when designing a 3D geomodel, to low-pass filter the small-scale variations of material parameters. This general strategy has been followed to define the new basin model used in the second part of E2VP.

Here we recall the main results of the article and explain how the conclusions of the study were accounted for when building the new set of synthetic calculations presented in this deliverable.

3.1   CANONICAL TEST CASES

Four test cases were presented in the article: two for which the velocity model is varying only in the vertical direction (1D geometry), and two for which the velocity model is a simplified, two-dimensional cross-section of the Mygdonian basin model (2D geometry). For each geometry (1D or 2D), two kinds of structural models were considered: one model, referred to as sharp, with internal discontinuities of the material parameters in the sedimentary part; and one model, referred to as smooth, where the vertical variation of the material parameters is continuous, piecewise linear within the sediments. The four test cases are denoted as 1D-sharp, 1D-smooth, 2D-sharp and 2D-smooth. The three-dimensional seismic wavefields include surface waves trapped in the sediments: for models with 1D geometry, the surface waves are excited by a surface force, whereas they are spontaneously generated from the conversion of body waves at the basin edges for models with 2D geometry. The 1D-sharp and 2D-sharp models consider 3 sedimentary layers overlying an elastic, homogeneous halfspace, the layer thicknesses and the material properties within each layer correspond to the structure below the central TST station of the Euroseistest array.

The 1D-smooth and 2D-smooth models consider the same 3 sedimentary layers, but with smoothly varying properties within the layers and no discontinuities of material parameters between the layers.

3.2 RESULTS IN 1D GEOMETRY

Figure 2 shows the vertical component of ground velocity along a 2D surface profile computed for the 1D-sharp case by the four methods: FDM-S, FDM-C, FPSM, and SEM-F (see the article for details). In the FDM-S, FDM-C, and FPSM calculations, the volume harmonic averaging of the elastic moduli and volume arithmetic averaging of mass density proposed by Moczo et al. (2002) is used to approximate the physical interfaces of the 1D-sharp model. The SEM-F calculations are performed following the F strategy, i.e. imposing that the interfaces of the model coincide with the spectral elements' boundaries. In FDM-S and FDM-C, the grid spacing is 5 m, which corresponds to a minimum of 10 grid points per S wavelength at the surface. The horizontal grid spacing is 20 m for FPSM and 10 m in average for SEM-F at the surface (i.e. the horizontal size of the surface spectral elements is 50 m and the polynomial order is N = 5). The vertical grid spacing increases in FPSM from 3 m at the surface to 100 m in the bedrock. In SEM-F it is set in average to 3.46 m in the first layer and to 14.5 m in the second layer. Each numerical solution is superimposed on the reference one – computed with the discrete wavenumber method – and the goodness-of-fit (GOF) in amplitude and phase between the two solutions are also shown.
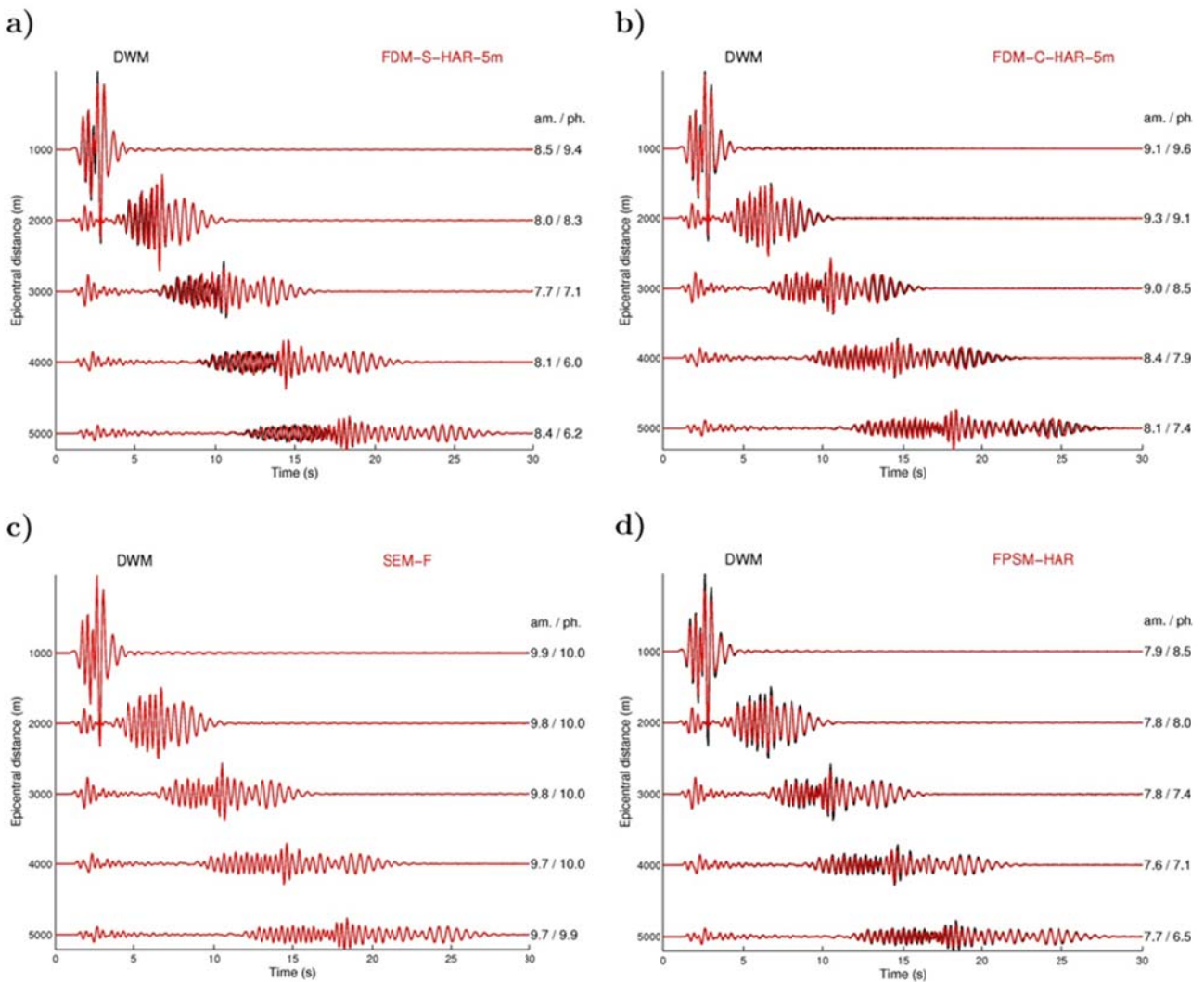
Figure 2: *Vertical component of ground velocity along the Northern surface profile computed for the 1D-sharp case by 4 different methods: a) FDM-S; b) FDM-C; c) SEM-F; d) FPSM. HAR indicates the harmonic averaging of the elastic moduli. Each of the seismograms (plotted in red) is superimposed on the reference solution computed with DWM (in black). The numbers to the right of each trace correspond to the goodness-of-fit scores in envelope (labelled to as "am") and phase (labelled to as "ph") with respect to the reference solution. A perfect match corresponds to a score of 10.*

Except for the SEM-F calculations, clear differences in phase and amplitude are seen in all the predicted surface wave trains. The excellent fit obtained for SEM-F is intrinsically related to the correct discrete representation of the interfaces in the 1D-sharp model by the F strategy. In Figure 3, we present the results obtained with a NF strategy, where instead of squeezing one element in the first layer, L1, two spectral elements of the same vertical size ($\simeq$ 45m) are used to describe the first two layers, L1 and L2. Note that only the first physical interface is interpolated in this modified mesh, the other two still coincide with elements' boundaries. The effect on the accuracy of the resulting numerical solution is tremendous. Apart from the direct S wave, all the other arrivals are affected by large phase and amplitude errors: the high-frequency 1D resonance occurs at a slightly lower frequency (around 2.5 Hz instead of 2.7 Hz) and the surface wave dispersion pattern is completely different. This is not a straightforward matter of the vertical spatial resolution in terms of the number of nodes per wavelength, but rather a problem of how the discontinuity in the material parameters is represented at the discrete level by the local spectral polynomial bases. The sensitivity of the surface-wave dispersion properties on the discrete implementation of the model can be recast under the general issue, faced by any grid-based numerical method, of how to represent spatial variations of the elastic parameters which are smaller than the size of the numerical grid cell (the extreme case being that of a material discontinuity). The main challenge is to "up-scale" the medium, i.e. to design an effective medium which realizes a physically consistent, low-pass filtering of the original model. Several up-scaling procedures have been derived in the last years: Moczo et al. (2002) proposed to use the volume harmonic average of the elastic moduli and arithmetic average of the mass density in the vicinity of a material discontinuity; Fichtner & Igel (2008) presented a non-linear minimization approach to design smooth models which preserve the phase velocities of a few target Love and Rayleigh modes; more recently Capdeville et al. (2010a,b) and Guillot et al. (2010) introduced a general numerical procedure to derive a fully anisotropic effective model using the framework of the homogenization theory; Kristek et al. (2014) and Moczo et al. (2014) extended their 2002 formulation to a more general effective medium with the orthorhombic anisotropy.
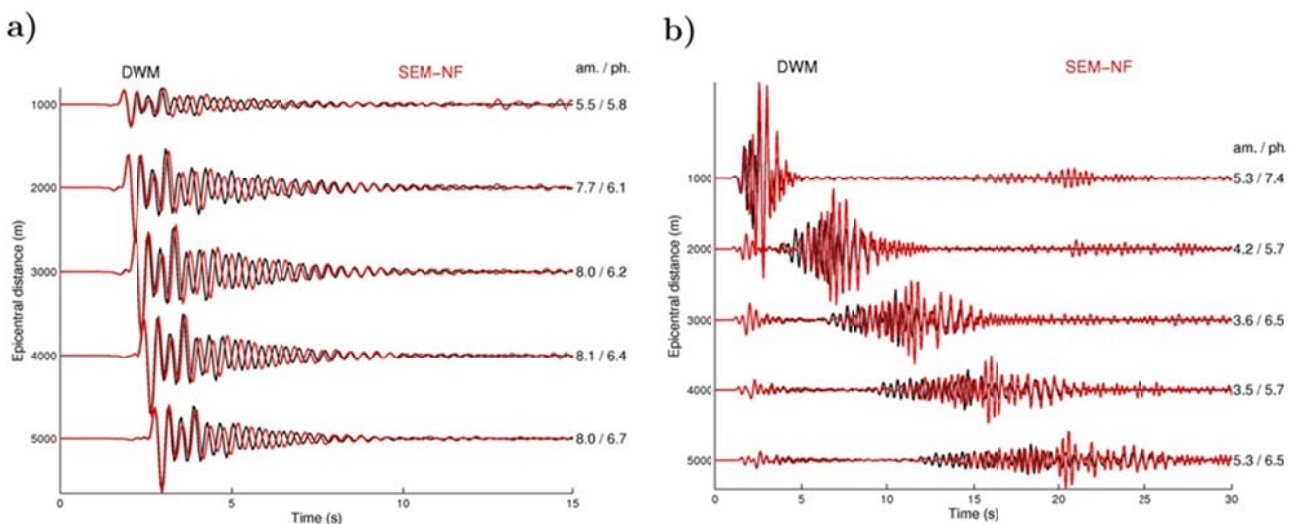
Figure 3:   East-West (left) and vertical (right) components of ground velocity computed for the 1D-sharp case using SEM-NF.

In Figure 4 we illustrate the performance of this new orthorhombic effective medium for numerical solutions for the 1D-sharp case computed with FDM-S. The advantage of using the orthorhombic approach is clearly seen in Figure 4, which involves Rayleigh waves propagating parallel to the discontinuities: the anisotropic solution computed with a grid size of 10 m outperforms the isotropic solution obtained with a grid size twice smaller, having inaccuracy only in the high-frequency Airy phase of the fundamental Rayleigh mode. Further reducing the grid size to 5 m in the anisotropic solution allows to reach the same level of accuracy as with SEM-F.
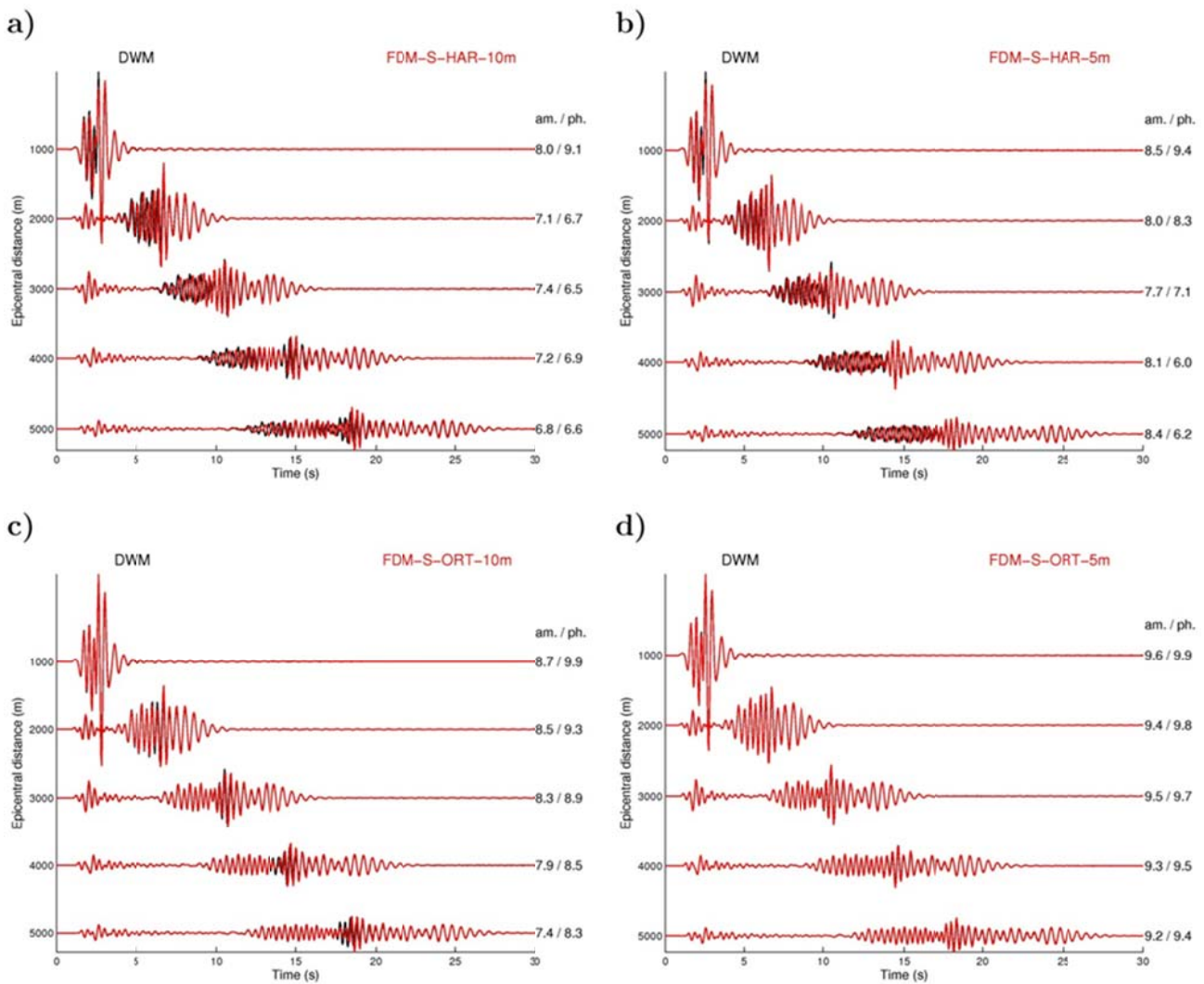
Figure 4:   *Vertical component of ground velocity along the Northern surface profile for the 1D-sharp case computed with FDM-S using different grid spacings and definitions of the effective media: a) harmonic averaging, 10 m; b) harmonic averaging, 5 m; c) orthorhombic averaging, 10 m; d) orthorhombic averaging, 5 m.*

The numerical solutions for the 1D-smooth case computed with the four methods (FDM-S, FDM-C, FPSM, and SEM-F) are shown in Figure 5. Compared to the 1D-sharp case, the level of goodness-of-fit with respect to the reference solution is systematically increased for surface waves. Note that the solution obtained with SEM-NF, in which the mesh design follows the NF strategy, is also sufficiently accurate, as shown in Figure 6. This is related to the ability of the polynomial bases used in the shallow spectral elements to represent the 1D-smooth velocity model. The comparison of the FDM-S solutions obtained with different effective medium implementations and grid spacings (see article) show that numerical accuracy in this case is controlled by the resolution of the grid rather than by the choice of the effective medium.
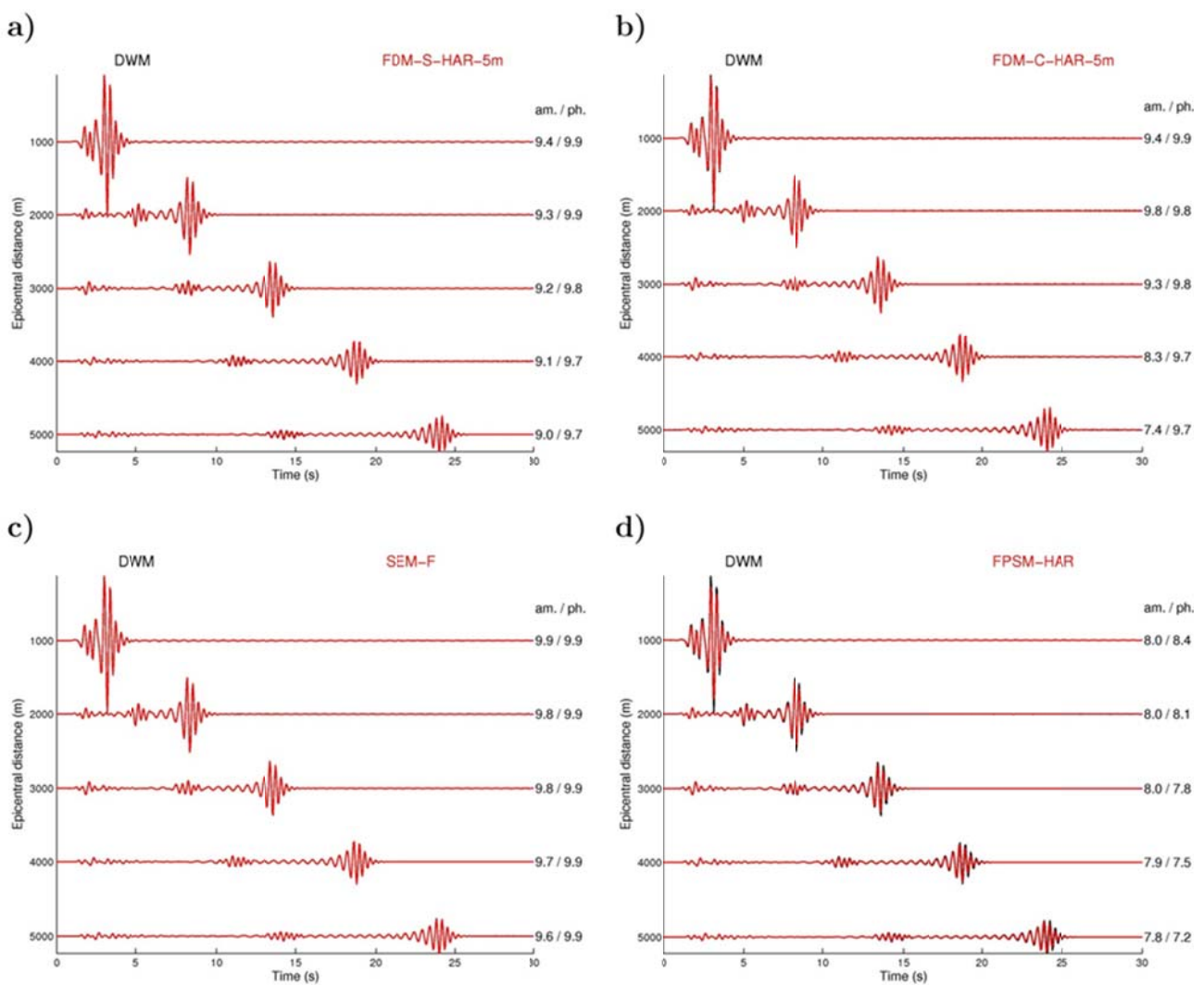
Figure 5:   Vertical component of ground velocity along the Northern surface profile computed for the 1D-smooth case by 4 different methods: a) FDM-S; b) FDM-C; c) SEM-F; d) FPSM.
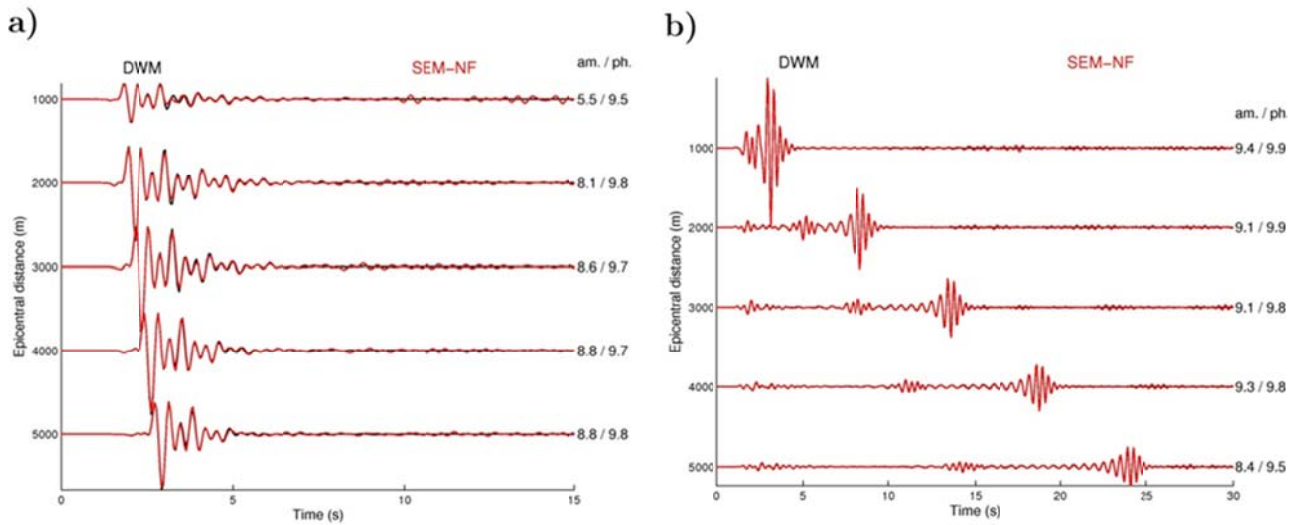
Figure 6:   East-West (left) and vertical (right) components of ground velocity for the 1D-smooth case computed with SEM-NF.

3.3   RESULTS IN 2D GEOMETRY

Figure 7 shows the horizontal in-plane component of the ground motion computed at a receiver located 1 km away from the vertical southern edge by FDM-S, FDM-C, FPSM, and SEM-BE. The numerical solutions were computed using the same spatial resolution as for the 1D-sharp case. In the SEM-BE solution, the mesh is designed in the "best-effort" (BE) mode, which is a compromise between the F and NF strategies: the boundaries of the elements follow the material interfaces only when these are horizontal or vertical.

Each prediction in Figure 7 is superimposed on the SEM-F reference, and the time-frequency GOF (in amplitude and in phase) with respect to the reference are shown as color images.

The agreement is very good for the first 8 s of the seismogram which consists of body and Rayleigh waves generated at the vertical Southern edge. The level of agreement considerably decreases for later arrivals consisting of Rayleigh waves excited at the Northern edge of the valley. The best fit is obtained with the SEM-BE solution, suggesting that the error in the numerical modelling of the surface wave generation at the Northern edge is not increased by the propagation of the surface waves towards the centre of the valley. For all the other solutions, the numerical error accumulates during propagation of the surface waves along the horizontal interfaces – as in the 1D-sharp case.

In Figure 8 we compare the horizontal in-plane component at the Southern receiver computed with FDM-S for different resolutions and definitions of the effective medium. As in the 1D-sharp case, the advantage of using the orthorhombic effective medium is clearly seen on the late Rayleigh waves generated at the Northern edge: the GOF levels for the anisotropic solution computed with 10 m grid spacing are much higher than for the 5 m isotropic solution. Halving the size of the grid in the anisotropic solution yields perfect match with the SEM-F solution, which provides an a posteriori justification for considering the latter a reference.

The analysis of the results of the 2D cases with smooth models (see article) confirms what was observed for the 1D models: the overall level of agreement between all solutions is very good, even for late Love and Rayleigh wave arrivals. This is because the grid spacing used in each numerical method is fine

enough to correctly represent the spatial variations of the material parameters of the models (in addition to correctly sample the seismic wavelengths).

Another feature of interest for the SEM is that a best-effort representation of the basin edges yields a reasonable level of accuracy, while preserving the computational efficiency of the method.
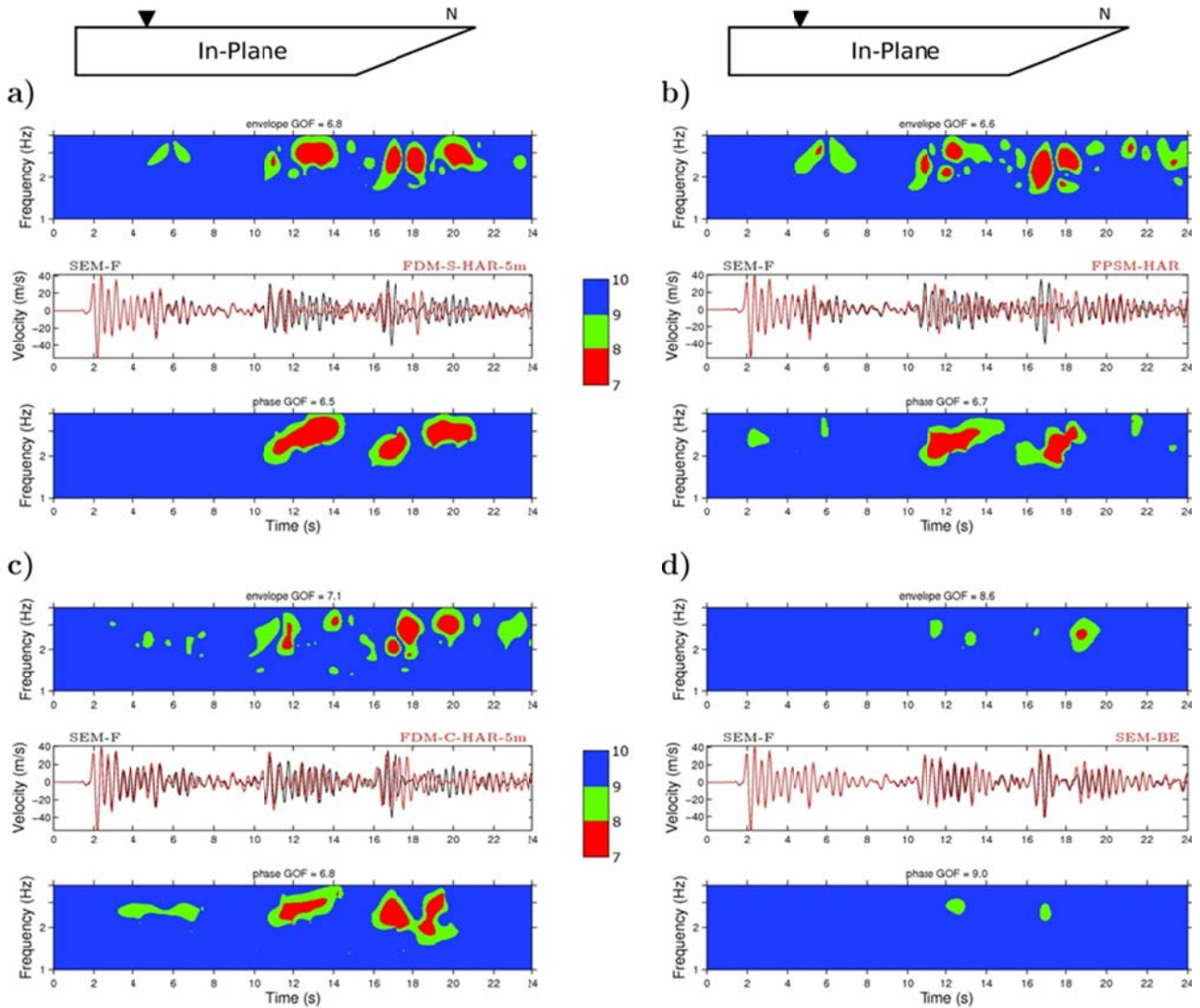
Figure 7: *North-South component of ground velocity at a receiver along the Western surface profile, 1 km away from the Southern edge, computed for the 2D-sharp case by four teams using a) FDM-S, b) FPSM, c) FDM-C, d) SEM-BE. The SEM-F solution is taken as a reference and is plotted in black. The level of agreement between each solution and the reference is quantified by the time-frequency goodness-of-fit (GOF) in amplitude (top panel) and phase (bottom panel). The colorscale indicates the level of GOF, from 7 to 10 (perfect fit). The average GOF is indicated on top of the time-frequency subplots.*
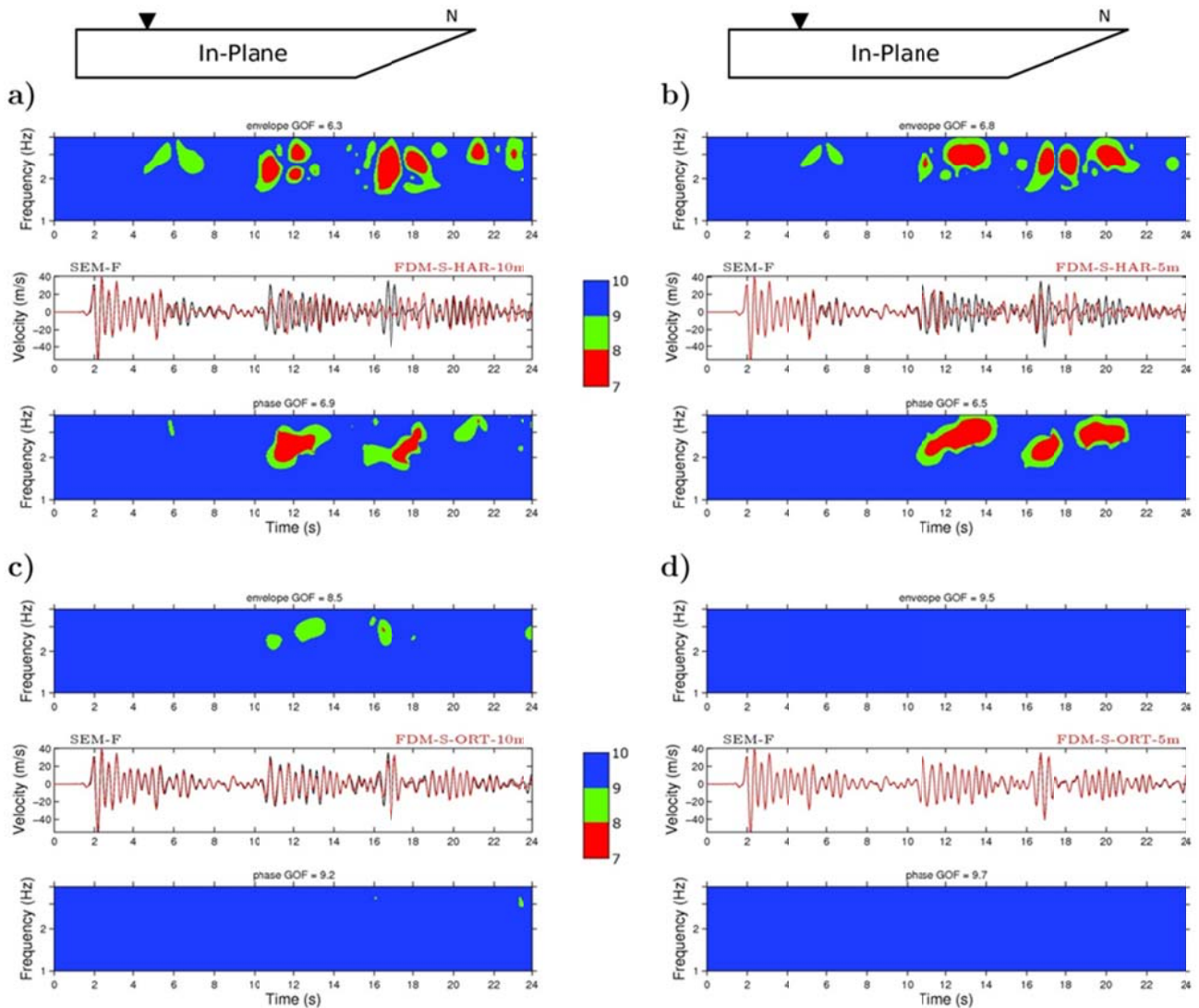
Figure 8:   *Same as Figure 7 for solutions computed with FDM-S using different grid spacings and definitions of the effective medium: a) harmonic averaging, 10 m; b) harmonic averaging, 5 m; c) orthorhombic averaging, 10 m; d) orthorhombic averaging, 5m.*

3.4   CONCLUSION

In order to better understand the origin of differences between 3D numerical predictions of earthquake ground motion in realistic models of the Mygdonian basin, we have designed four canonical models derived from the realistic 3D model of the Mygdonian basin. The models have 1D or 2D geometry and consider sharp or smooth models of the basin material properties.

We have compared several numerical solutions of the four cases for frequencies up to 4 Hz. The solutions were computed with the Fourier pseudo-spectral method (FPSM), the Legendre spectral-element method (SEM) and two formulations of the finite-difference method (FDM-S and FDM-C).

The comparisons show that both the accuracy of individual solutions and level of agreement between solutions vary with the type of seismic waves and depend on the smoothness of the velocity model. The level of accuracy is high for the body waves in the numerical solutions for all the models considered, whereas it systematically decreases in the sharp models for the surface waves.

The accuracy of the numerical solutions for the sharp models is shown to depend strongly on the discrete representation of the material interfaces (at which material parameters change discontinuously) inside the sediments. We have illustrated the dual nature of the implementation of interfaces in SEM: solutions computed with a mesh of elements whose boundaries follow the interfaces (F strategy) are optimally accurate, whereas solutions computed by interpolating the discontinuities on the polynomial basis local to the elements can be extremely inaccurate for surface waves propagating along the interfaces. For all the numerical methods considered, except SEM if the F-strategy can be applied, a proper implementation of interfaces requires the definition of an effective medium consistent with the interface boundary conditions. We have tested the efficiency of two explicit effective media: the isotropic volume harmonic and arithmetic averaging of elastic moduli and densities, respectively, and its generalization to an orthorhombic effective medium.

Our results show that using the isotropic effective medium yields numerical solutions of limited accuracy for surface waves. They also indicate that reaching an acceptable accuracy by solely decreasing the size of the numerical grid may be extremely computationally expensive. Using instead the orthorhombic effective medium is shown to significantly improve the accuracy of the solutions and to preserve the computational efficiency of the methods.

The conclusions drawn from the analysis of the results of the canonical cases greatly help to explain the origin of the differences between numerical predictions of ground motion in realistic models of the Mygdonian basin. The persistent misfit between even the most similar solutions can be fairly attributed to the differences in the discrete representation of the material interfaces in sediments.

These results have important implications regarding the accuracy of numerical prediction of earthquake ground motion in sedimentary basins, in particular with respect to local surface waves which play a critical role in the lengthening of ground motion duration and local amplifications at the basins edges. An improper discrete representation of the interfaces can cause considerably inaccurate numerical modelling of surface waves. Therefore, preparation of the computational model needs special care in this respect. Homogeneous layers within sediments should not be artificially introduced.

Whenever small-scale, or localized, strong variations of the material parameters have to be considered in the sediments, e.g. based on firm geological, geotechnical or geophysical evidence, an effective medium relevant for the chosen frequency range should be used. Depending on the degree of knowledge of the model heterogeneity and on the desired level of accuracy of the predictions, the effective media can be defined as follows: In the common situation where the level of uncertainty in the model (including the presence of interfaces) is large, a simple volume arithmetic average of the densities and slownesses, or a volume arithmetic average of the densities and harmonic average of the elastic moduli, should be used to provide an isotropic effective medium ready for numerical simulations. In all other situations, an upscaling procedure should be adopted to design an anisotropic effective medium, either by solving a homogenization problem, or by following an explicit approach based on the orthorhombic averaging.

Finally, our results confirm that there is no single numerical-modelling method that can be considered the best in terms of accuracy and computational efficiency for all structure-wavefield configurations. We recommend that any numerical method and code that is intended to be applied for

numerical prediction of earthquake ground motion should be verified through stringent models that would make it possible to test the most important aspects of accuracy. We believe that the canonical cases presented in this article, and made freely available to the seismological community (http://www.sismowine.org), can serve this purpose.

Based on these conclusions, we have designed a new basin model for the calculations performed in the second phase of E2VP. The basin model is presented in section 4. It relies on the parameterization of the basin velocity model into two sedimentary subregions, which correspond roughly to Mygdonian (M) and Pre-Mygdonian (P) deposits. The anchor depth of the interface between M and P units varies laterally, but there is no discontinuity of the material parameters across the MP interface. This input model was furthered smoothed using a simple homogenization procedure, which consists in applying an arithmetic vertical average of the slownesses and densities, with an average length of 50 m. Verification was done by comparing the response of the new basin model computed by two independent codes implementing the spectral element method (specfem3D and efispec) by the UJF and BRGM teams. The results obtained by the two codes form the synthetic database that was used in the different sections of this deliverable (4,5 and 6).

4   <u>VALIDATION</u>

4.1   SOURCE PARAMETER OPTIMIZATION

Following the learnings of the first phase of E2VP, it was decided to define a new catalog of seismic events with improved source parameters (location of hypocentres and focal mechanisms) for the validation phase of E2VP2. This work was performed by A. Kiratzi and Z. Roumelioti from Aristotle University and coordinated by EPPO-ITSAK. The details of the work can be found in Appendix 3.

This work included careful relocation and determination of focal mechanisms through waveform fitting of Broad-Band and accelerometric recordings with 1D synthetics computed by the Discrete Wavenumber Method in the crustal velocity model of Novotny et al. (2001).

This task was made difficult because of several factors: (i) retrieval of the BB data from the unified Hellenic network is automatized only for events that occurred after 2008, (ii) only few recordings (usually 2-4, once 7) were used per events as the small magnitudes considered prevent the existence of good quality recordings at low-frequency, (iii) some events were immediately followed by aftershocks which affect the waveform analysis.

Nonetheless, the results of the inversion were usually found to be stable in terms of hypocentral depths and focal mechanisms (only one event resulted in poorly constrained parameters).

Note that for those events that were considered in both validation phases of E2VP, the new source parameters can vary significantly with respect to the old ones. For example, the largest event (Mw=4.4) used in the first phase (labelled II4, then) was moved by 5 km vertically and 4.5 km horizontally to define the S3 event of phase 2, resulting in a change of the epicentral distance of the central TST station from 6.5 km to 8 km.

The results of this analysis provide valuable information for 19 events (shown in Table 3 and Figure 9): a preferred hypocentral location and focal mechanism are given as well as at least one alternative solution. The depth uncertainty is given for each event, and is usually around 2 km.

For the sake of consistency, all the synthetic 3D calculations presented in section 4.4, 5 and 6 make use of the same crustal velocity model (*i.e.*, Novotny et al., 2001) than the one used in the relocation analysis. In the validation work presented in section 4.4, only the preferred solutions have been used, the alternative solutions will be tested in the next months. The sensitivity of absolute and relative ground motion parameters to source parameters uncertainty is studied in section 4.4 and 5.

4.2   NEW 3D PROPERTY MODEL

During the E2VP-phase 1, we used the preexisting 3D model as proposed by Manakou 2007 and Manakou et al. 2010. For E2VP-phase 2, we build a new 3D model "from scratch" in order to avoid any bias due to preexisting interpretation choices. This next model is extended to the whole Mygdonian basin and gathering all available data (and a few new one collected in the framework of E2VP2).

Table 3:   *Characteristics of the 19 selected real events that occurred near the Mygdonian basin, whose recordings by the Euroseistest accelerometric array are compared to 3D numerical predictions in the validation phase 2. Only the preferred solutions of the inversion for source parameters are shown.*

Event ID	Date	Lat. (°)	Long. (°)	Depth (km)	Mag. Mw	TST hyp. dist. (km)	Strike (°)	Dip (°)	Rake (°)
S1	2006/05/10	40.5208	23.4052	5	4.38	19.3	245	54	-105
S2	2006/08/17	40.5433	23.1732	11	3.59	20.0	80	57	-149
S3	2005/09/12	40.7255	23.3408	10	4.40	12.8	281	52	-98
S4	2009/06/21	40.6895	23.1148	11	3.14	18.7	100	61	-102
S5	2012/10/21	40.6950	23.2580	11	3.44	11.9	81	53	-127
S6	2004/06/08	40.5520	23.5233	9	3.30	25.0	71	82	-121
S7	2004/07/15	40.6800	23.4378	7	3.70	14.4	73	53	-118
S8	2004/07/15	40.6952	23.4733	9	3.70	18.2	258	47	-96
S9	2004/11/09	40.7648	23.3520	3	3.10	12.7	253	46	-98
S10	2004/12/12	40.6760	23.2853	4	2.70	4.2	240	51	-89
S11	2005/04/20	40.8121	22.9129	4	3.50	36.1	103	58	-94
S12	2005/09/12	40.7012	23.3586	4	3.00	8.1	301	52	-77
S13	2005/10/09	40.7889	23.4375	8	3.40	20.2	64	74	-116
S14	2007/12/27	40.7230	23.1700	11	3.50	16.4	276	59	-95
S15	2008/08/28	40.6617	23.3292	3	2.80	4.4	80	48	-83
S16	2008/10/13	40.6120	23.4200	9	2.90	15.3	306	58	-52
S17	2009/10/05	40.6920	23.3850	10	3.40	13.1	63	60	-174
S18	2010/08/08	40.5603	23.5785	8	4.60	28.1	235	52	-157
S19	2011/07/25	40.6265	23.3047	5	2.80	6.6	14	84	0
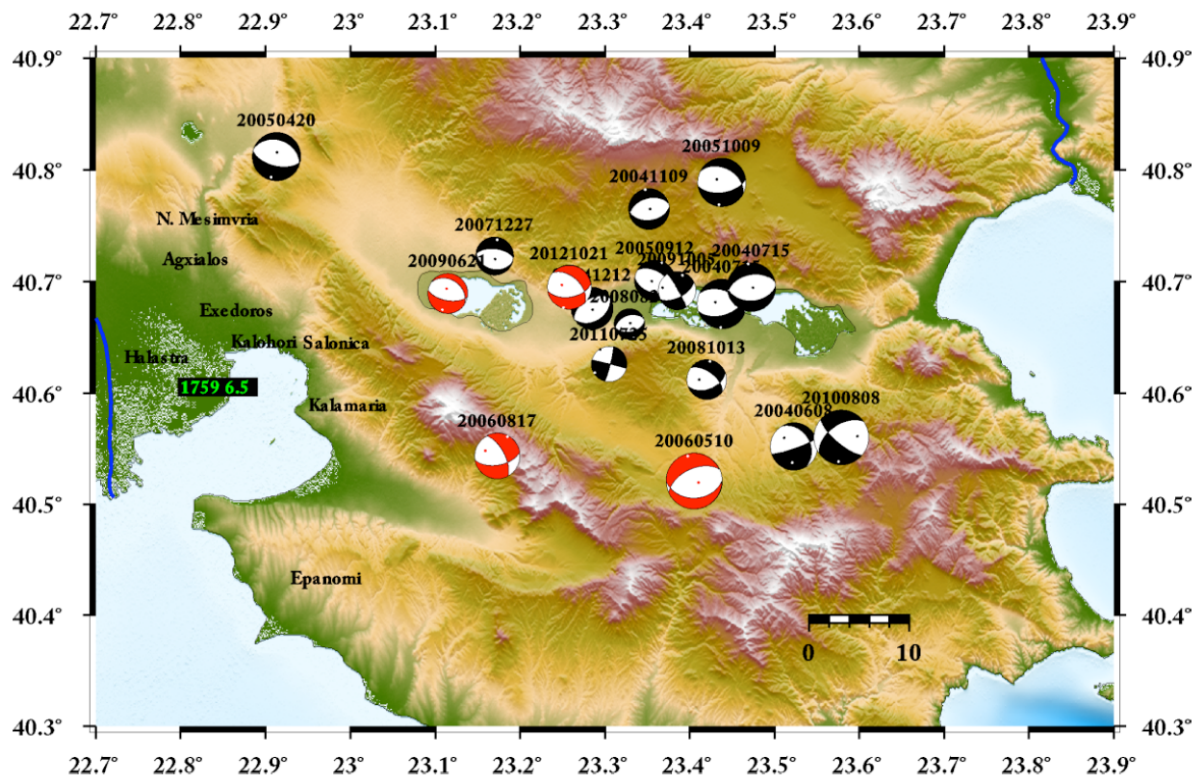
Figure 9: Map of the 19 seismic events that were considered in the Validation part of E2VP2. The focal mechanisms are indicated with beach-balls, the size of which is proportional to the magnitude of the event. Most of the events show normal faulting, consistently with the extension regime of the area.

On important thing to mention in order to understand the "philosophy" of E2VP2 validation effort, is that we did our best to build the new 3D model using geological, geophysical and geotechnical available data but only these data. Indeed, we did not try to "retro-fit the model" in an *ad hoc* approach in order to perfectly fit simulated ground motion with real records as we could have done by using the E2VP-phase1 results.

The used database is heterogeneous and composed of hydrogeological and geotechnical boreholes, seismic refraction surveys, array microtremor measurements, electrical and geotechnical surveys. We propose an integrated workflow, adapted to heterogeneous geological, geophysical and geotechnical data in order to integrate this database in 3D. All available data were compiled in 3D using the geomodeller GOCAD (Caumon et al., 2009; Mallet, 2002) to build a 3D geological model of the entire Mygdonian basin. The results presented and discussed in this paper have been derived from information provided by the 3D geological model such as 3D geometry of 1/ the "geophysical" bedrock (i.e. Paleozoic basement), 2/ the main faults surfaces as well as thickness maps of the entire filling of the Mygdonian basin.

This 3D geological model led to the 3D geometry of the main geophysical/geological boundary of the basin and to precisely quantify the 3D volume of the sedimentary filling of the basin. The results of this study will be used in the second phase of the E2VP project for numerical simulations at the scale of the entire Mygdonian basin.

4.2.1   Geology of the Mygdonian basin and present-day structure

The Mygdonian basin is located in a seismically active zone, belonging to both Serbomacedonian massif and Circum Rodope zone. This basin can be subdivided into two different parts: the eastern part close to the Volvi Lake, striking E-W and the western part close to the Lagada Lake, striking NW-SE. The Euroseistest site is located at the center of the basin, between the two lakes.

The present-day structure of the basin (Figure 10) is composed of three structural units, from shallower to deeper unit: (1) the Mygdonian system (2) the ProMygdonian system and (3) the Paleozoic basement (Manakou, 2007; Manakou et al., 2010). The Mygdonian and ProMygdonian systems are two sedimentary units with thickness variation of 140 meters, for the eastern part (close to the Volvi Lake) to 400 meters, for the western part (close to the Lagada Lake). The Mygdonian system is composed of fluvial-lacustrine, deltaic, lacustrine, lagoonal and estuarine deposits (Psilovikos, 1977; Sotiriadis et al., 1983), Pleistocene to Holocene age (Quaternary). The ProMygdonian system is composed of conglomerates, sandstones, silt-sand and red-beds sediments (Raptakis et al., 2005), Tertiary age. These two sedimentary units underlie the Paleozoic basement, composed of gneiss, amphibolites, two-mica schists and marble intrusions. These structural units are affected by a complex fault system. In the entire basin, the faults are mostly striking NW-SE, excepted in the eastern part (Volvi Lake) where the faults strike E-W and N-S. The main features are the 12 km long Vasiloudi - Gerakarou - Nikomidino - Stivos fault system, running through the southern and western part of the basin (F-GNSP for the main fault system and F-VL & F-Sx for its two segments, Figure 10). This fault system presents a constant dip to the North (70°-80°), reduced to about 35° with increasing depth.

Figure 10:   Simplified structural sketch of the Mygdonian basin, modified from Mygdonian geological and neotectonic maps, scales 1:100 000 to 1:50 000[9].

4.2.2   Database

4.2.2.1   Hydrological and geotechnical boreholes

190 hydrological and geotechnical boreholes were used in this study. These boreholes are extracted from IGME, ITSAK and AUTH databases. 85 boreholes are located in the center of the Mygdonian basin between Lagada and Volvi lakes, most of them located near the Profitis-Stivos section and south border of the basin, close to the main fault (F-GNSP) of the basin. 78 boreholes are located in the western part of the basin, 27 boreholes are located in the eastern part of the basin, mainly in the south border of the Volvi Lake. Boreholes have a total depth (True Depth) reaching 7 to 473 m. They are mainly drilled in Quaternary, Pleistocene and Miocene siliciclastic deposits and Palaeozoic rocks, for boreholes reaching the basement of the Mygdonian basin. 56 boreholes reach the Paleozoic basement, with an average depth of 100 m, varying from 1 to 408 m. Three boreholes have been drilled directly in the Paleozoic basement. 131 boreholes don't reach the Paleozoic basement. They reach 100 m depths in average in the sedimentary filling of the basin, some of them reaching depths until 473 m depth, in the eastern part of the basin, in front of the Volvi Lake.

4.2.2.2   Geophysical surveys

Geophysical surveys have been mostly acquired to investigate bedrock depth and geometry, others to detail faults geometries of the Mygdonian basin. The goal of this study is to reveal the true 3D deep structure, not only in the center of the basin, between the two lakes, but of the entire Mygdonian basin. To achieve this goal, we collected and compiled all available geophysical surface and subsurface data, which

were integrated in 3D in order to perform a 3D geological model of the entire Mygdonian basin. All these collected data are presented below.

4.2.2.3 *BRGM seismic surveys*

Seismic lines used in his study were acquired between 1970 and 1971 by BRGM, in the case of the hydrological study of the Mygdonian basin, for management of water irrigation of Thessaloniki city. Six seismic refraction profiles (AA' to FF') have been acquired by the BRGM between 1970 and 1971. Two profiles strike NE-SW and are located in the western part of the Mygdonian basin. One profile, located in the eastern part, strikes N-S whereas three profiles are located in the center of the Mygdonian basin, between the two lakes (Lagada and Volvi lakes), with two of them striking N-S and one striking E-W. These seismic profiles (along 58,344 km) have been calibrated with 165 electrical boreholes. Five profiles (profiles AA' to CC' and EE') are perpendicular to the axis of the basin, one (profile DD') is parallel. The seismic stratigraphy was established by correlating the electrical boreholes stratigraphy with adjacent seismic lines. This geophysical study allowed producing a map of the depth of the geophysical bedrock, identified as the impermeable bedrock, i.e. the Paleozoic basement.

4.2.2.4 *CSRMT measurements*

Five CSRMT profiles (Controlled Source/Radio MagneoTelluric) have been measured by (Bastani et al., 2011) in 2008 (Profiles 3 to 7). CSRMT data have been acquired along these profiles in order to precisely map the geometry of faults surfaces, especially the "F-GNSP" normal fault (Manakou, 2007; Manakou et al., 2010), located along the south border of the Mygdonian basin. This fault, striking E-W and 12 km long, is located between Vasiloudi and Peristerona villages.

CSRMT profiles have been collected close to Stivos village. The profile 3, striking NNW-SSE, is located along the Profitis-Stivos section and is 3,1 km long, starting from Stivos village. Profiles 4 to 7 are parallel to profile 3. These four profiles strike NNW-SSE and are located to the east of profile 3, close to Stivos village.

4.2.2.5 *H/V measurements*

347 H/V measurements have been collected in the center of the basin, between Lagada and Volvi lakes.

4.2.3 Modelling workflow

The 3D geological model of the Mygdonian basin was built using all available geophysical and geological data. These data are compiled in 3D using a modeling workflow in the framework of the gOcad geological software (Caumon, et al., 2009; Le Carlier de Veslud, et al., 2005; Mallet, 1989; 1992; 2002; Spottke, et al., 2005, ParadimGeo). The Mygdonian basin 3D geological model is georeferenced in the World Geodetic System 84 (Universal Transverse Mercator 34°N). The following modelling workflow has been applied to is composed of the following 3 steps, modified from (Guyonnet-Benaize, et al., 2010).

4.2.4 3D structure of the Mygdonian basin

The 3D view of the 3D geological model of the Mygdonian basin is shown in Figure 11. This model is 12 km wide, 65 km long and is 400 m deep in average. Figure 11 displays the fault pattern and main geological/geophysical interface ("Paleozoic" bedrock) as well as the topography of the basin. It has been built using all available geophysical, geotechnical and geological data.
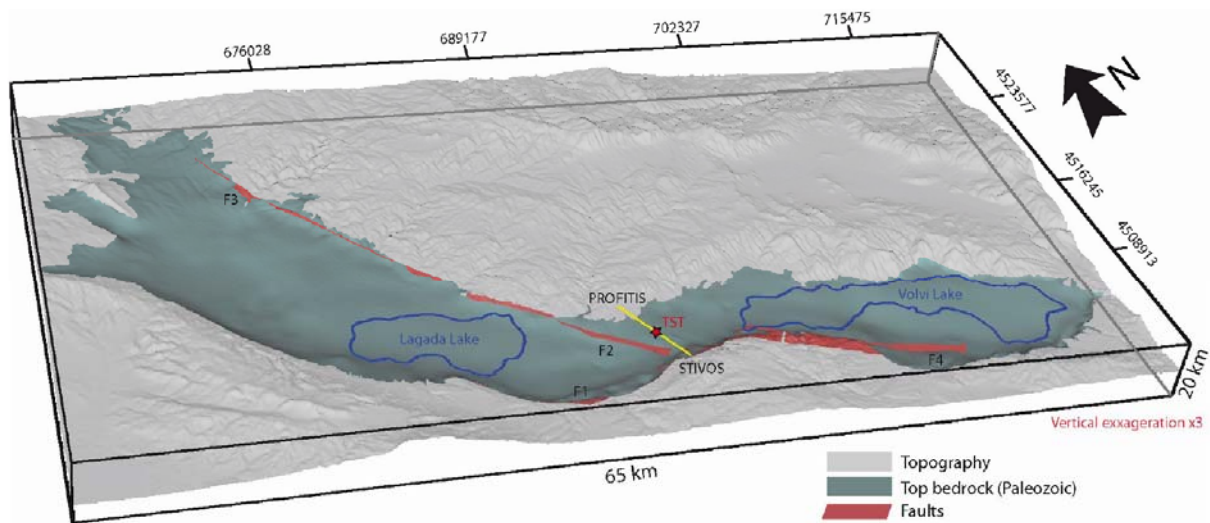
Figure 11:   3D view of the 3D geological model of the Mygdonian basin.

The model includes 4 main faults of plurimetric scale, extracted from the neotectonic map (Moundrakis et al., 1995). These faults have been chosen to be modeled because they affect directly the Paleozoic bedrock and the geometry of its surface, under the limits of the Mygdonian basin. These changes have to be taken into account in numerical simulations. These faults present two main strikes: two faults strike NW-SE and two faults strike E-W. These faults present a vertical faulting geometry (faults 2 to 4), except for one fault showing a listric faulting geometry (fault 1: F-GNSP, located at the southern border of the basin, (Manakou, 2007; Manakou et al., 2010)). 3 faults are located at the basin borders. One fault is located at the center of the basin, between the two lakes. This fault divides the studied area in two homogeneous structural blocks: a western block (Lagada area) and an eastern bloc (Volvi area).

4.2.4.1   Bedrock geometry

Figure 12 displays the present-day geometry of the top surface of the bedrock (i.e. Paleozoic basement), shown in depth. Throughout the studied area, the mean depth of this surface is close to -65 m, with a range from -414 to 400 m. The top bedrock surface 3D geometry is characterized by two major depressions striking NW-SE and E-W, respectively to the western and the eastern parts of the Mygdonian basin (Lagada and Volvi areas, Figure 12a). These two depressions are separated by a high located between the two lakes ranging from -176 to 180 m depth. Figure 12b displays a closest view of this area. This view highlights an asymmetrical shape of the bedrock geometry. Compared to the present-day axis of the basin (orange dashed line), the axis of the bedrock is shifted to the south (red dashed line). Along Profitis-Stivos section, the top bedrock surface presents low dip values (5-8° to the southeast) between stations PRO1 and TST0. Between TST0 and FRM1, the deepest part of the bedrock is flat, in average. Finally, from stations FRM1 to STE1, the top bedrock surface presents high dip values (more than 15-35° to the northwest).

4.2.4.2   Sedimentary thickness

Figure 13 illustrates the present-day thickness of the entire filling of the Mygdonian basin, corresponding to both ProMygdonian and Mygdonian units. The thickness of the entire sedimentary serie increases both parts of the center of the basin (Figure 13a). The thickness map highlights two main sedimentary depot-centers: the first is located to the northwestern part of the Lagada lake and is 465 m thick, the second is located to the east of the basin in front of the Volvi lake and is 450 m thick. These two sedimentary depot-centers are separated by a structural high with less sedimentary thickness,

corresponding to the center of the basin, between the two lakes (Figure 13b). In this area, the sedimentary thickness ranges from 100 to 250 m in average, except with a zone located southeast of the Lagada lake where sedimentary deposits are 350 m thick. The axis of the sedimentary depot-center (red dashed line) through Profitis-Stivos section is close to the south border of the basin, illustrating the asymmetrical shape geometry of the basin along this section.

The Figure 14 presents the whole model that is used in E2VP-phase 2 (box of 69 x 69 km) including position of accelerometric stations and modeled earthquakes (see Table 3), the DEM on the whole arear and the elevation of the top of the bedrock within the basin.
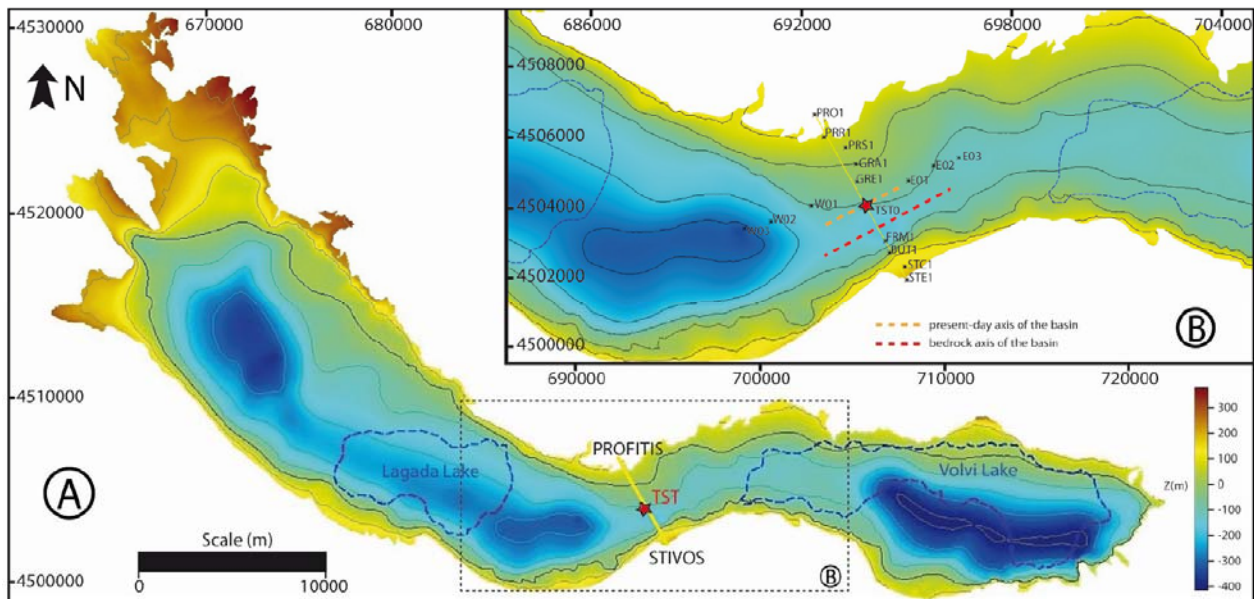
Figure 12: Present-day geometry of the top surface of the bedrock.
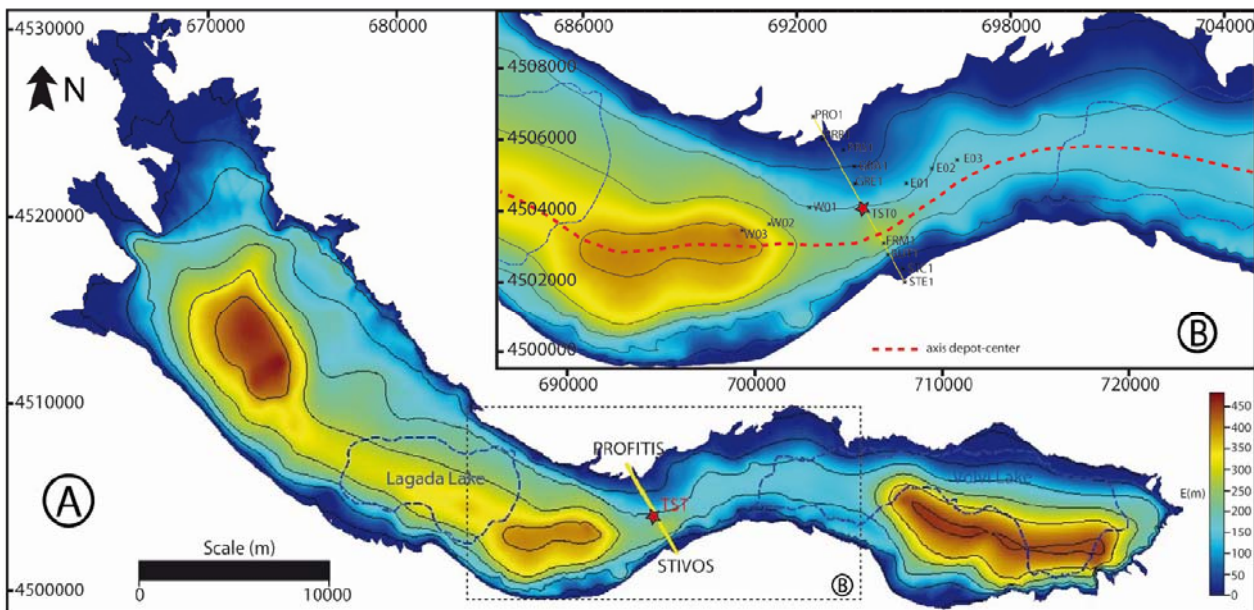
Figure 13: thickness of the entire sedimentary serie increases both parts of the center of the basin.
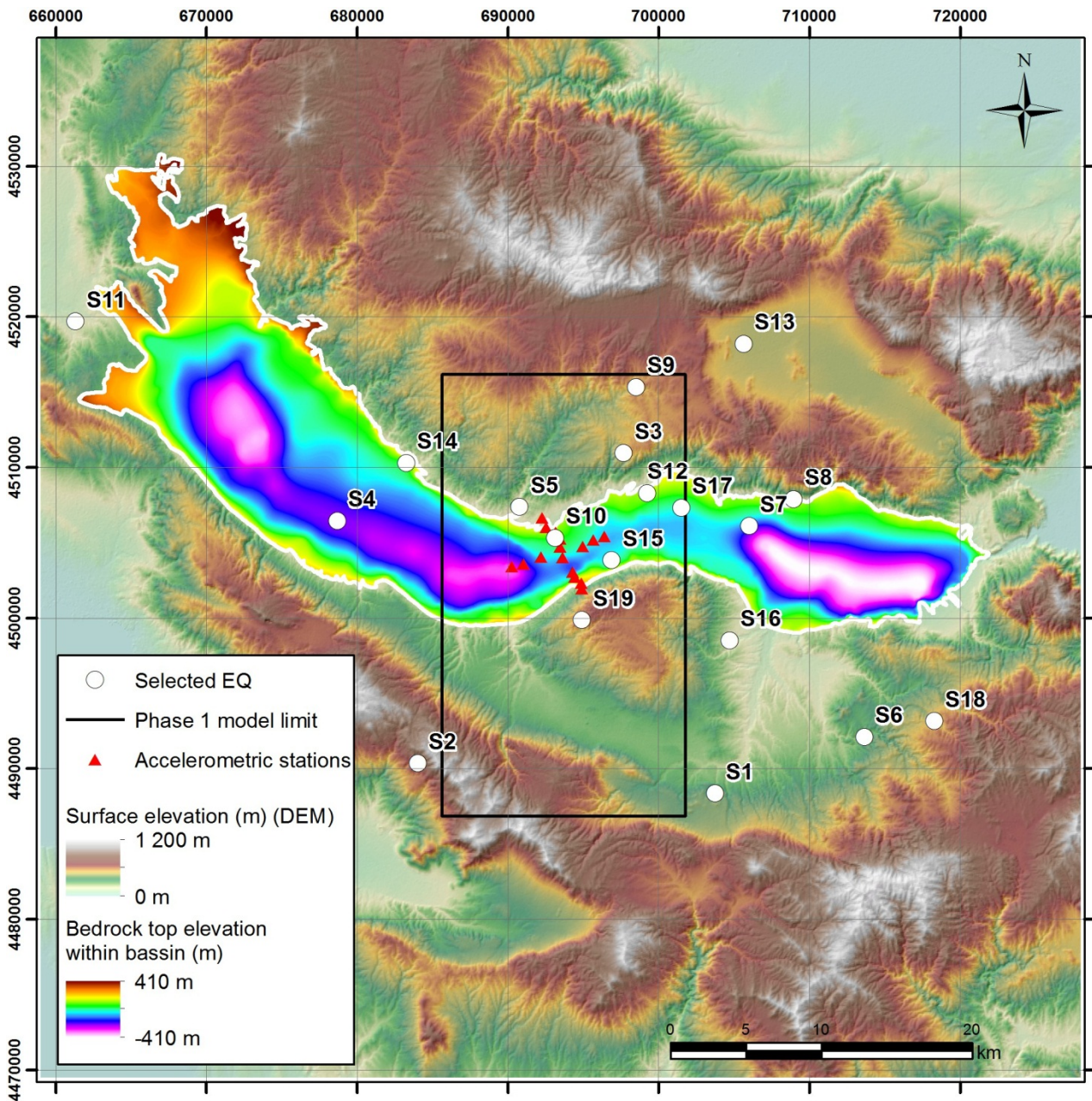
Figure 14: *Map of the whole model used for E2VP phase 2 modeling (box of 69 x 69 km), with the location of the area of the "phase 1" modeling box, accelerometric stations, modeled earthquakes, DEM et elevation of the top of the bedrock within the basin.*

4.2.5 Properties model

In order to define the physical properties within the basin, we gathered 74 profiles (7 from geotechnical tests like cross-hole or down-hole, 67 from geophysical survey like refraction seismic refraction and ambient vibration arrays).

We first considered that there was no reason to prefer a constant velocity layered model instead of a "gradient like" model. We then proposed to use "double gradient" concept:

— the first linear gradient from the surface to an intermediate surface within the basin,

— the second linear gradient from this intermediate surface to the bedrock

The intermediate surface corresponds to a limit where the velocity trend changes within the basin. This could be associated to the Mygdonien / Premygdonien limit (so we named this surface M/P limit) but do not consider this surface as a strict geological interface, rather a geophysical interface. Table 4: Gives the "anchor" chosen values.

Table 4: V_S, V_P, ρ, Q_S and Q_P "anchor" values used to build E2VP2 properties model within the basin.

	Vs	*Vp*	ρ	*Qs*	*Qp*
Surface	130	1500	2075		
M/P limit	475	2100	2130	= Vs/10	= max [Vp/20, Vs/5]
Bedrock top	800	2700	2250		

For a sake of consistency, within the bedrock, we used the model from Novotný et al. (2001), since this one was also used in the improved characterization of the seismic sources (see Section 4.1), insead of the Papazachos (1998) model previously used in E2VP phase 1.

4.2.6 Main differences between E2VP1 and E2VP2 3D models

The Figure 15 aims to compare the E2VP-phase 1 and E2VP-phase 2 models in terms of geometry. Two main differences have to be pointed out here:

─ Along the Stivos-Profitis (STE-PRO) cross-section, the new model produces an asymmetric shape, with a maximum depth South to TST, whereas the old model was more symmetric, with a maximum shape near to TST.

─ The global first-order shape of the new model is rather cylindrical at the scale of the accelerometric network, with a progressive deepening to the West, whereas the previous shape was more a "saddle point".

The Figure 16 presents de differences between the velocity profiles below the TST stations. This illustrated the "constant velocity layers" paradigm used for phase 1 by opposition with the new gradient approach. The first-order consequence of these changes is illustrated on 1D transfer function between TST5 (downhole) and TST0 (surface) on Figure 17. We can see that the fundamental frequency is strictly the same between the new and old model. The difference in amplitude of fundamental peak is very week. There is nevertheless a consequence on higher modes. This illustrate that the difference we will comment in section 4.4 is clearly mainly due to the geometry.
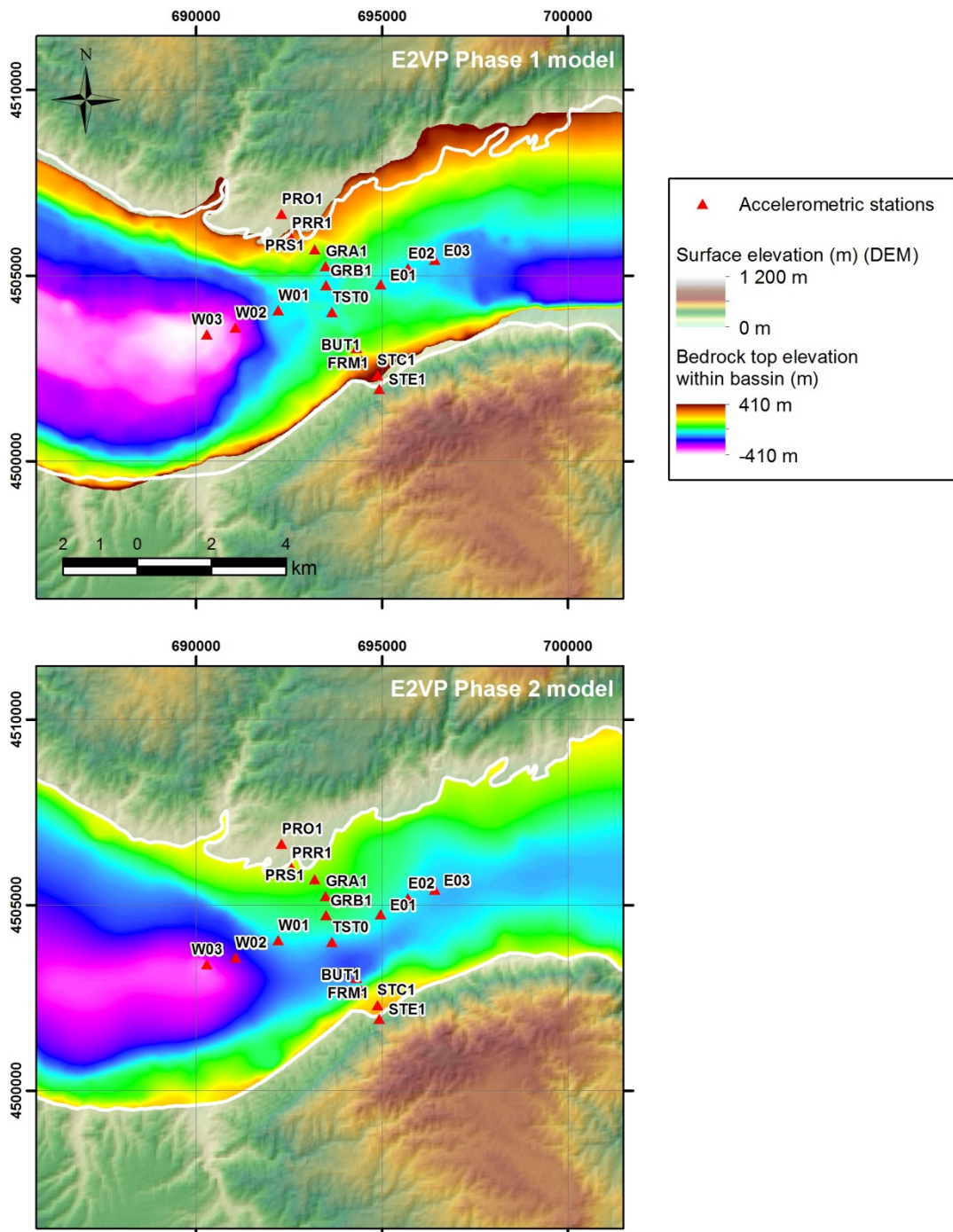
Figure 15:   Comparison between E2VP-phase 1 (top) and E2VP-phase 2 (bottom) models in terms of bedrock top elevation.
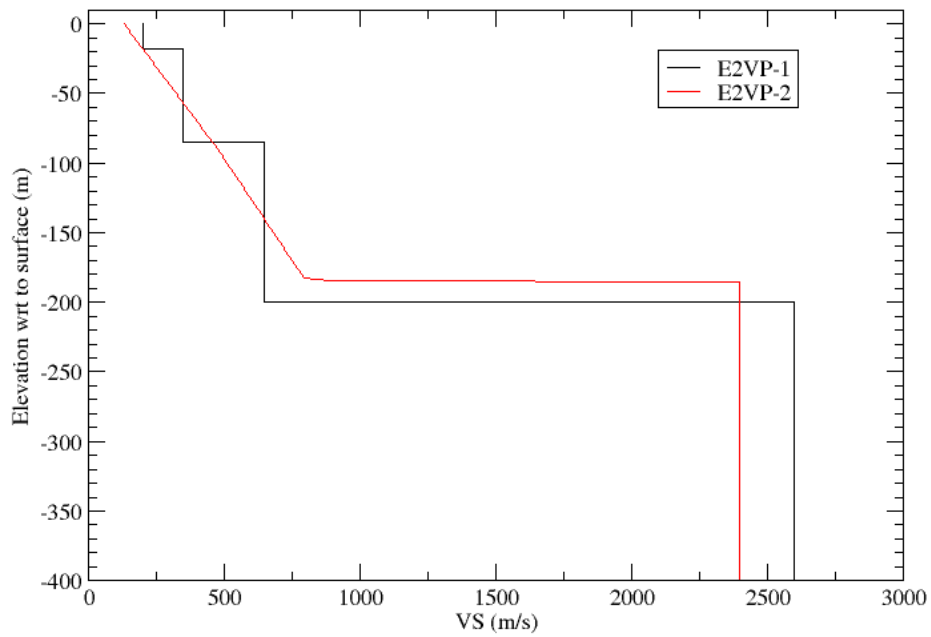
Figure 16: Comparison between E2VP-phase 1 (black) and E2VP-phase 2 (red) models in terms of V_S profile below TST.
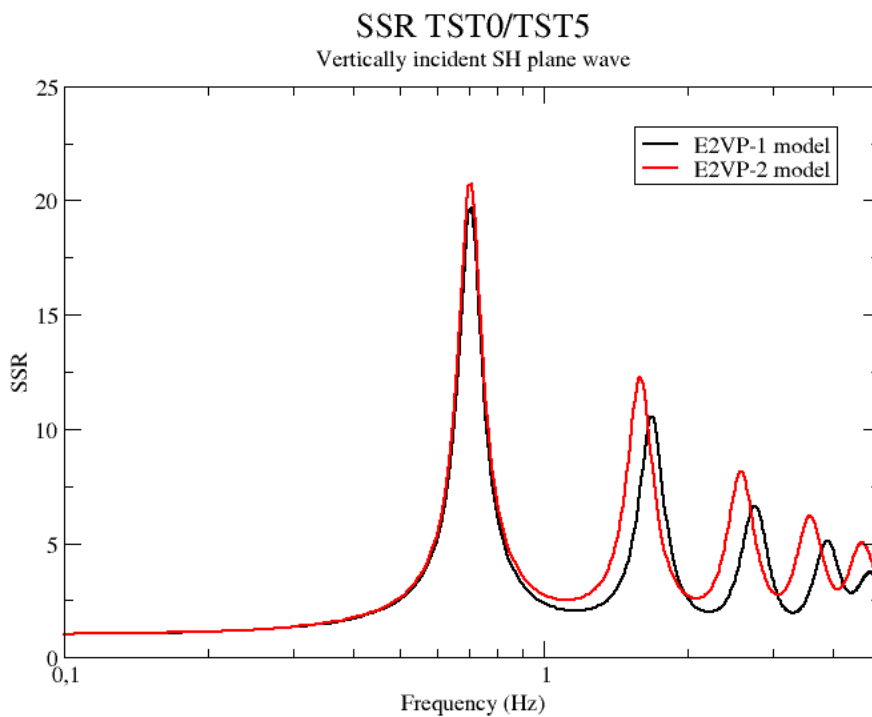
Figure 17: Comparison between E2VP-phase 1 (black) and E2VP-phase 2 (red) models in terms of 1D-SH equivalent transfer function between TST5 and TST0.

4.3   PROCEDURE TO COMPARE ACTUAL RECORDINGS WITH THEIR NUMERICAL PREDICTIONS

The "validation" is defined as the demonstration of the capability of the theoretical model (i.e., the mathematical-physical model and its numerical approximation) to predict/reproduce observations.

The validation in phase 1 of E2VP aimed at providing an objective, quantitative comparison between recorded and numerically-simulated earthquake ground motions in the Mygdonian basin. This exercise, the proposed procedure and the results of phase 1, are the object of a manuscript that is currently submitted for publication in Bulletin of the Seismological Society of America (Maufroy et al., 2014, also in Appendix 2). We summarize the validation procedure and the main results of phase 1 hereafter. The figures and tables cited in the following all refer to the content of that manuscript.

Differences between numerically-simulated seismograms and earthquake records can be relatively large. We defined an objective and quantitative way of comparing signals on the basis of 5 ground-motion parameters chosen to evaluate the similarity between two seismograms on 5 different characteristics of the seismic signal commonly considered in earthquake engineering. Three of them are representative of the signal amplitude in different frequency bands: peak value of the acceleration time series (PGA, C1); elastic spectral acceleration at intermediate frequencies (1.5-3.0 Hz, C2); elastic spectral acceleration at lower frequencies (0.375-0.750 Hz, C3). These different frequency bands are chosen according to the observed characteristics of the real signals at the center of the Mygdonian basin: the frequency range covered by C3 includes the fundamental resonance frequency of the basin, while C2 covers the two higher modes. The two last criteria are representative of the total amount of energy contained in the signal (Cumulative Absolute Velocity, C4) and of the duration (Relative Significant Duration between 5% and 95% of the Arias intensity, C5), respectively. Arguments for the selected characteristics, details on their computations and on the way to handle the horizontal components are provided in Maufroy et al. (2014) (in Appendix 2).

The direct quantification of the difference between two signals is expressed in % of misfit on each of the 5 ground-motion parameters, with a positive (resp., negative) sign for the over- (resp., under-) prediction of the first signal (the recordings) by the second (the numerical prediction).

In phase 1 of E2VP, the validation consisted in the quantitative comparison between numerical predictions and actual recordings in the frequency range up to 4 Hz. The discrepancies between real and predicted ground motions may have multiple origins: inaccuracies of the numerical-modeling methods as seen in the verification, uncertainties in the determination of source parameters (hypocenter location, focal mechanism and magnitude), uncertainties in the description of the geological medium (geometry and/or velocity distribution) and intrinsic ground-motion variability. The comparison was performed for 6 local weak-to-moderate magnitude events, spanning various azimuths, hypocenter depths and distances (see Figure 2). Requirements on the selected events were: (a) available focal mechanism and (b) a sufficient number of high-quality recordings by the local seismic array. The corresponding synthetics were computed in the first 3D viscoelastic layered model of the Mygdonian basin (Table 2).

The misfit values on the E2VP criteria C1 to C5 were found to be highly variable on the whole array: considering the strongest event (#4), an almost perfect fit (~0%) was achieved on a few receivers but some high misfits (greater than ± 100%) were also observed (Figure 10). The misfit values were also highly variable from one criterion to another. The visual comparison of recorded and synthetic waveforms indicated a good level of agreement at the surface soil site TST0 and at the corresponding downhole sensor TST5 at 197 m depth (Figure 9). The level of agreement on event #4 at the surface soil site TST0 was therefore found to be excellent (misfits closed to 0%) or reasonable (below 20%) for criteria C1, C2, C3 and C4 (the duration criterion C5 having a particular behavior, as detailed in the manuscript). The misfits for the borehole

station TST5 also drop to a satisfactory level. For the other stations, even if the waveforms are different, the numerical prediction is sometimes able to reproduce some characteristics of the ground motion.

Still the validation results on phase 1 remain very variable, even inside one event. A global overview of the validation is given in Figure 11 that gathers misfit values on the E2VP criteria for the verification exercise (misfits between synthetics obtained by different teams) and for the validation exercise (misfits between recordings and predictions) for all receivers or for TST0-only, for all events or for event #4 only. One can observe an overall misfit around 25% for the verification while the misfit values are much higher for the validation (around 80%). When considering only TST0, the validation misfits are reduced to approximately 60% for all events and to 40% for event #4 only. This synthesis shown in Figure 11 clearly demonstrates the robustness of the statement that the smallest differences between recordings and their numerical predictions are significantly larger than the usual distances between simulations.

One important question was: can we identify the origins of the validation misfits? The details of the waveforms are highly sensitive to the source parameters (hypocenter location and focal mechanism), to the shape of the sediment-basement interface and to the internal sediment layering of the basin. Each of these items may affect the validation misfits. Are the misfits due predominantly to inaccuracies in the description of the sources and/or of the 3D model?

In order to tackle that question, two analyzes were performed. First, the prediction of the Fourier transfer function from the downhole sensor to the surface sensor at the vertical array TST is evaluated through the comparison of TST0/TST5 Standard Spectral Ratios from recordings and from synthetics, as those SSR remove (some of) the errors due to uncertainties in source parameters and focus on the site effect alone. The frequencies at which amplification of ground motion occurs are well reproduced in all synthetics (Figure 13). However the amplitudes of the different maxima are not all accurately predicted and the contribution of the surface waves around 1 Hz is especially underestimated. The numerical predictions have well reproduced some features of the site effect, but not all.

This analysis is deepen in a second step with the computation of "hybrid" time histories that maximize the impact of numerical estimate of site-effect component and minimize the effect of uncertainties in source description. This is achieved by multiplying in Fourier domain the actual recordings at the downhole sensor TST5 with the synthetic surface-downhole transfer function TST0/TST5. The inverse Fourier transform returns a hybrid time histories in the sense that the input signal is a real signal (integrating actual source parameters) while the site-effect part is coming from the numerical predictions. The E2VP evaluation criteria are then applied between the actual recordings at TST0 and those hybrid time histories (Figure 14). We conclude that fully-numerical signals exhibit a trend to overestimate most parameters, while the hybrid signals exhibit an opposite trend to underestimate the same parameters, in prefect agreement with the surface/downhole spectral ratios previously analyzed.

It suggests that: (a) uncertainties in source description tend, in E2VP phase 1, to produce overestimation of the ground motion in the validation exercise (that could be explained by an overestimation of the magnitude, for example); (b) the site effect itself is globally underestimated at TST site. That global trend for underestimating the actual amplification by all the 3D simulations at TST site could have several explanations: incorrect estimates of damping, incorrect internal sediment layering structure, over-emphasis on the buried-pass/saddle-point structure just underneath TST site (which would result in larger off-profile diffraction), or finally overestimation of the hypocentral depth resulting in too weak excitation of surface waves.

We draw several conclusions from that first validation exercise. Having sensitive in-situ instrumentation proves to be invaluable for checking the reliability of numerical simulation results, with a

special emphasis on vertical arrays which allow constraining the site-effect component. The validation also showed the importance of completing such data with high-quality metadata, concerning both the source parameters and the site model. The gross characteristics of the amplification at the valley center are satisfactorily reproduced by the 3D model, both in terms of spectral contents and signal duration, with however a slight underestimation. In the present case, the differences between recordings and predictions appear to have an approximately-balanced origin shared between inaccuracies in source parameters and uncertainties in the site model. The former are associated to some over-prediction of ground motion, while the latter would underestimate the site amplification. The small number of candidate seismic events that was considered in that first validation phase is a typical situation for moderate/weak seismicity areas. The next validation phase would certainly benefit from the possibility to include more events.

The whole validation procedure as defined in phase 1, which includes (a) calculation of the 5 evaluation criteria, (b) comparison on SSR and (c) computation of hybrid time histories, will be followed in the validation phase 2.

4.4 VALIDATION RESULTS FOR PHASE 2 OF E2VP

Nineteen seismic events, well recorded by the Euroseistest accelerometric array, are used in the second validation phase of E2VP. Details of their characteristics are given in Table 3. Their selection and characterization are described in Section 4.1. This exercise is performed in the new extended model of the Mygdonian basin (Section 4.2). The 3D numerical simulations of the 19 events are performed with the code EFISPEC3D (De Martin 2011) implementing the Spectral Element Method. The simulations include the effects of surface topography and of intrinsic attenuation.

Pre-processing of the data to perform the validation exercise includes: (1) filtering the real data with a Butterworth filter between 0.3 Hz (order 6) and 3.0 Hz (order 10), in order to get a similar frequency content between the recordings and the synthetics; (2) synchronization of recordings with the corresponding synthetics on the first *P*-wave arrival; (3) all couple of signals to be compared are cut to the same length in duration; and (4) a study of the signal-to-noise ratio is performed on all recordings to determine the frequency band where that ratio is greater than 3.

4.4.1 Validation results at rock sites

Results of the comparison between actual recordings and their numerical predictions at 3 rock sites in Euroseistest are given in Table 5. The level of misfit obtained on the 5 criteria of the E2VP evaluation procedure (see Maufroy et al., 2014, in Appendix 2) is expressed by the average misfit computed per criterion from the selected events that were recorded at the corresponding rock site. The misfit values obtained here are similar or below in absolute value to the misfits obtained in the first validation phase at PRO and STE rock sites, giving a first confirmation that the surface ground motion outside the basin is in general well predicted by the numerical simulations. Only borehole site TST5 exhibits anomalously-high misfit values at the highest frequencies considered in the validation.

To get another estimation of the level of misfit outside the basin, Figure 18 shows the Fourier spectral ratios computed between recordings and their numerical predictions for the events recorded at these 3 rock sites. Concerning northern rock site PRO (Figure 18a), the median ratio of observed ground motion over predicted is globally satisfactory (i.e., around and closed to value 1), except for the lowest frequencies that are under-estimated. Reason for that low-frequency under-estimation of the ground motion at PRO is not yet understood. At southern rock site STE (Figure 18b) the median ratio is satisfactorily closed to 1 in all frequencies. But it is noteworthy that the validation results at STE can also be bad for a few events (the colored lines giving the result for each individual event are far from the value 1 in a few cases).

At borehole site TST5 (Figure 18c) that is located right below the sediments at 200 m depth, as previously shown by the evaluation criteria, the actual ground motion appears to be significantly over-estimated by the synthetics in the higher frequencies. This could have a strong impact on the ground motion predicted at the surface and center of the basin, if the incoming wavefield below the sediments is already over-estimated. A few hypotheses are investigated to determine the origin of that problem. At first, the impact of the new crustal-propagation model is examined: the model from Papazachos (1998) was previously used in E2VP phase 1, to be later replaced by the model from Novotný et al. (2001) also used in the improved characterization of the seismic sources (see Section 4.1). Figure 19 shows the simulation result ratio between the two crustal models at 200 m depth (Figure 19a) and at the surface (Figure 19b, without sediments). The crustal model used in phase 2 induces only a slight overestimation (30-60%) in every frequency of the ground motion computed with the model previously used in phase 1. This effect, although it could participate, cannot fully explain the high-frequency overestimation found at borehole site TST5.

Table 5: *Average in % of horizontal misfits on the E2VP evaluation criteria between the actual recordings and their numerical predictions at 3 rock sites: northern rock site PRO, southern rock site STE and borehole TST5. The number of events recorded by each station and considered in the average is indicated in the last column.*

	C1 PGA	C2 2.0 Hz	C3 0.5 Hz	C4 CAV	C5 RSD	Number of events
PRO	-21	-24	-54	-9	-73	9
STE	34	39	1	8	-124	17
TST5	128	129	53	88	-161	16
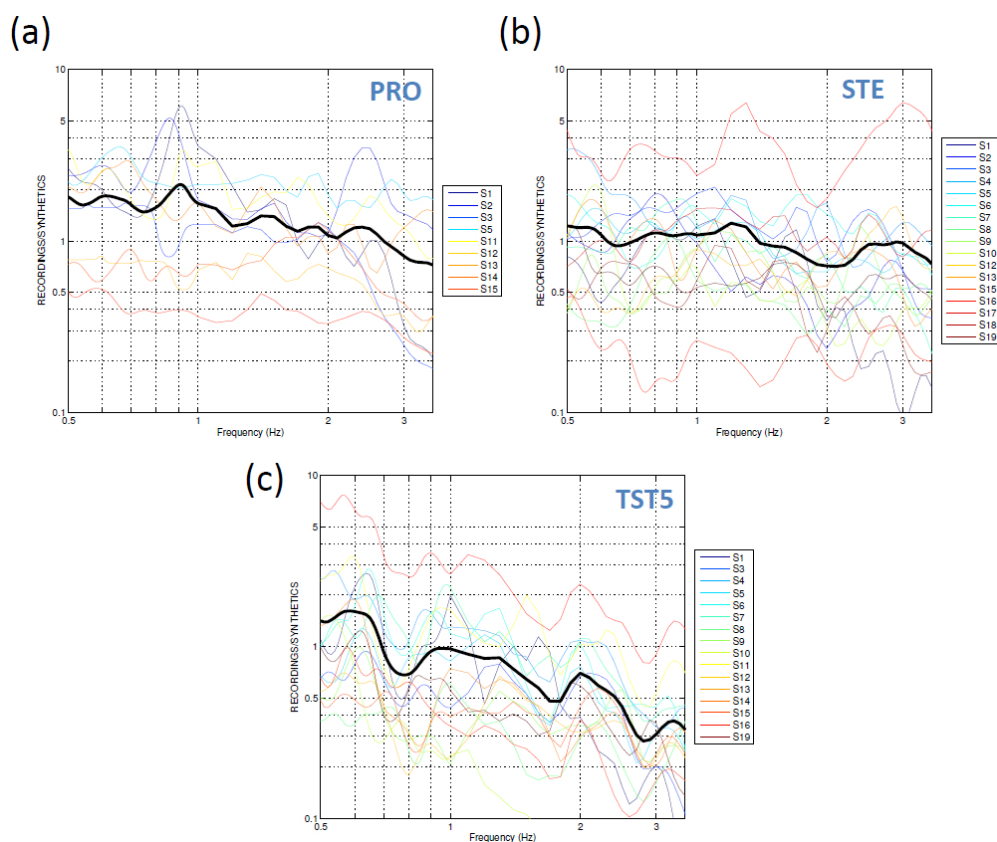
Figure 18 : *Fourier spectral ratios between recordings and their numerical predictions at 3 rock sites: (a) northern rock site PRO, (b) southern rock site STE and (c) borehole TST5. Each colored line shows the result for one seismic event of the validation. The solid black line indicates the average ratio in each panel.*
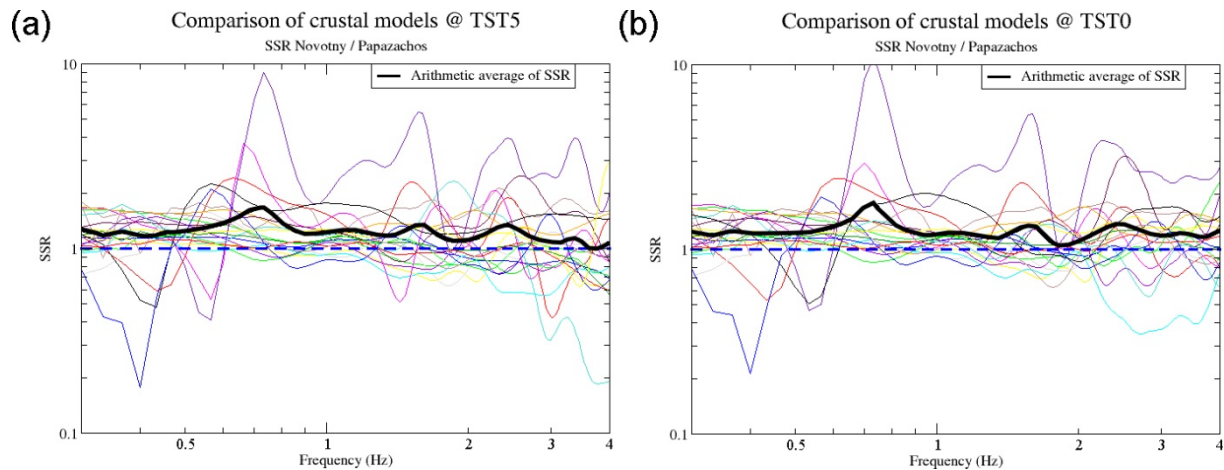
Figure 19:   *Fourier spectral ratios between synthetics computed taking as crustal model either Novotný et al. 2001 (E2VP2) or Papazachos 1998 (E2VP1) for stations (a) borehole 200 m depth TST5 and (b) surface TST0 here modeled without sediments. The solid black line in each panel indicates the average ratio over the 19 selected seismic events. The crustal model from Novotný et al. (2001) used in E2VP2 induces a slight global overestimation (30-60%) of the ground motion computed with the model from Papazachos (1998) previously used in E2VP1.*

Another hypothesis is that borehole site TST5, located right below the sediments, might be too much affected by the basin propagation in the new basin model of E2VP phase 2. The strongest argument in favor of that hypothesis is found in Figure 18c. The average ratio (solid black line) shows the considered overestimation of the recordings by the synthetics at TST5, but that line also presents three inversed peaks. The frequencies of those peaks, roughly at 0.75 Hz, below 2 Hz and below 3 Hz, coincide with the frequencies known as being amplified by the basin at TST0. Indeed the fundamental resonance frequency observed at TST0 and the two higher modes are precisely identified at those 3 frequencies (see for example the SSR computed in phase 1 or at the end of Section 0). This figure demonstrates that a footprint of the frequency-dependent site effect at TST0 is found at TST5 in the new numerical simulations. Moreover, the overestimation of recordings by the predictions at TST5 also clearly increases with increasing frequency. Those observations suggest a too weak attenuation in the new basin model: compared to the recorded motion, the borehole site TST5 receives some extra energy from the basin, which even increases with frequency. Therefore synthetic ground motion at TST5 is amplified in the highest frequencies, which explains those high misfit values on the E2VP evaluation criteria (Table 5). Validation results at surface soil site TST0 will also be affected by the too-low attenuation, as seen in the following.

4.4.2 Validation results in the Mygdonian basin

Once the validation is globally satisfactory at some rock sites (PRO and STE), validating the crustal propagation, the evaluation procedure is applied to all stations for all selected events. The validation results for each event are given in Figure 20 to Figure 38, one map per event and per criterion. See Maufroy et al., 2014 (in Appendix 2) for a description of each criterion and of the followed procedure. To summarize: Criteria C1, C2 and C3 evaluate the amplitude of the signal in different frequency bands. These frequency bands are chosen according to the observed characteristics of the real signals at the center of the Mygdonian basin: the frequency range evaluated by C3 includes the fundamental resonance frequency of the basin, while C2 covers the two higher modes. C1 evaluates the highest frequencies available in the synthetics. C4 and C5 evaluate the total energy of the signal and its duration, respectively.

The study of the signal-to-noise ratio over recordings revealed that the lower investigated frequencies are sometimes not strong enough in the signal for that ratio to be greater than 3. This can potentially affect the validation evaluation on criterion C3: when the signal-to-noise ratio is consistently lower

than 3 in the frequency range 0.375-0.750 Hz over the two horizontal components, a red cross is added to the C3 map (see for example Figure 23). One should remain cautious when interpreting the validation misfits on the marked maps.

In most cases the ground motion in the basin is much over-estimated. The study of the validation results at TST5 revealed that the attenuation might be too weak in the numerical model of the basin. Indeed the site effect predicted at TST0 is consequently too strong and produces high misfit values; this will be further analyzed in the comparison of observed TST0/TST5 SSR with numerical SSR.

The signal duration (criterion C5) is systematically under-estimated in every case, which is interpreted as being due to the absence of any scattering in the numerical simulations.

Event S16 (Figure 35) is the only case where the numerical prediction globally under-estimates the observed ground motion, even at rock sites. This is probably due to some remaining uncertainty in the source-characteristics estimates. A similar case, though reversed, is observed for event S18 (Figure 37) where the ground motion is everywhere over-estimated, even at rock site STE. Other events identified with anomalously strong misfits at rock sites are S9 and S10.
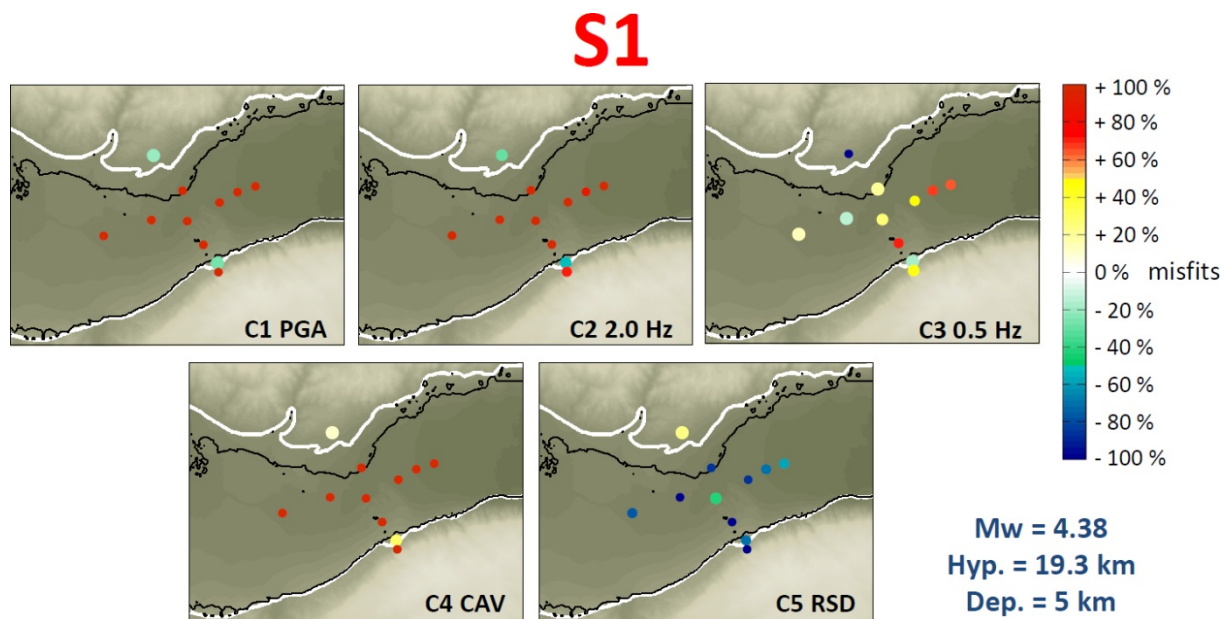
Figure 20:   Maps of horizontal misfits on the E2VP evaluation criteria between the recordings of the real event S1 (see Table 3) and its 3D numerical prediction. C1 is based upon peak ground acceleration, C2 upon elastic spectral acceleration ranging 1.5 – 3.0 Hz, C3 upon elastic spectral acceleration ranging 0.375 – 0.750 Hz, C4 upon cumulative absolute velocity and C5 upon 5-95% relative significant duration (see Maufroy et al., 2014, in Appendix 2, for details). Each colored dot corresponds to the misfit obtained at the corresponding real surface receiver. Red/yellow tones are for overestimation of the recordings by the prediction; blue/green tones are for underestimation.

S2

Mw = 3.59
Hyp. = 20.0 km
Dep. = 11 km
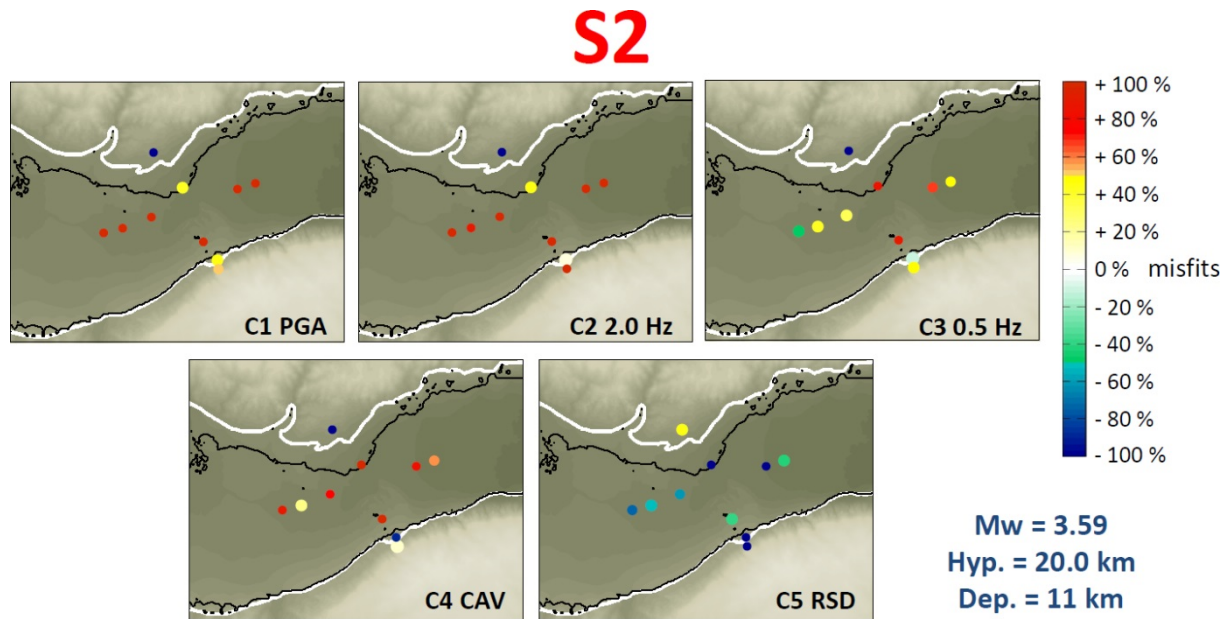
Figure 21 : Same as Figure 20 for event S2.

S3

Mw = 4.40
Hyp. = 12.8 km
Dep. = 10 km
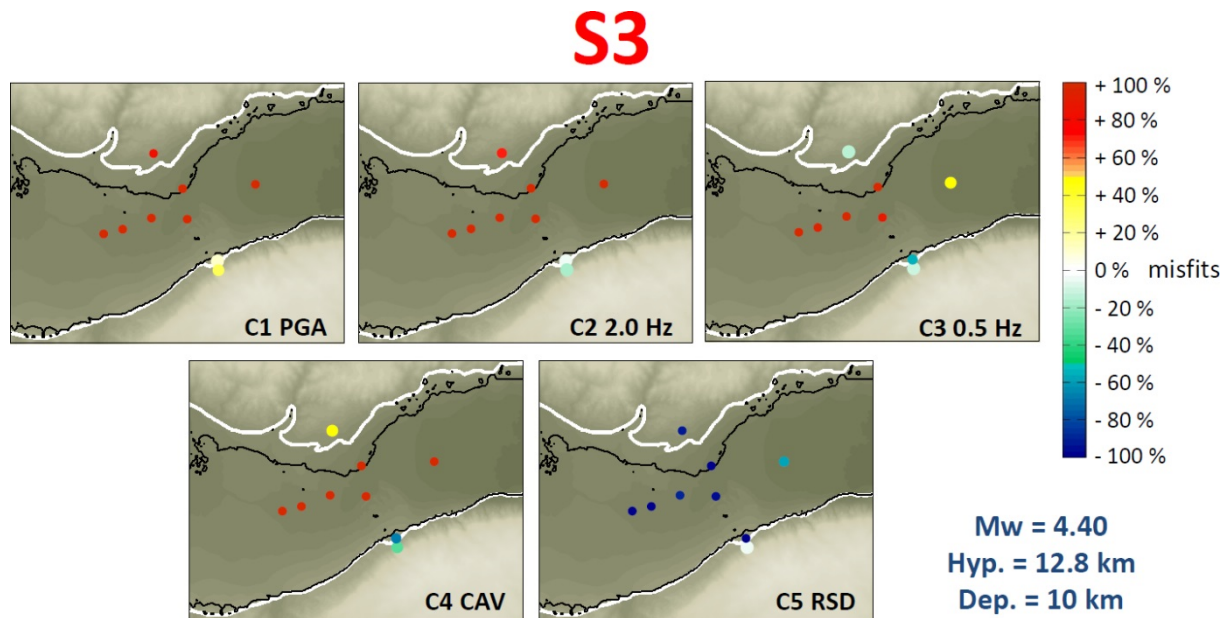
Figure 22 : Same as Figure 20 for event S3.

S4
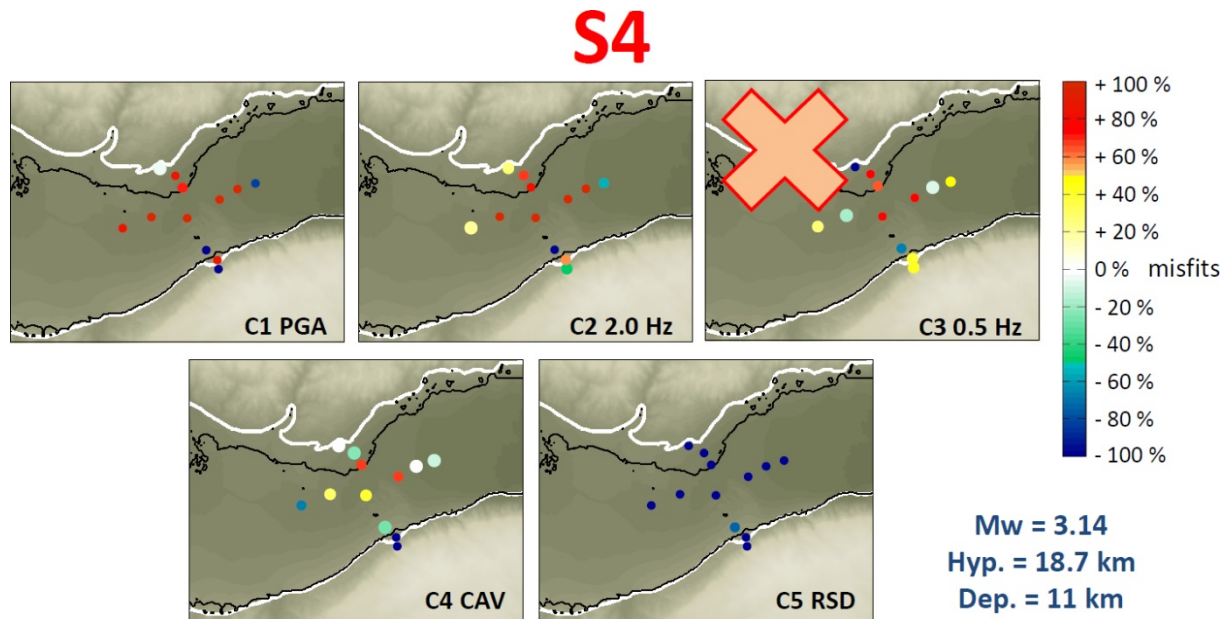
Figure 23 : Same as Figure 20 for event S4.

S5
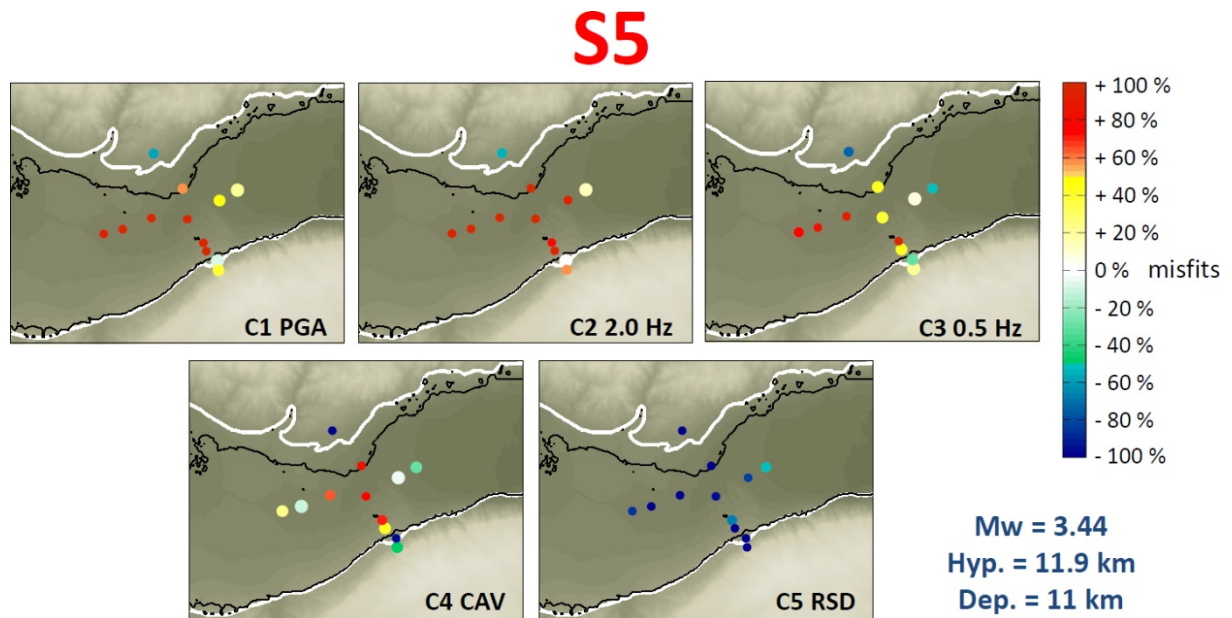
Figure 24 : Same as Figure 20 for event S5.
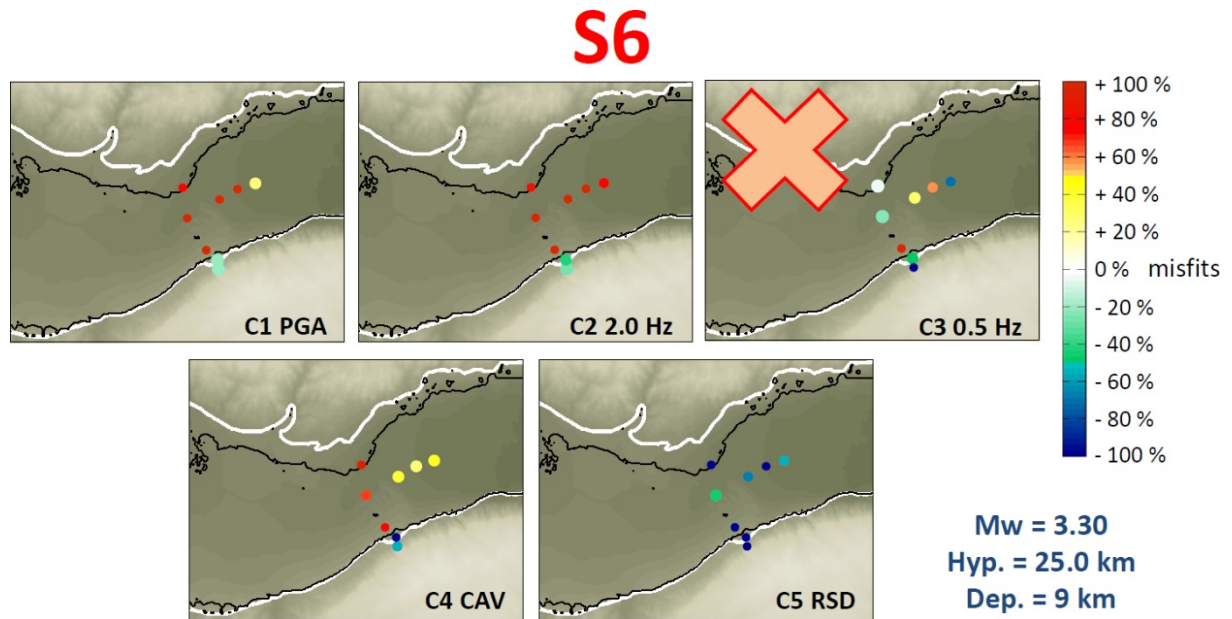
Figure 25 : Same as Figure 20 for event S6.
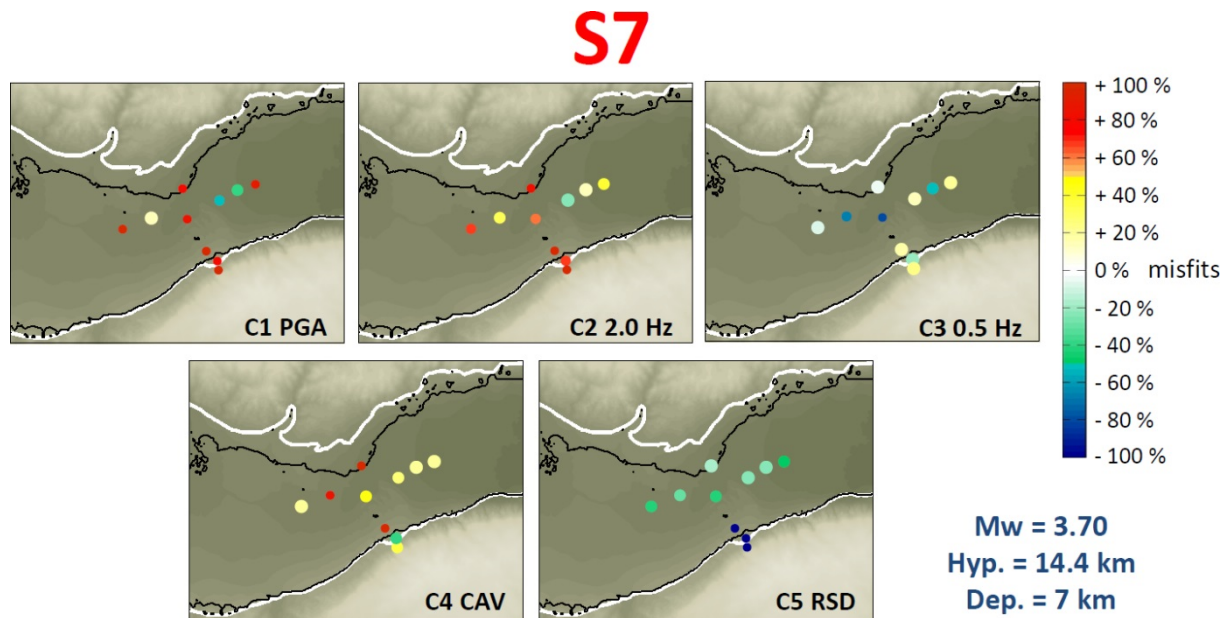
Figure 26 : Same as Figure 20 for event S7.
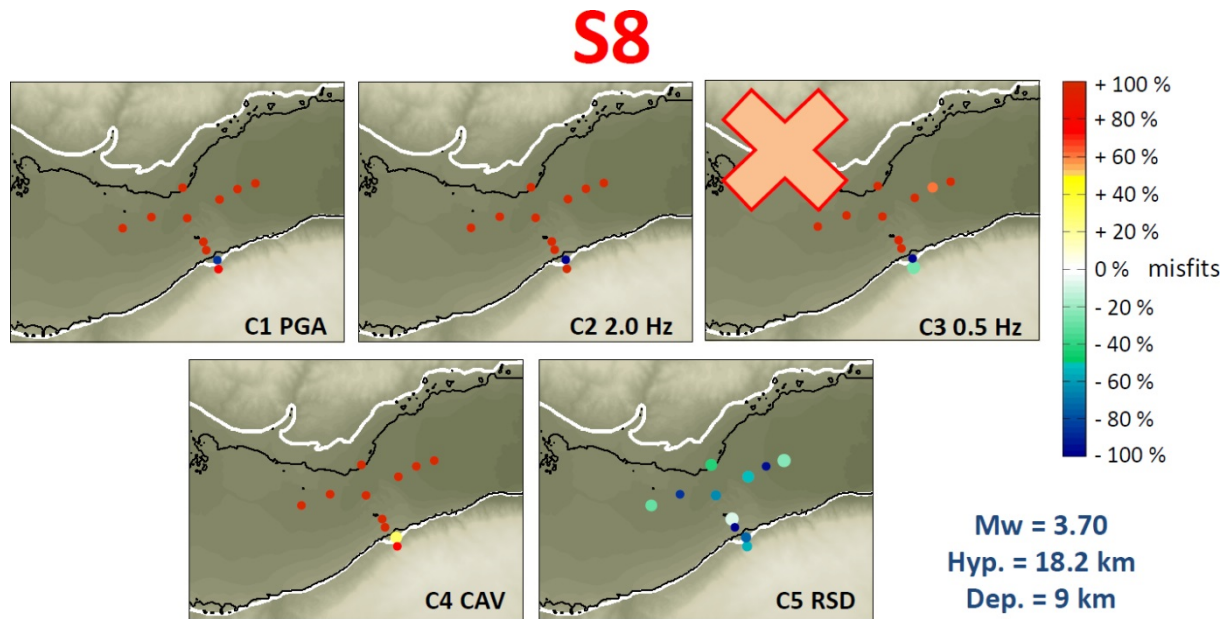
Figure 27 : Same as Figure 20 for event S8.
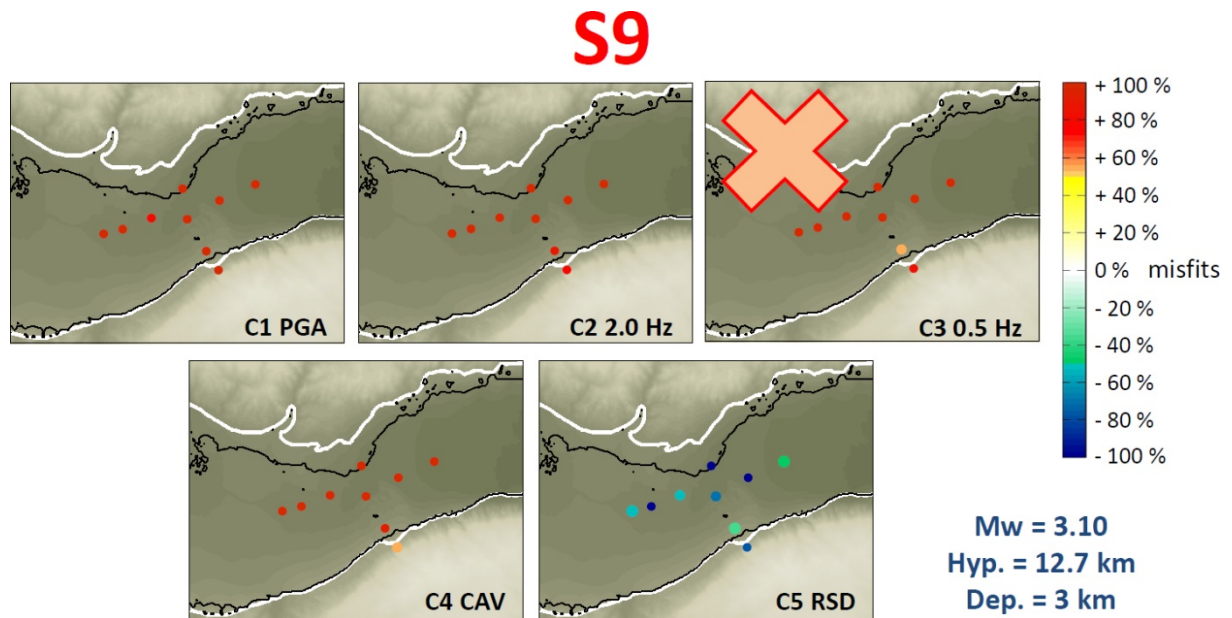
Figure 28 : Same as Figure 20 for event S9.

S10
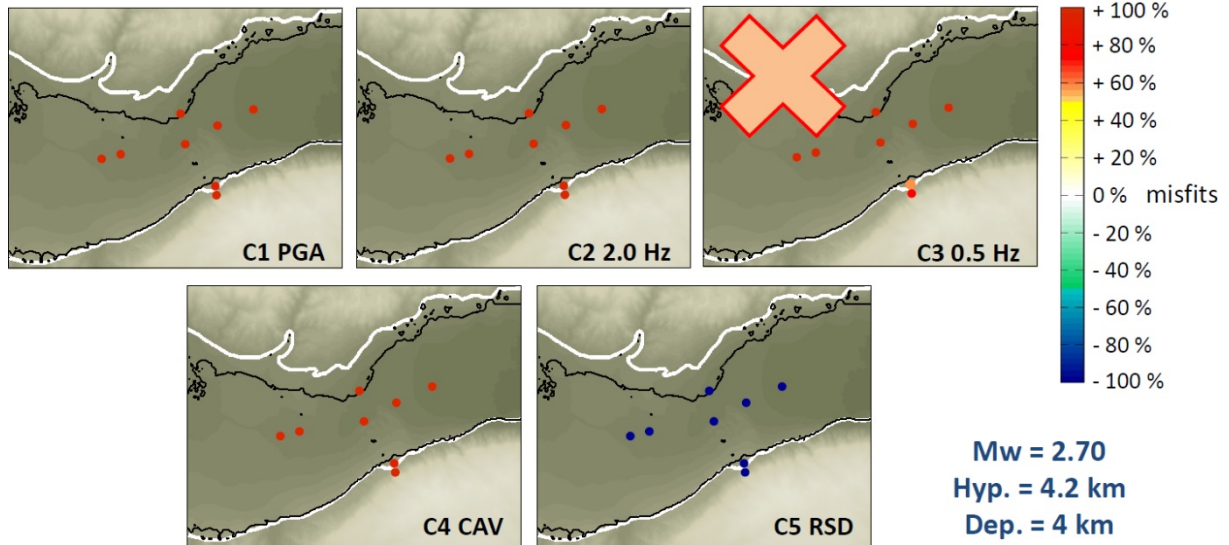
Figure 29 : Same as Figure 20 for event S10.

S11
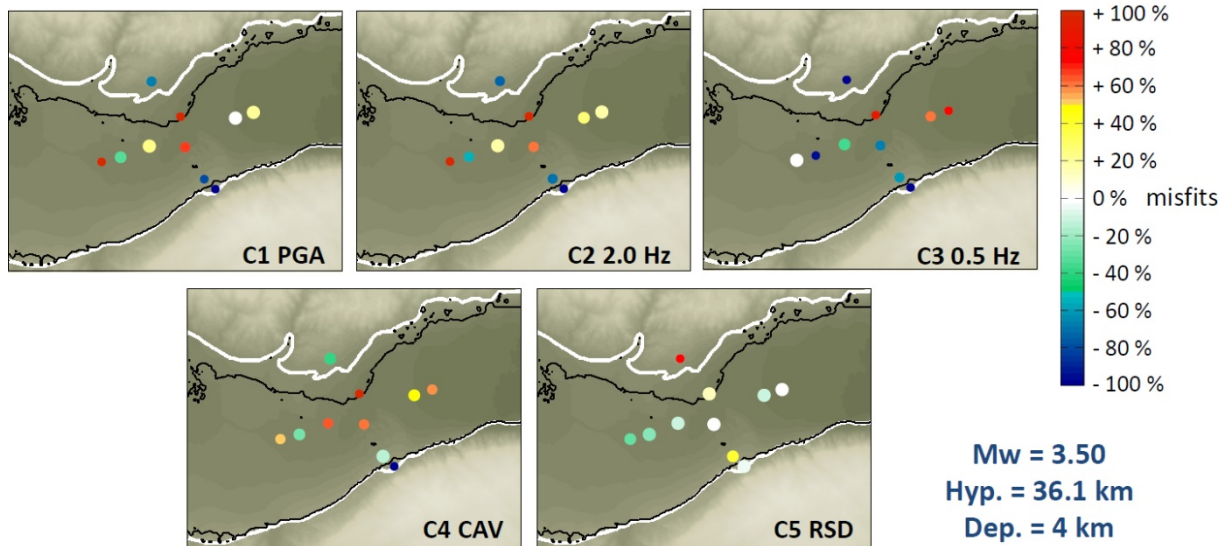
Figure 30 : Same as Figure 20 for event S11.

S12
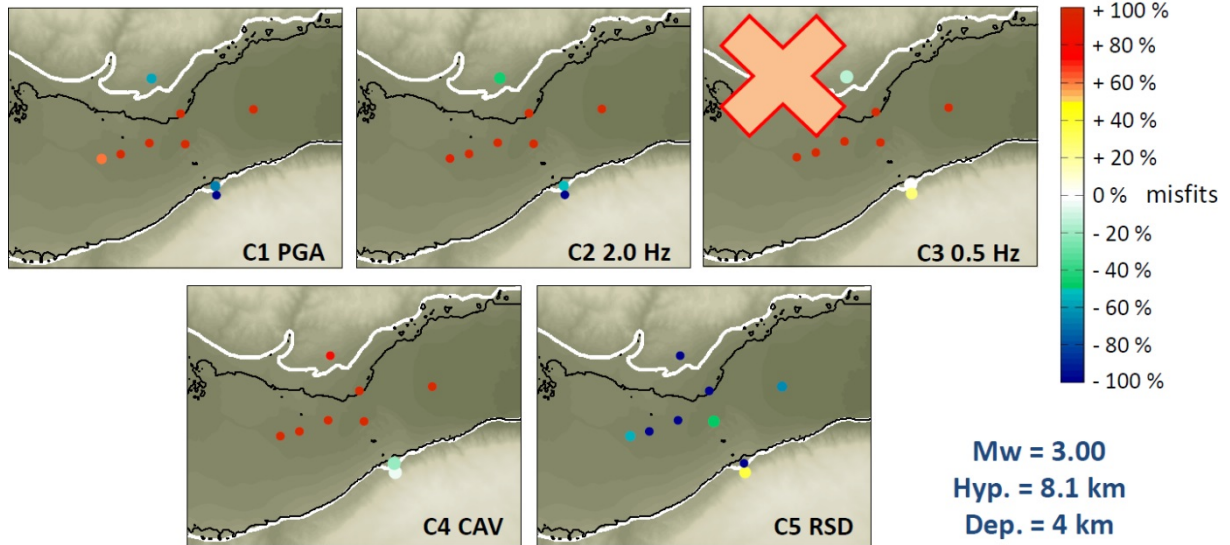
Figure 31 : Same as Figure 20 for event S12.

S13
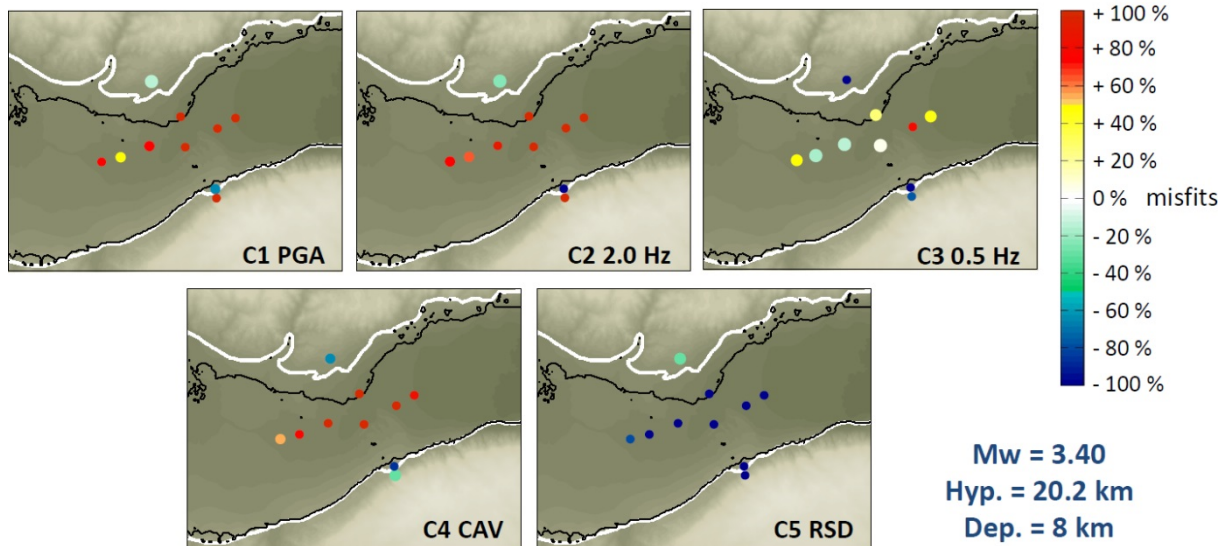
Figure 32 : Same as Figure 20 for event S13.

S14
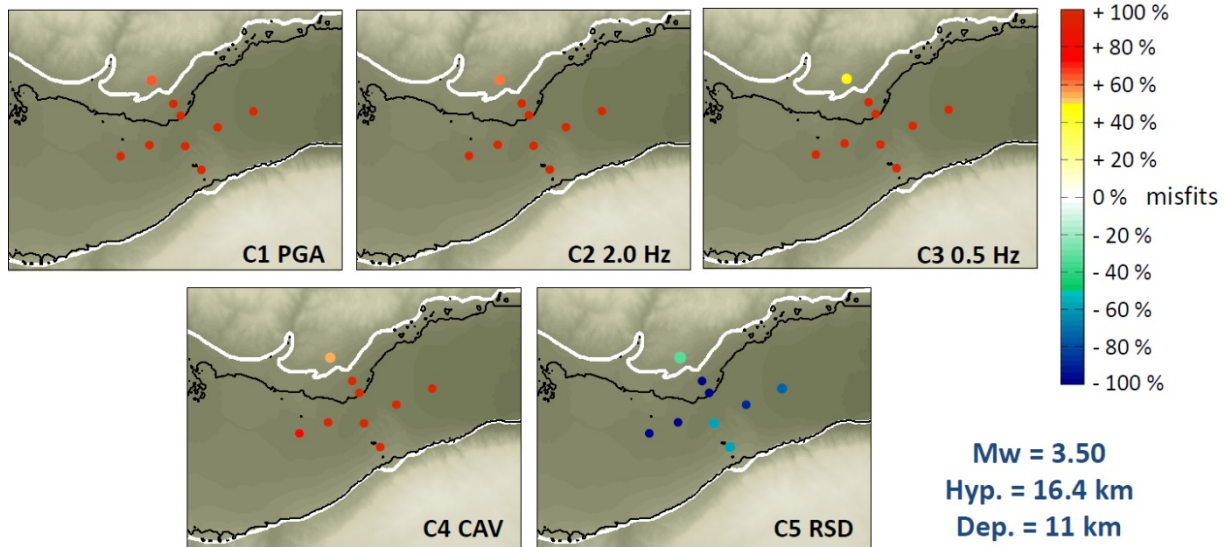
Figure 33 : Same as Figure 20 for event S14.

S15
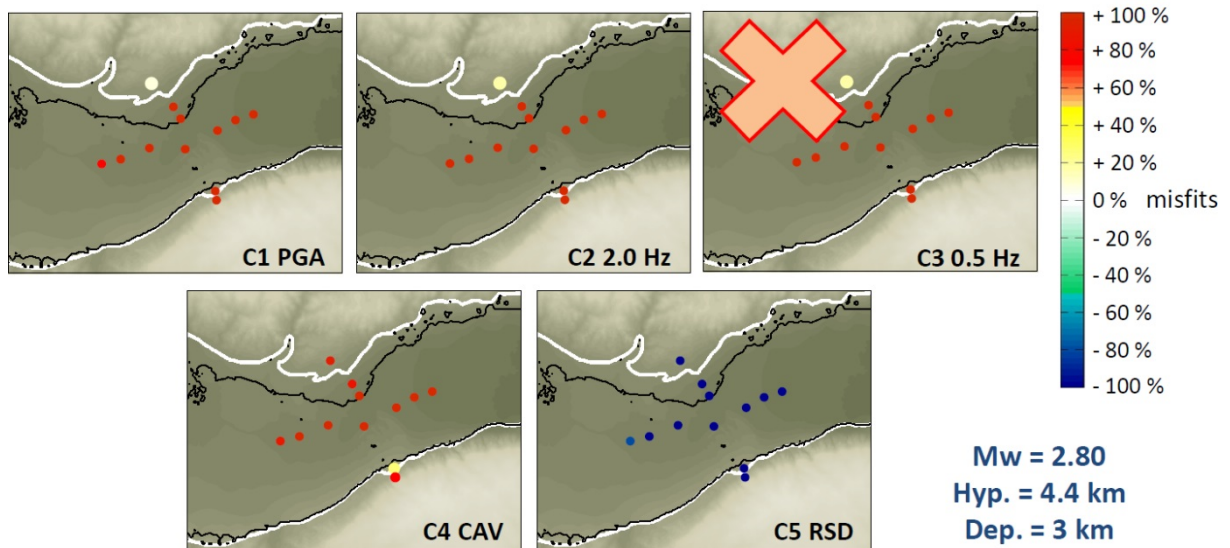
Figure 34 : Same as Figure 20 for event S15.

S16

Mw = 2.90
Hyp. = 15.3 km
Dep. = 9 km
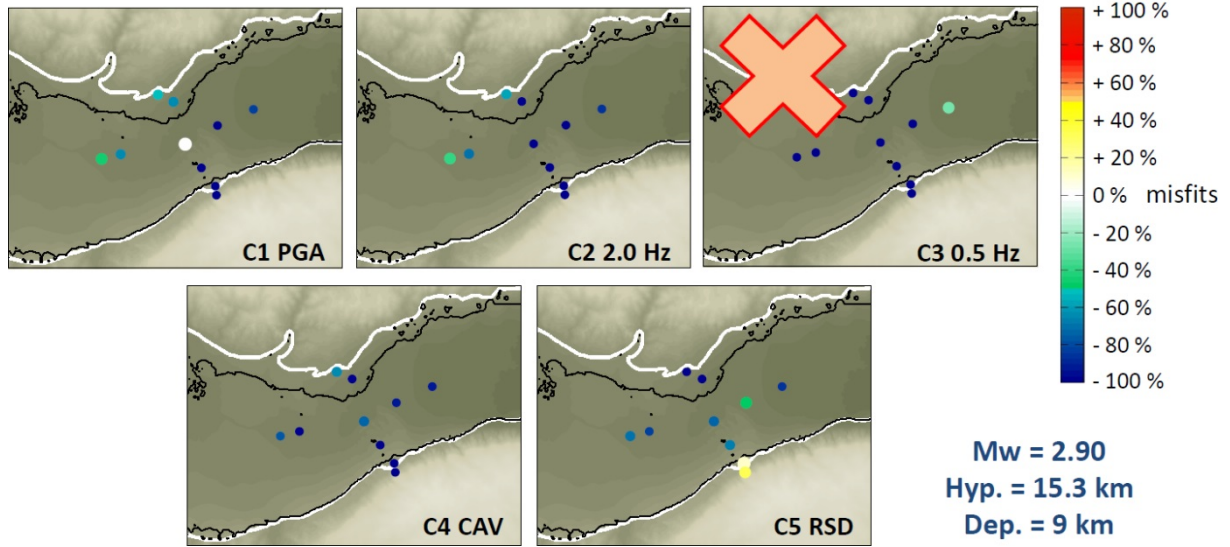
Figure 35 : Same as Figure 20 for event S16.

S17

Mw = 3.40
Hyp. = 13.1 km
Dep. = 10 km
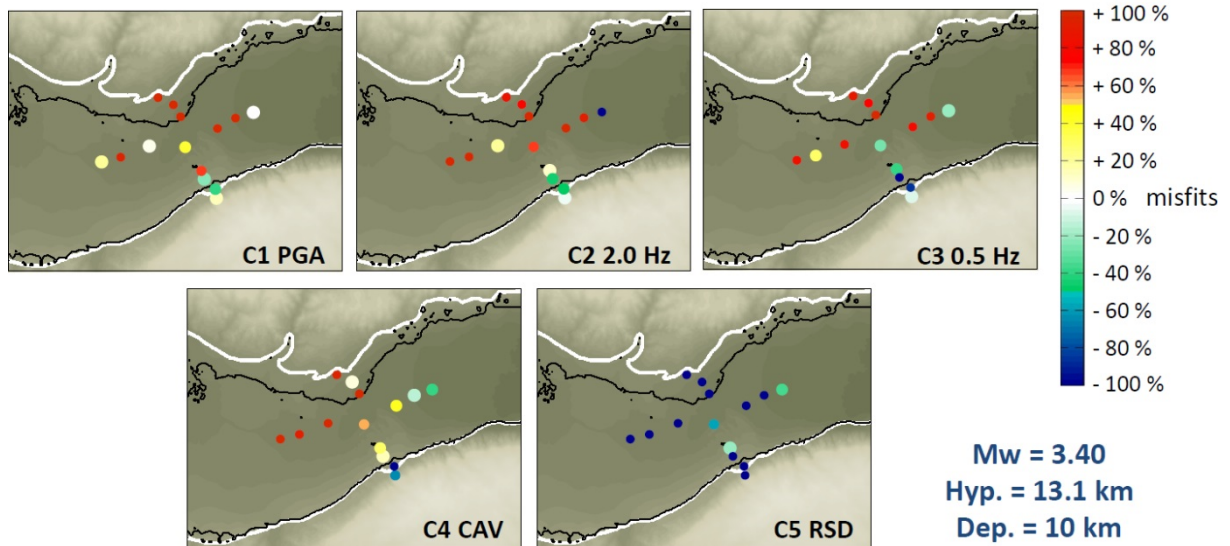
Figure 36 : Same as Figure 20 for event S17.

S18
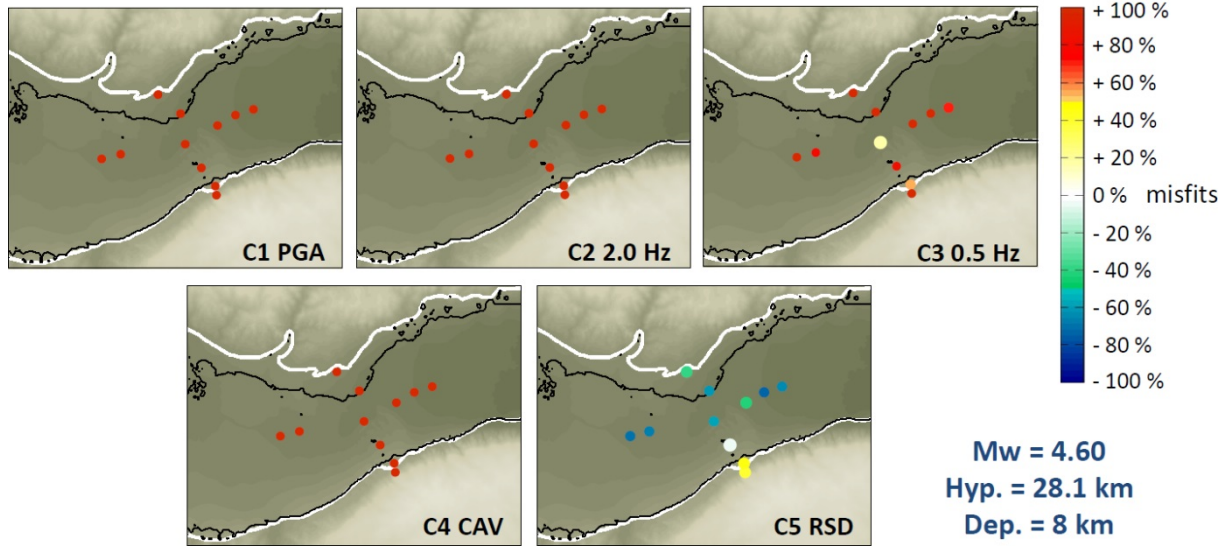
Figure 37 : Same as Figure 20 for event S18.

S19
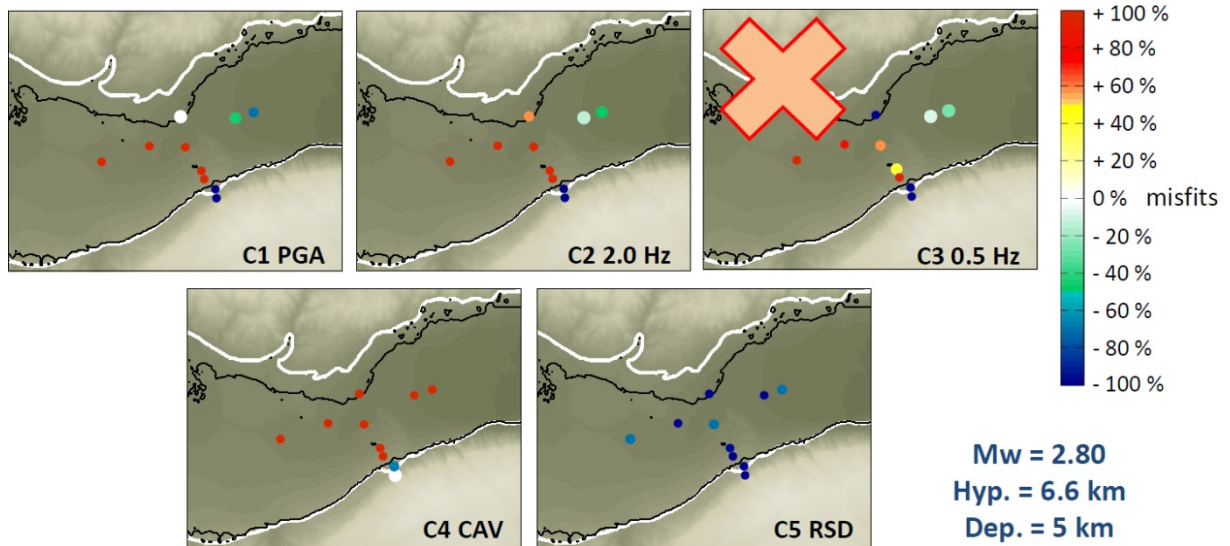
Figure 38 : Same as Figure 20 for event S19.

The worst validation results are obtained for events S10 and S15 (Figure 29 and Figure 34, respectively), both cases strongly over-estimated by the numerical prediction, even if misfits on C1 and C2 are low at PRO for event S15. It is noticeable that those two events have the lowest magnitudes of all selected events (Mw = 2.7 and 2.8, respectively), together with the shortest hypocentral distances to TST (4.2 and 4.4 km, respectively) and shallowest depths (4 and 3 km, respectively). The combination of these source characteristics appears to considerably affect the validation misfits. In the next section, a numerical study of the robustness of the site-effect estimation related to source parameters is performed: this study demonstrates that shallow seismic events being closed to the considered site are the most sensitive to uncertainties in hypocenter location, and consequently are not the best candidates for a validation exercise. Low-magnitude events might also be prone to higher magnitude uncertainties that impact the validation exercise.

Some satisfactory validation results are observed at low frequencies (criterion C3) for events S1, S5 and S13, and at more criteria for events S7, S11 and S17. However concerning event S11, rock site PRO shows a strong under-estimation of the ground motion, and therefore of the incoming wavefield, which potentially explains the low misfits at soil sites due to some compensation of the over-estimation in the basin (this is also the case for S13 at low frequencies).

The validation exercise performed on the E2VP evaluation criteria, which are measures of absolute ground-motion parameters, is a difficult task due to the high sensitivity of the waveforms to cumulative uncertainties in source parameters, in crustal and regional propagations, and in the local site effect. It remains difficult, when high misfit values occur, to distinguish the origin(s) of the discrepancies. The source parameters and the propagation model at all scales (crustal, regional and local) have to be all precisely estimated for an accurate numerical prediction of the absolute ground motion. If one is only concerned by the prediction of the local site effect, an estimation based on relative criteria might be an interesting option.

4.4.3   Hybrid time histories computed at the center of the basin

Following the procedure of the first validation phase (Maufroy et al., 2014, in Appendix 2), "hybrid" time histories are computed to further investigate the ability of the numerical predictions to predict the site-effect component of the ground motion. Hybrid time histories combine the recorded signal at TST5 (real input holding actual source parameters) with the site-effect part coming from the simulation (synthetic borehole-surface transfer function) to compute the hybrid ground motion at soil site TST0. This way the hybrid time histories maximize the impact of numerical estimate of site-effect component and minimize the effect of uncertainties in source description or in crustal propagation.

Table 6 summarizes the validation misfits obtained with the 5 criteria when comparing actual recordings with full synthetics and with hybrid time histories computed at TST0. The results are only available for the events that were recorded both at TST0 and TST5. Performing hybrid time histories allows compensating potential uncertainties in source parameters. This procedure does not improve the fit between recordings and their numerical predictions on the total energy of the signal (C4) and on its duration (C5). However it greatly helps to improve the fit on the amplitude-frequency criteria C1 to C3.

The misfit values obtained on criteria C1, C2 and C3 for the hybrid time histories are significantly lower than for the full synthetics, being in absolute value closed to the values obtained in validation phase 1 (see Figure 14 in Maufroy et al., 2014, in Appendix 2). The typical average misfit values encountered in phase 1 for hybrids were ranging from -20% to -50%. In the second phase, the corresponding average values equal 27%, 29% and 1% on C1, C2 and C3 respectively. However, when not taking into account events S10 and S15 (identified as being bad candidates for validation due to their proximity and low magnitude), those values decrease to 19%, 16% and -22% on C1, C2 and C3 respectively (–48% on C3

when considering only events with signal-to-noise ratio greater than 3). This represents a general improvement of the validation results on the site-effect component.

One important change from validation phase 1 to phase 2, is that the site-effect component was globally under-estimated in phase 1 (negative average misfit values for hybrid time histories at TST0), while it is now mostly over-estimated in phase 2 (positive average misfit values on C1 and C2). This point is further analyzed in the following, where we compare various TST0/TST5 Standard Spectral Ratios (SSR) obtained from different recorded or synthetic datasets.

At last, one may also notice the change from an almost-systematic under-estimation of signal duration (criterion C5) by the full synthetics to an almost-systematic over-estimation by the hybrid time histories. This is another indication in favor of an under-estimation of the damping value within the sediments.

Table 6: *Values of horizontal misfits on the E2VP evaluation criteria between the actual recordings at central soil site TST0 and their numerical predictions. Values in % evaluate the predictions by full synthetics vs. hybrid time histories (see text). For each criterion the average is computed over the 16 events that were recorded both at TST0 and TST5, and over 14 events (deleting S10 and S15 that give anomalously-high misfits).*

	FULL SYN.	HYBRIDS	FULL SYN.	HYBRIDS	FULL SYN.	HYBRIDS	FULL SYN.	HYBRIDS	FULL SYN.	HYBRIDS
	C1	**C1**	**C2**	**C2**	**C3**	**C3**	**C4**	**C4**	**C5**	**C5**
S1	154	10	129	11	27	-58	196	72	-39	92
S3	177	19	186	39	89	-48	156	13	-93	-63
S4	142	62	128	84	78	52	42	95	-169	-6
S5	147	32	166	35	40	-12	76	-4	-93	1
S6	128	81	117	104	-22	106	68	198	-44	98
S7	87	-24	63	-19	-77	-90	47	25	-41	64
S8	130	12	173	12	156	-73	192	62	-61	47
S9	186	-3	192	20	164	15	152	34	-70	27
S10	471	75	506	98	431	203	365	94	-205	101
S11	68	35	63	32	-65	4	61	66	4	47
S12	201	5	201	29	136	-72	146	-16	-48	-26
S13	243	46	153	-47	5	-134	123	-12	-109	-19
S14	234	2	214	-5	188	-1	184	-15	-57	15
S15	310	92	338	134	262	129	253	114	-102	29
S16	2	9	-119	-120	-143	-17	-72	31	-71	47
S19	99	-15	139	50	58	19	126	146	-69	53
AVERAGE	**173**	**27**	**166**	**29**	**83**	**1**	**132**	**56**	**-79**	**32**
AVERAGE without S10 S15	143	19	129	16	45	-22	107	50	-69	27

4.4.4 Comparison of TST0/TST5 SSR from various recorded and synthetic datasets

Another way to evaluate the capability of the numerical simulations to predict the site-effect component is to compare the TST0/TST5 SSR from actual recordings with the predicted ones. The SSR obtained from 3 real datasets are compared in Figure 39: the "HC" dataset is the most complete one currently available, including 21 events both recorded at TST0 and TST5; the median SSR from this dataset

(black line with variability shown in gray) is compared to the median SSR from the 5 real events selected in E2VP1 (dashed red line) and to the median SSR from the 16 real events selected in E2VP2 (solid red line). This figure shows that, depending on the events included in the computation of the SSR, the obtained spectral ratio can vary significantly: the amplifications at fundamental resonance and overtones stay consistent both in frequency and amplification level, but a strong variability of the median SSR occurs in-between (although it remains inside the variability estimated from the most complete dataset). That effect, due to the variable contribution of the surface waves propagating in the basin, is clearly observable around 1 Hz. It is also noteworthy that, at this frequency, the real SSR from E2VP1 selection gives a much higher ratio than from the E2VP2 selection.
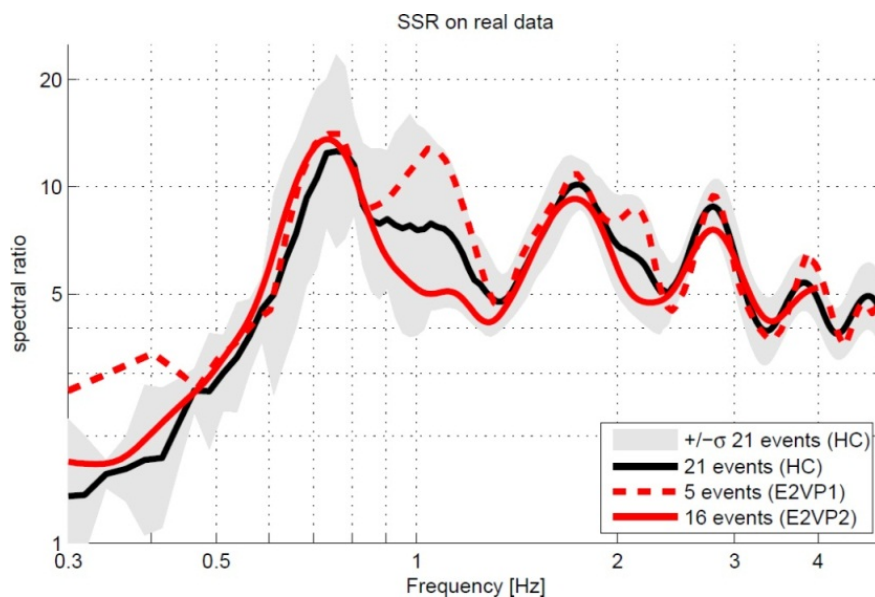
Figure 39: Median of SSR (Standard Spectral Ratios) at TST0 with TST5 as the reference station, computed for the actual recordings of 21 events (black line, associated variability shown in gray), for the 5 events selected in E2VP1 (dashed red line) and for 16 events selected in E2VP2 (solid red line), that were recorded both at TST0 and TST5.

The SSR results from validation phase 1 are recalled in Figure 40 (red line for median SSR from actual recordings and blue line for the corresponding numerically-predicted SSR). This figure confirms that the site-effect component was globally under-estimated by the synthetics in phase 1 of E2VP, although the real SSR computed on only 5 events rather stands in the highest part of the site-effect variability (Figure 39). The SSR results obtained for validation phase 2 are shown in Figure 41 with the associated variability on the 16 events considered. Now the site-effect component appears globally over-estimated in the new model of the Mygdonian basin, but it is slightly weaker than the under-estimation in E2VP1 (as shown previously by the misfits on evaluation criteria for the hybrid time histories). The misfit values in E2VP2 obtained on the three amplitude-frequency criteria (from hybrids: 19%, 16% and -22% on C1, C2 and C3 respectively) are in total agreement with the SSR results shown in Figure 41, where the site-effect is rather under-estimated in the lowest frequencies (C3, -22%, evaluates 0.375-0.750 Hz) and over-estimated above 0.8 Hz (C2, 16%, evaluates 1.5-3.0 Hz, and C1, 19%, the highest frequencies).

Those results must however be moderated by considering the variability of the actual SSR. The highest differences between actual and predicted SSR occur at the most variable frequencies, where the SSR estimates from recordings are highly dependent on the considered events. Indeed, around 1 Hz, there

is a significant over-estimation of SSR by the synthetics in Figure 41, but this over-estimation still remains inside the variability shown by the most-complete actual dataset of 21 events (gray area in Figure 39).

It is noteworthy that the results shown in Figure 41 also indicate some shift of the amplified frequencies in numerical predictions compared to recordings towards the higher frequencies. This effect didn't really occur in phase 1 (Figure 40) and is therefore imputed to the 3D structure of the new basin model in E2VP2. Several elements from the previous comparisons also tend to indicate a lack of attenuation in the new model, and this is surely at the origin of the global over-estimation of E2VP2 SSR by the synthetics (though we consider that the prediction of the site-effect component is already much satisfactory).
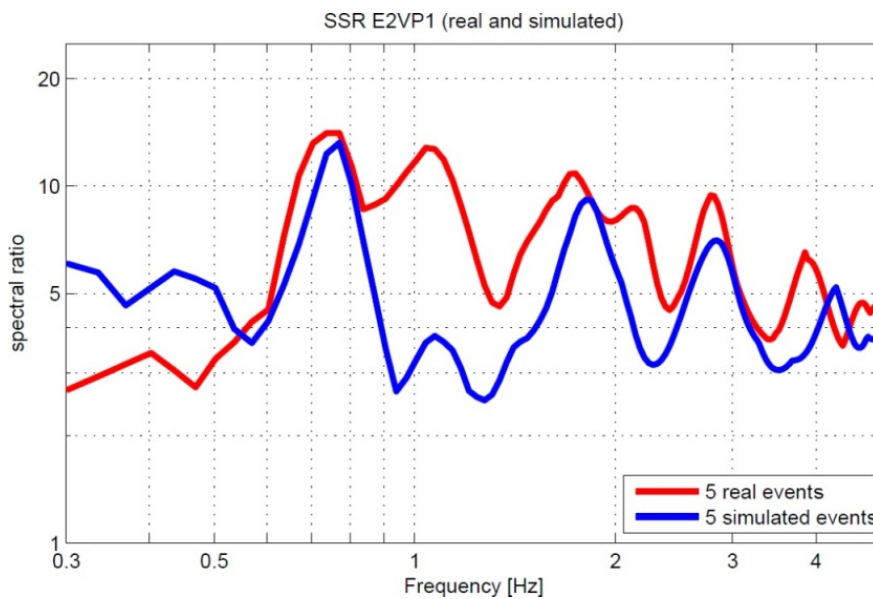
Figure 40 : Median of SSR (Standard Spectral Ratios) at TST0 with TST5 as the reference station, computed for the 5 events selected in E2VP1 where actual recordings (red line) were compared to their numerical predictions (blue line).
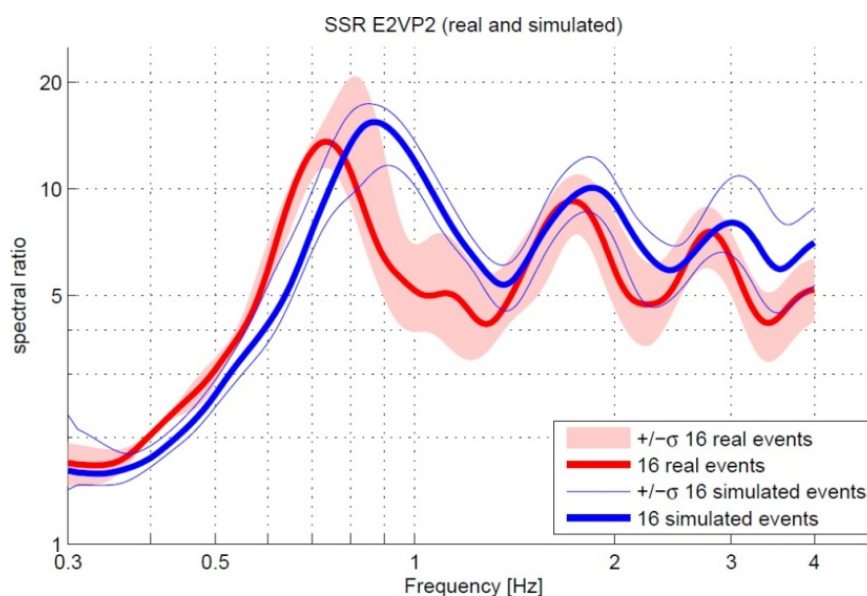
Figure 41:   Median of SSR (Standard Spectral Ratios) at TST0 with TST5 as the reference station, computed for 16 events selected in E2VP2 where actual recordings (bold red line, associated variability in light red) are compared to their numerical predictions (bold blue line, associated variability shown by thin blue lines).

4.4.5   Conclusions of validation phase 2

The validation exercise performed in phase 2 of E2VP shows a strong sensitivity of the validation results to the source parameters, to their variability and/or uncertainties. In the next section we perform a numerical analysis of the robustness of the site-effect estimation to the seismic source parameters. This exercise takes into account a large number of virtual seismic sources (1260) around the Mygdonian basin, eventually reduced to a realistic number (52 hypocenters being comparable to the events included in the real database; see next section for more details on that virtual database). Figure 42 and Figure 43 evaluate the capability of the new E2VP2 basin model to predict the site-effect component at TST0 from those 1260 virtual sources, reduced to 52 events, respectively. Those results (magenta lines) are superimposed to the actual SSR variability observed on 21 real events recorded both at TST0 and TST5 (gray area). The results are rather stable when considering 1260 or 52 events, and remain globally inside the actual SSR variability for most frequencies. However the numerical variability appears to be significantly shifted towards higher ratios above 3 Hz: it is interpreted as the consequence of a lack of attenuation in the new basin model. The frequency shift of the amplified peaks also has to be understood.

We also showed that the actual basin response is much complicated around 1 Hz: the impact of that element on the estimated SSR is strong, but it is also strong on the associated variability. The relation between the frequency-dependent variability in the Mygdonian basin and the considered seismic events is the object of current studies in E2VP.

The validation phase 2 also demonstrated that rock sites are important to calibrate the general amplitude level of the simulations compared to recordings, in order to validate the source parameters and the crustal/regional propagation. When those elements are not validated, the impact of their uncertainties strongly affects the validation results measured on absolute parameters of the ground motion. Any validation exercise would certainly benefit from a higher number of rock sites (more than 1 or 2) around the area of interest.

The use of relative parameters (SSR, hybrid time histories) to evaluate the numerical prediction of the isolated site-effect component proves to be essential in validation phase 2. The validation results on absolute ground-motion parameters helped to detect a lack of attenuation in the new basin model (a parameter that is not yet satisfactorily measured), together with the identification of few events still giving large anomalous misfits imputed to source uncertainties. The results on relative parameters however recognize a general improvement of the site-effect prediction at the center of the basin.
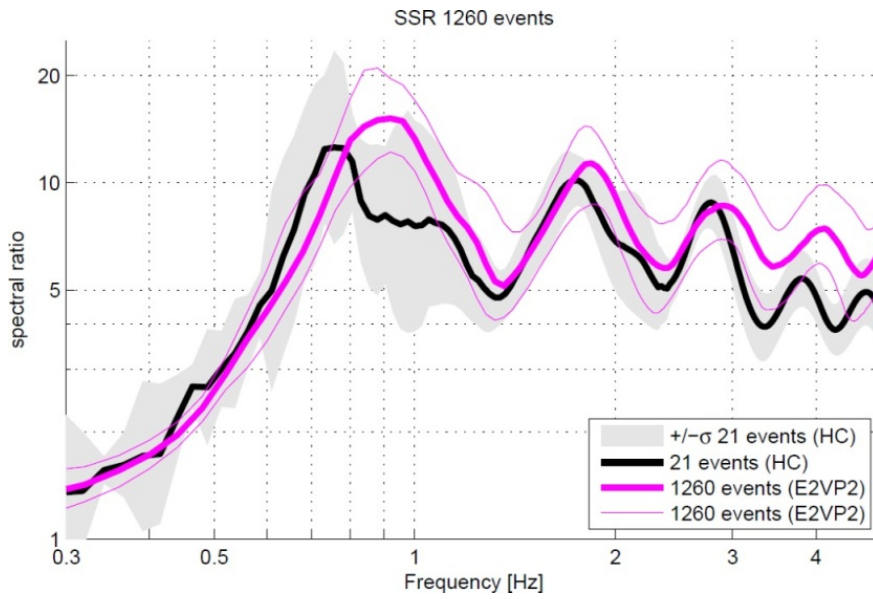
Figure 42: *Median of SSR (Standard Spectral Ratios) at TST0 with TST5 as the reference station, computed for the actual recordings of 21 events (black line, associated variability shown in gray) to be compared to the synthetic median obtained for the 1260 sources of the extended virtual dataset (bold magenta line, associated variability shown by thin magenta lines; see Section 6).*
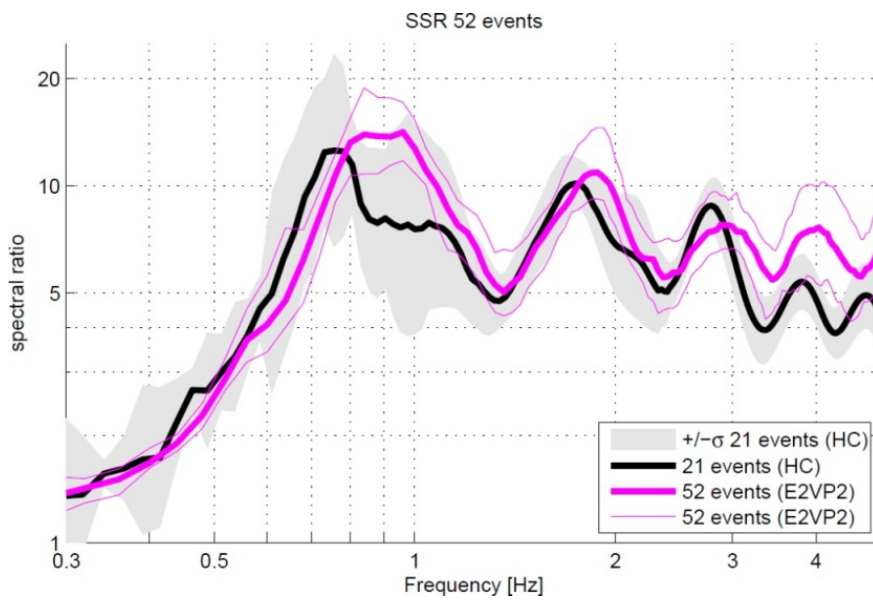
Figure 43: *Same as Figure 42, for the 52 sources of the real-catalog dataset (bold magenta line, associated variability shown by thin magenta lines; see Section 6).*

5   NUMERICAL STUDY OF SOURCE-RELATED VARIABILITY OF GROUND MOTION AND OF SITE-EFFECT ESTIMATION IN THE MYGDONIAN BASIN

We present the results of a numerical analysis of the robustness of the site-effect estimation and of the sensitivity of the earthquake ground motion to seismic source parameters, focusing on the Mygdonian basin. This exercise is performed in the new extended model of the basin (see Figure 44). The velocity model in the basin is defined by two linear gradients, one between the surface and the pre-Mygdonian/Mygdonian limit, and the second one down to the sediment-bedrock interface. The surface S-wave velocity is 137 m/s.

The 3D numerical simulations are performed with the SPECFEM3D code implementing the Spectral Element Method. They rely on a robust, semi-automated, mesh design strategy together with a simple homogenization procedure to define a smooth velocity model of the basin, allowing numerical accuracy for frequencies up to 4 Hz. The simulations include the effects of surface topography and of intrinsic attenuation.
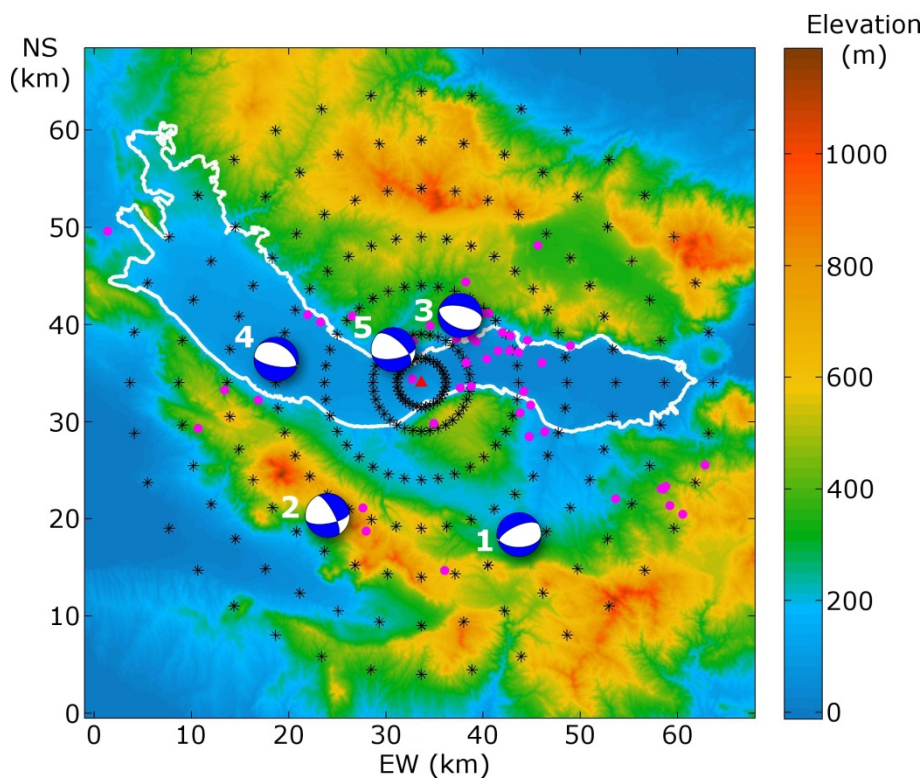
Figure 44:   Location of the Mygdonian basin (bold white line) related to the seismic sources considered in the numerical study. The response of the basin is computed to five real events (beachballs) and to 1260 sources considered in the reciprocity-based calculations (black circular crosses) at the central soil site TST indicated by the red triangle. The real catalog of local events is also shown by the magenta dots. Elevation is given in meter by the color scale.

5.1   GROUND-MOTION SYNTHETIC DATABASE

The synthetic results presented hereafter are obtained with reciprocity-based calculations where the ground motion due to many different seismic sources is computed at a few stations in the basin (central soil site TST0, corresponding borehole TST5 and northern rock site PRO).

The response of the basin is available for five real events (beachballs in Figure 44), which occurred in the last years. These events correspond to the first 5 selected events of the validation exercise (S1 to S5, see source parameters in Table 3). These events were well recorded by the Euroseistest accelerometric array which is centered on the TST site (red triangle in Figure 44). For each of the 5 real events, the basin response is computed for 125 point sources which hypocenters were shifted by +/- 1 km or +/- 2 km in the X, Y, Z directions around the original hypocenter. This setting allows investigating the sensitivity of the ground motion and of the site-effect estimation at TST to uncertainties in the hypocenter location.

The response of the basin was also computed for a circular setting of numerous point sources (circular crosses in Figure 44). We consider epicentral distances varying from 2.5 to 30 km, source depths from 1 to 15 km, and we span the range of possible back azimuths with a 10-degrees bin. Therefore the reciprocity-based calculations consider 1260 different source hypocenters. This second setting allows investigating the variability of the amplification caused by site effects, as measured by standard spectral ratios, due to the source characteristics.

The focal mechanism of each source in the circular setting is randomly generated in relationship with the typical mechanisms encountered around the Mygdonian basin, which commonly indicate normal faulting. Thus the random focal mechanisms in the synthetic database follow a Gaussian distribution around the corresponding values: strike = 86° ± 18°, dip = 52° ± 15°, rake = -101° ± 51°. This dataset is called "extended virtual" in the following.

A sub-dataset is derived from the complete one, decimating the number of included hypocenters so that their number (52) and locations closely match the real database of observed recordings at the Euroseistest. The exact locations of the real events (magenta dots in Figure 44) are only approximated in that sub-dataset, as only the hypocenters included in the circular setting can be considered (see the impact of that approximation in Figure 45). This sub-dataset is called "real catalog" in the following.
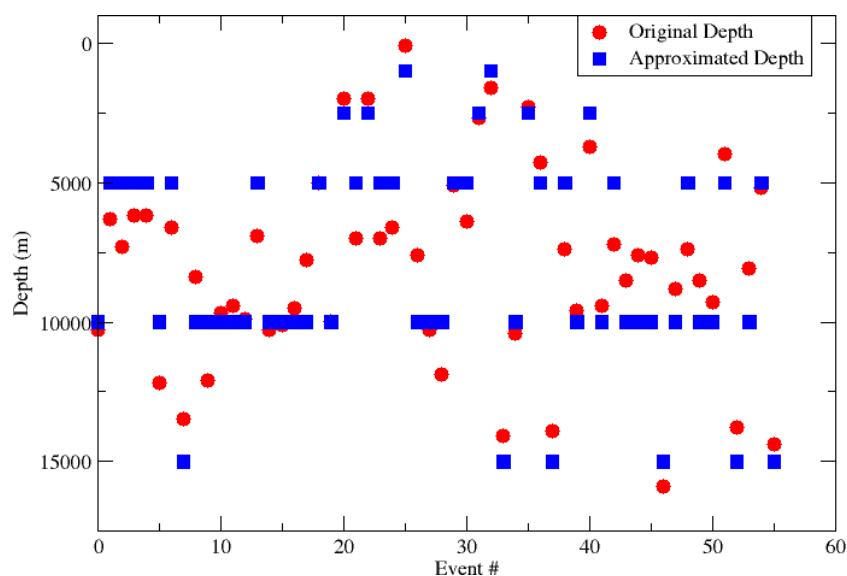
Figure 45:   Original depth of hypocenters from the catalog of local real events (red dots) approximated by the blue squares in the corresponding synthetic "real catalog" sub-dataset.

5.2 VARYING THE HYPOCENTERS OF 5 REAL EVENTS

Considering the 5 selected real events and the 125 point sources surrounding their hypocenter, the variability of the acceleration spectrum at TST0 and of the amplification measured by Standard Spectral Ratio (SSR, between TST0 surface and TST5 borehole) are shown for the most energetic horizontal component, in Figure 46 and Figure 47, respectively. Colors indicate the source depth from blue (shallow) to red (deep). The median spectrum and ratio are represented by the black bold line in the corresponding panel, while the 16% and 84% percentiles are shown by the lower and upper dashed lines, respectively.

Significant differences appear between the 5 sources scenarios. The acceleration spectrum appears more or less sensitive to the hypocenter uncertainty depending on the considered source: the y-scale of each panel being comparable, the acceleration spectra for events S2, S3 and S4 appear less variable than for events S1 and S5, in all considered frequencies (Figure 46). The largest variability of the acceleration spectrum due to hypocenter uncertainty is observed for event S5, that is a deep source (depth = 11 km) but the closest to the receiver (hypocentral distance = 12 km). The second largest impact of hypocenter uncertainty occurs for event S1, that is a shallow distant source (depth = 5 km, hypocentral distance = 19 km). The hypocenter uncertainty on the 3 other events induces much less variability of the computed ground motion at TST0.
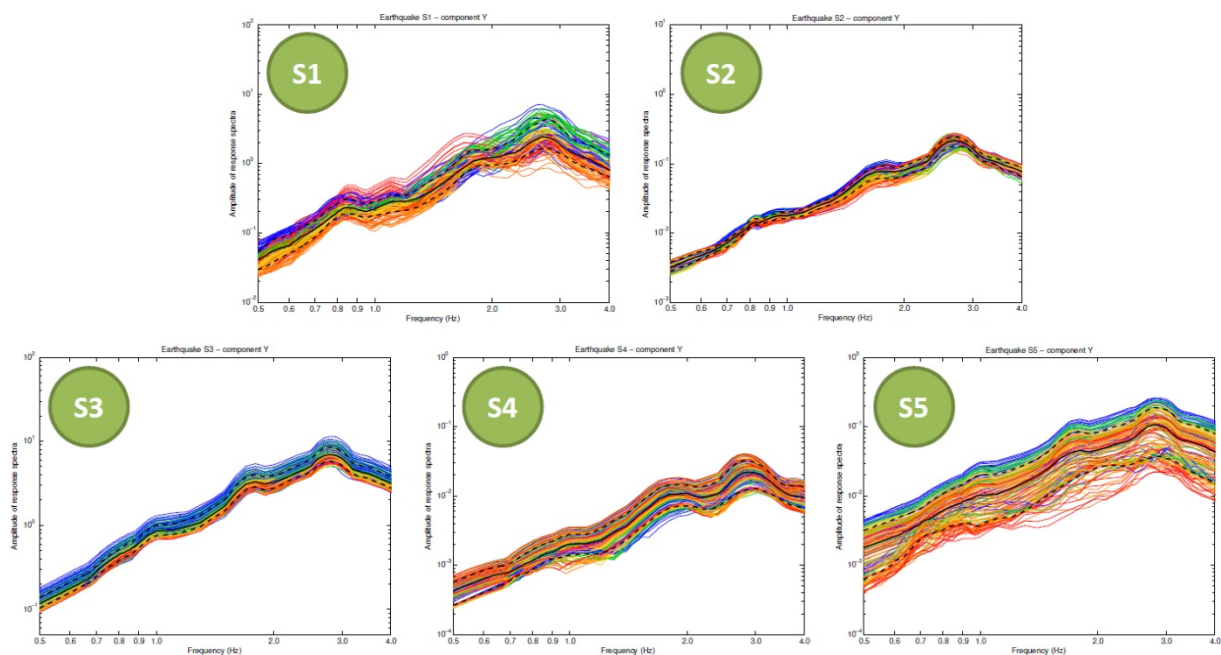
Figure 46: Acceleration spectra at TST0 computed for the 5 selected real events shown by beachballs in Figure 44. Variability of the acceleration spectra due to hypocenter uncertainty (see text) is indicated by the colored lines, from blue (shallower hypocenter) to red (deeper hypocenter). The median spectrum is given in each panel by the solid black line, surrounded by the upper (84%) and lower (16%) percentiles as dashed lines.

The amplification factor at surface soil site TST0 measured by SSR with TST5 as the reference station shows a similar sensitivity to the hypocenter uncertainty depending on the seismic event (Figure 47). The SSR are more variable for events S1 and S5, and less variable for events S2, S3 and S4. The same is also observed when northern rock site PRO is used as the reference station (Figure 48).

The computed ground motion at TST0 and the related site-effect estimation logically appear more sensitive to hypocenter uncertainty when the source is closer to the receiver. But these results also demonstrate that the sensitivity can be as high when the source is distant but very shallow. As a consequence, an important recommendation for the validation exercise is to remain cautious when comparing recordings and their numerical predictions for events located close to the array, but also for more distant (though still local) shallow events, as they can potentially give bad validation scores for a slight error on the hypocenter location.

5.3 SENSITIVITY OF THE BASIN RESPONSE TO THE SOURCE VARIABILITY AND ROBUSTNESS OF THE AMPLIFICATION ESTIMATE

The previous exercise revealed that the amplification estimate shows some amount of variability related to the hypocenter location. Indeed a small variation of hypocenter location can potentially induce large differences in the level of amplification, but when comparing the various SSR obtained for the 5 sources, differences in the frequency peaks that are amplified also appear from one source to another. The following exercise aims at quantifying the level of variability reached on the amplification estimate for a large amount of sources around the target station.

The basin response at the TST0 station (red triangle in Figure 44) is computed for 1260 point sources located at epicentral distances 2.5, 5, 10, 15, 20, 25 and 30 km, and at depths (relative to sea level) 1, 2.5, 5, 10 and 15 km. These 1260 sources are therefore distributed on 35 circles, each of these circles including 36 point sources at same distance and depth, but with different back azimuths (10-degrees bin). The focal mechanisms of these sources follow a Gaussian distribution around values corresponding to the average regional mechanism (normal faulting).
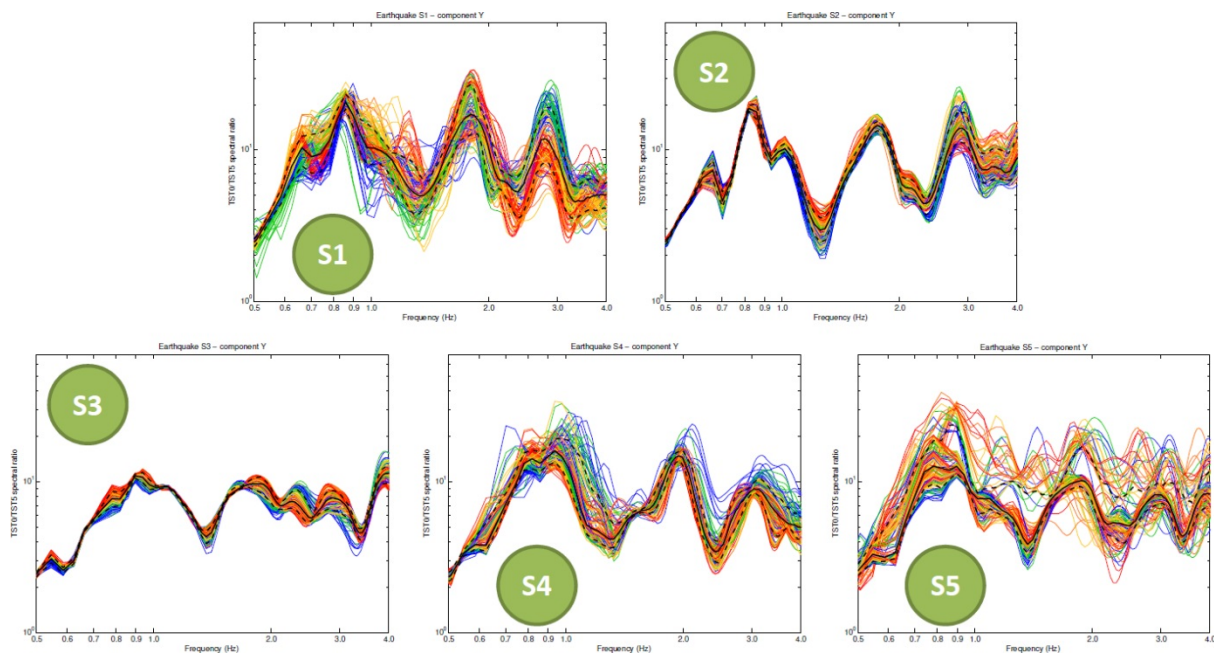
Figure 47: Standard Spectral Ratio at TST0 with TST5 as the reference station, computed for the 5 selected real events shown by beachballs in Figure 44. Variability of the spectral ratio due to hypocenter uncertainty (see text) is indicated by the colored lines, from blue (shallower hypocenter) to red (deeper hypocenter). The median ratio is given in each panel by the solid black line, surrounded by the upper (84%) and lower (16%) percentiles as dashed lines.
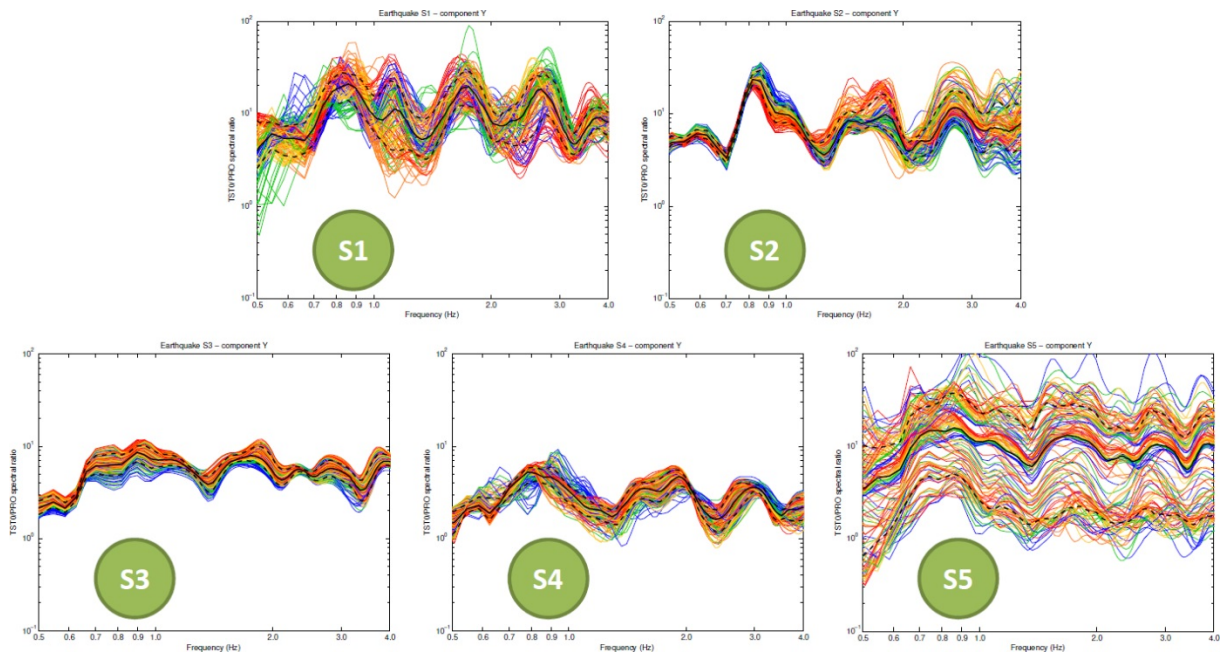
Figure 48:   Same as Figure 47 with northern rock site PRO as the reference station.

We compute the median PGA and duration for each circle of sources, together with the associated standard deviation on the log values. Figure 49 shows the evolution with epicentral distance of the median PGA for the 3 considered stations. The curves are gathered by source depth values. The expected influence of source distance and depth over the PGA is clearly observable at every station, with a global level of PGA much higher for soil site TST0 due to site effect compared to borehole site TST5 and rock site PRO.

Figure 50 shows the evolution obtained for the standard deviation of log PGA. No tendency appears with source distance or depth. The level of variability is comparable (around 0.18) for both stations TST0 and TST5. However a higher level of variability is observed at rock site PRO (around 0.21). No soil effect is present at PRO in the numerical simulations; therefore there must be another explanation for that increase of variability. The circular setting of the sources is centered on the TST site, but the PRO site is located 2.5 km northward. This could have an influence on the variability values for the closest sources (indeed it is noticeable in Figure 50), though one could expect that it becomes of minor importance for the farthest sources. The standard deviation of log PGA remains slightly higher at PRO even for the distant sources (around 0.20). Topography could explain part of that increase in variability at PRO (Maufroy et al., 2014, showed that an increase of 0.1 in standard deviation of log PGA in comparable frequencies could be explained by source-site interaction at topographic rock sites), but further analyses are required to explore this hypothesis.

The same analysis is performed considering the signal duration at the 3 sites, as shown in Figure 51. The increase of duration with distance is clearly observable at stations TST5 and PRO, associated to another increase of duration due to shallow sources compared to deep ones. However this tendency totally disappears at TST0, where the signal duration appears to be almost-exclusively controlled by the local basin response rather than source distance.

Figure 52 shows the evolution obtained for the standard deviation of log duration. Again the tendency observed at TST0 is different than the one observed at the two other sites. There is only a weak variability of duration at soil site TST0 that is not related to source distance or depth. Even if that variability is also not related to source distance or depth at the two other sites, the amount of duration variability is much

higher at both borehole site TST5 and rock site PRO. This larger variability on log scale is probably related to the significantly shorter duration at rock sites.
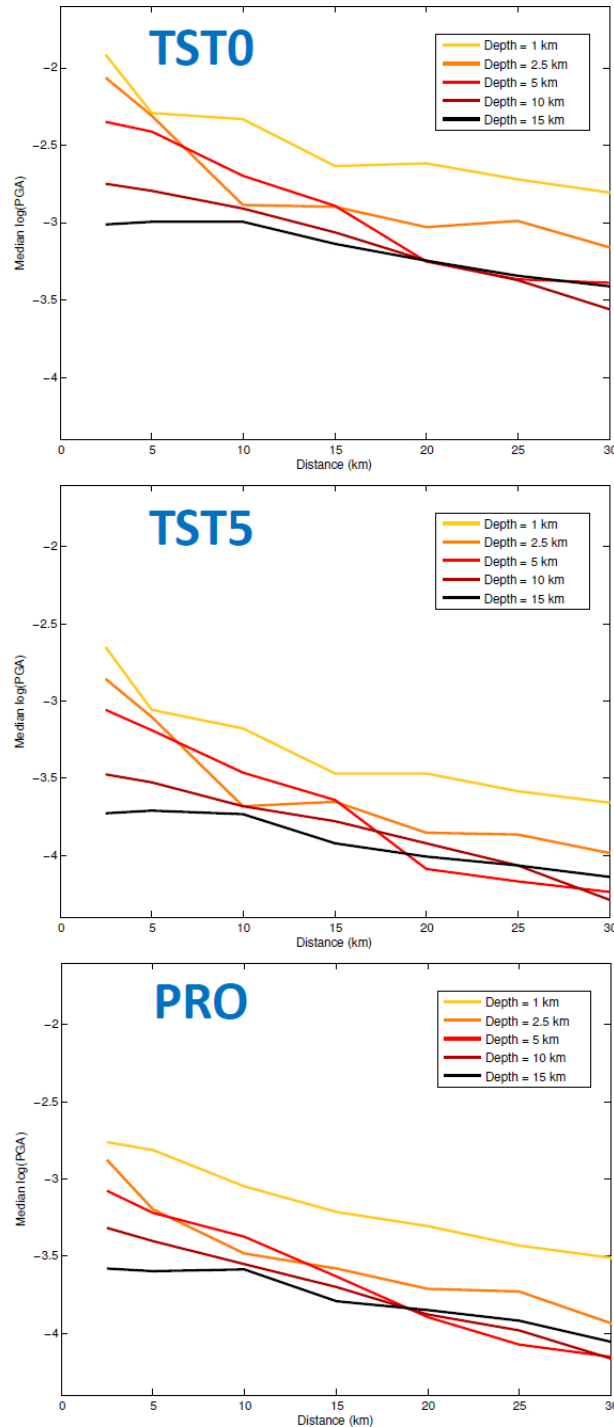
Figure 49:   Evolution with the epicentral distance of the median PGA (log_{10} of m/s²) for the 3 stations considered in this study. The curves are gathered by source depth values (colors).
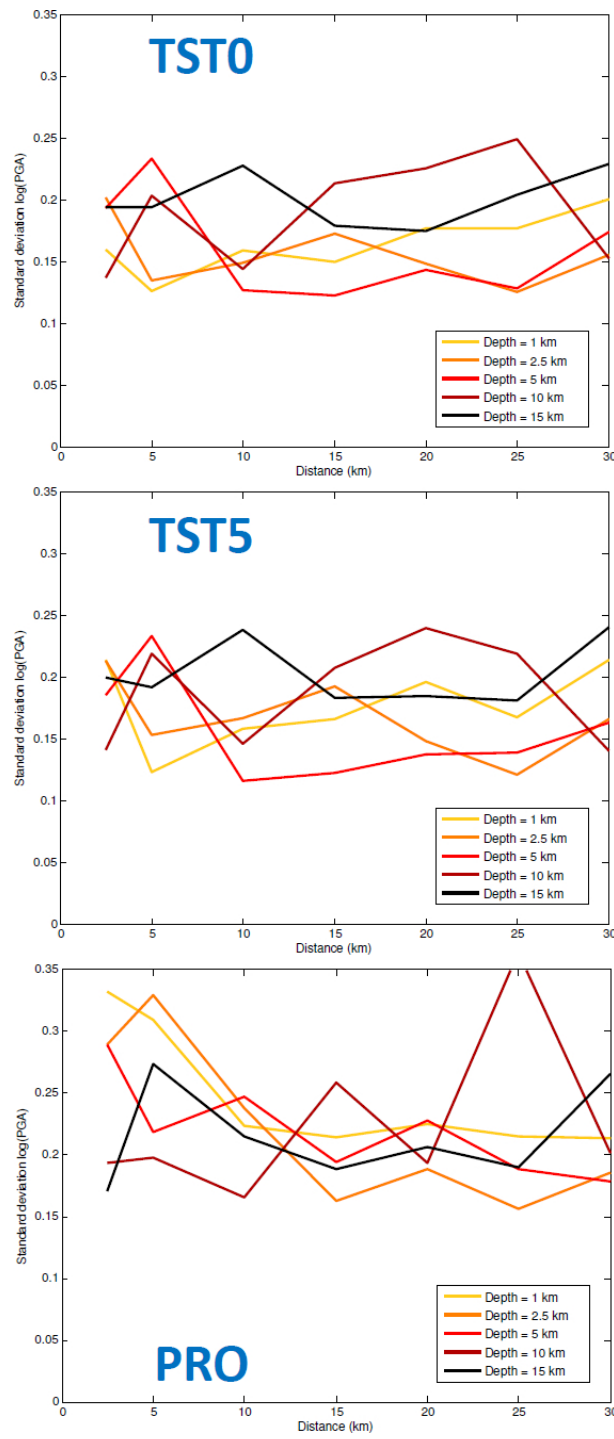
Figure 50:   Same as Figure 49 for the standard deviation of log_{10} PGA.
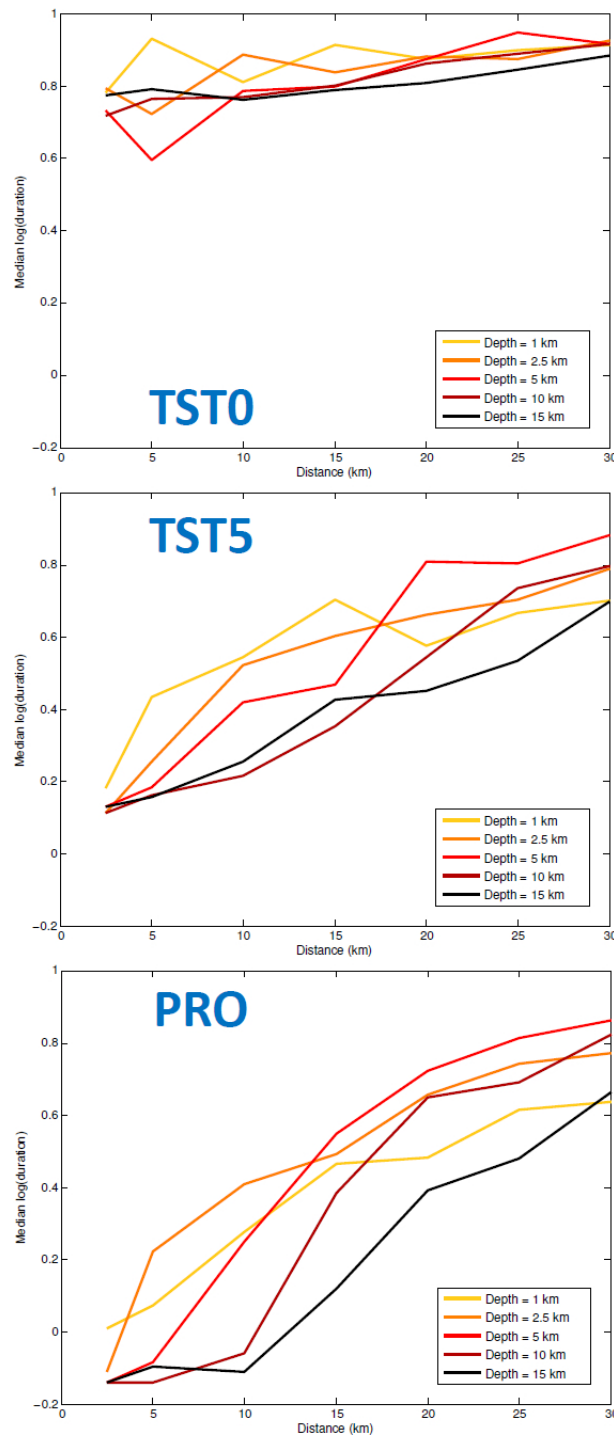
Figure 51:   *Evolution with the epicentral distance of the median duration for the 3 stations considered in this study. The curves are gathered by source depth values (colors). The duration is evaluated by the Relative Significant Duration, defined as the time interval between 5-95% of the Arias Intensity (Trifunac and Brady 1975; Kempton and Stewart 2006).*
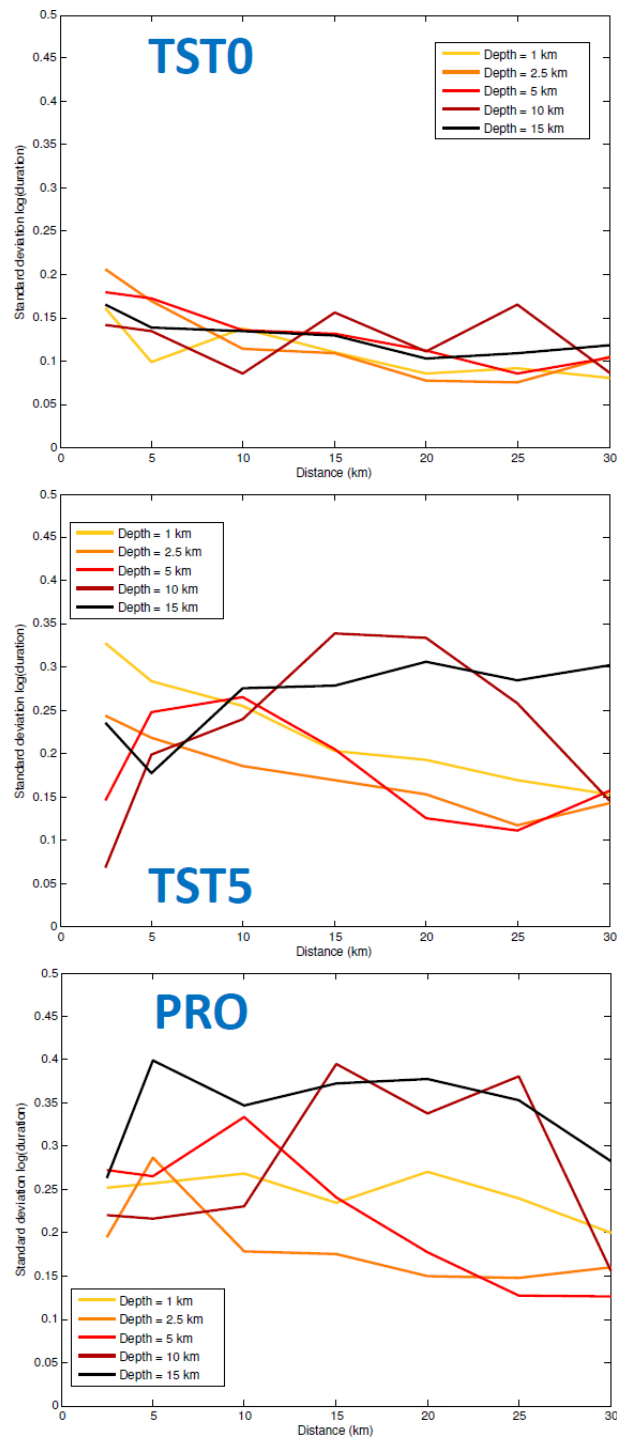
Figure 52:   Same as Figure 51 for the standard deviation of log duration.

The robustness of the amplification estimate is evaluated through the computation of the SSR at TST0, using either TST5 or PRO as the reference station, for the whole dataset of 1260 sources on the circular setting ("extended virtual" dataset), and for the sub-dataset of 52 sources that closely matches the real database available ("real catalog" dataset).

The TST0/TST5 SSR obtained for the extended virtual dataset are shown in Figure 53, together with the median SSR and upper/lower percentiles. The inconsistency, or variability, of the estimated SSR due to source variability remains moderate, compared to the average standard deviation on instrumental SSR (usually a factor of 2, i.e., σ [log10(SSR)] = 0.3).
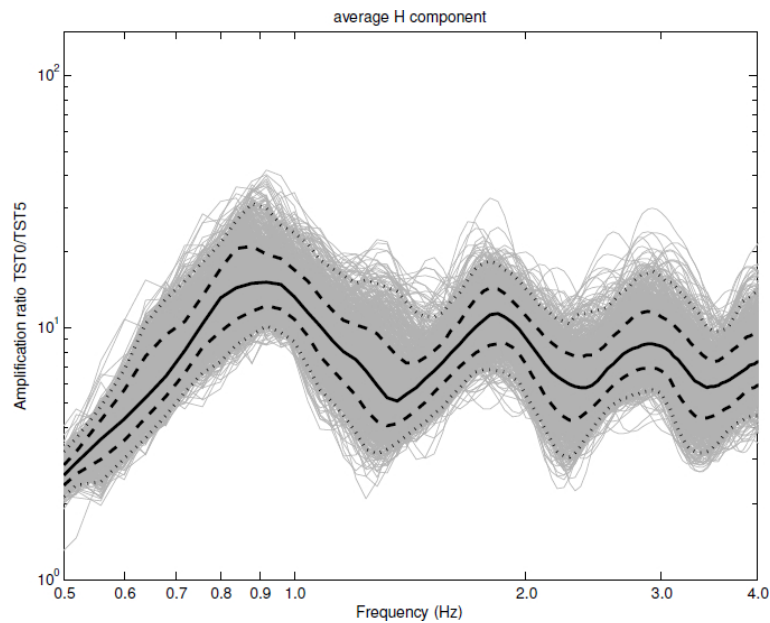
Figure 53: Standard Spectral Ratios at TST0 with TST5 as the reference station, computed for the 1260 sources of the "extended virtual" dataset. The median ratio is indicated by the solid black line, surrounded by the 16% and 84% percentiles (lower and upper dashed lines, respectively), and by the 2% and 98% percentiles (lower and upper dotted lines, respectively).
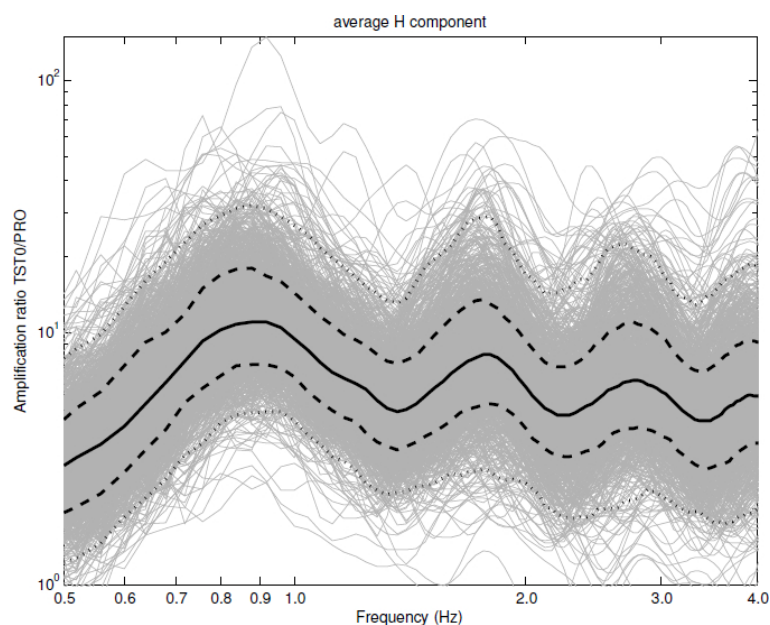
Figure 54: Same as Figure 53 with northern rock site PRO as the reference station.

Figure 54 shows the TST0/PRO SSR obtained for the extended dataset: the robustness of the estimated SSR appears much more impacted than in the previous case. This could have two potential origins: (1) the distance separating TST0 and PRO (2500 m) is much more important than the distance separating TST0 and TST5 (200 m); (2) there is a higher variability of the ground motion at PRO, which impacts the robustness of the SSR at TST0 when taking PRO as the reference station. The resulting standard deviation corresponds approximately to a factor of 2, i.e., to the value usually obtained on instrumental SSR (see Riepl et al., 1998, for the Euroseistest case).
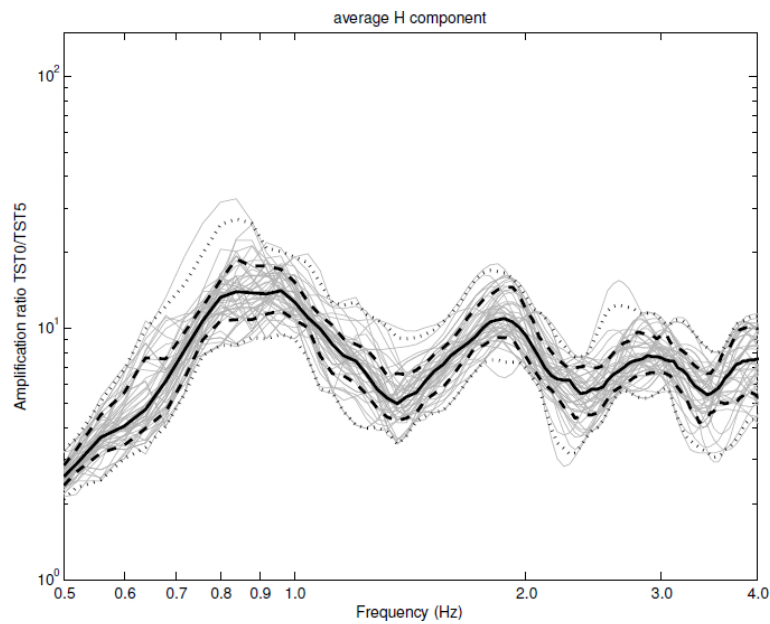
Figure 55:   Standard Spectral Ratios at TST0 with TST5 as the reference station, computed for the 52 sources of the "real catalog" dataset. The median ratio is indicated by the solid black line, surrounded by the 16% and 84% percentiles (lower and upper dashed lines, respectively), and by the 2% and 98% percentiles (lower and upper dotted lines, respectively).
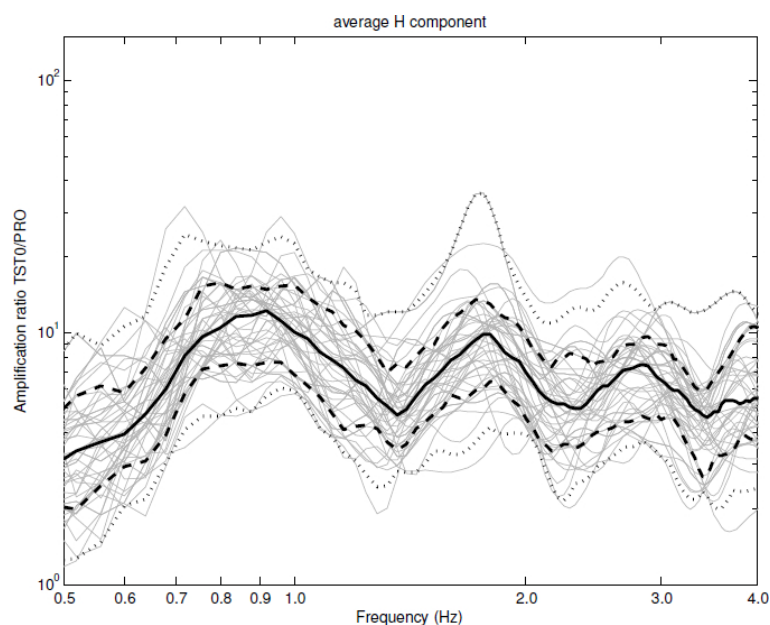
Figure 56:   Same as Figure 55 with northern rock site PRO as the reference station.

The same analysis is performed taking into account only the 52 sources of the "real catalog" sub-dataset: Figure 55 shows the TST0/TST5 SSR estimates and Figure 56 the TST0/PRO estimates. The observations made for the extended dataset are also valid here: the estimation of SSR appears more robust when taking TST5 as the reference station rather than PRO.

The robustness of the SSR depending on the completeness of the sources catalog (in terms of covered distances, depths and back azimuths) is illustrated through Figure 57 and Figure 58, that show the SSR variability for the extended virtual dataset (black lines) compared to the SSR variability for the real-catalog sub-dataset (magenta lines), when using TST5 or PRO as the reference station, respectively. It appears that the sub-dataset efficiently samples the extended dataset, despite the drastic decrease in number of events (52 vs. 1260), as the SSR estimate remains much comparable in the two cases. Indeed the median SSR and associated percentiles are satisfactorily superimposed, whatever station is taken as the reference. Some loss of robustness in the SSR estimate occurs in the higher frequencies, but it remains reasonable.

This numerical study shows that the variability of the ground motion computed in the Mygdonian basin is impacted by the hypocenter location (characterized by distance, depth and back azimuth – magnitude was not considered here). We distinguish two effects associated to hypocenter location that can affect the robustness of the site-effect estimate at TST0: (1) the uncertainty in the hypocenter location for one particular source scenario; and (2) the variety in the hypocenter locations around the basin. The first effect becomes important when the considered source is close to the studied stations, and also when it is farther but very shallow. The second effect relates to the different interactions that occur between the incident wavefield and the 3D structure of the basin. The variability of SSR at TST0 due to those 3D interactions appears to be significant enough to justify the characterization of the local site effect by a statistical distribution.

The numerical-simulation tool proves to be useful to investigate whether the real-sources catalog represents an accurate and complete-enough sample to estimate the site-effect amplification and to embrace its associated variability.
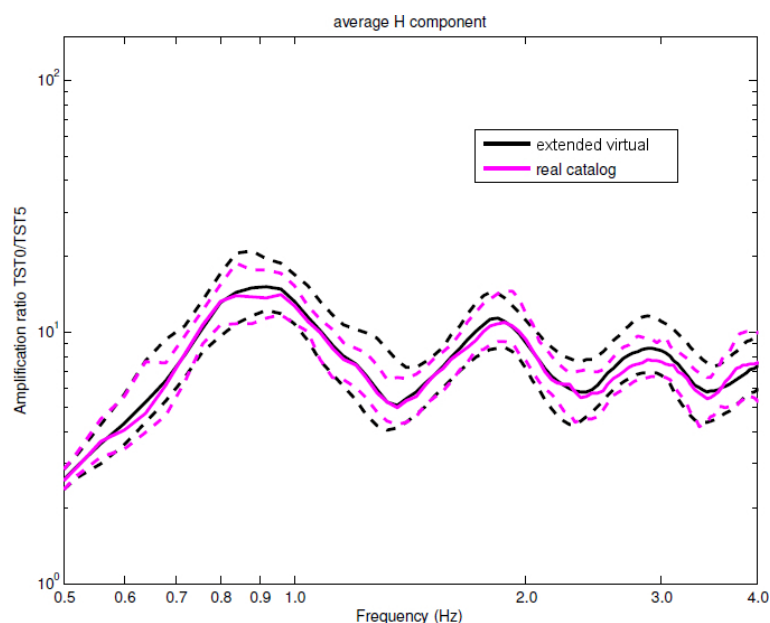
Figure 57: Standard Spectral Ratios at TST0 with TST5 as the reference station, for the "real catalog" sub-dataset (magenta lines) compared to the "extended virtual" dataset (black lines). The median ratio in each case is indicated by the solid line, surrounded by the 16% and 84% percentiles as dashed lines.
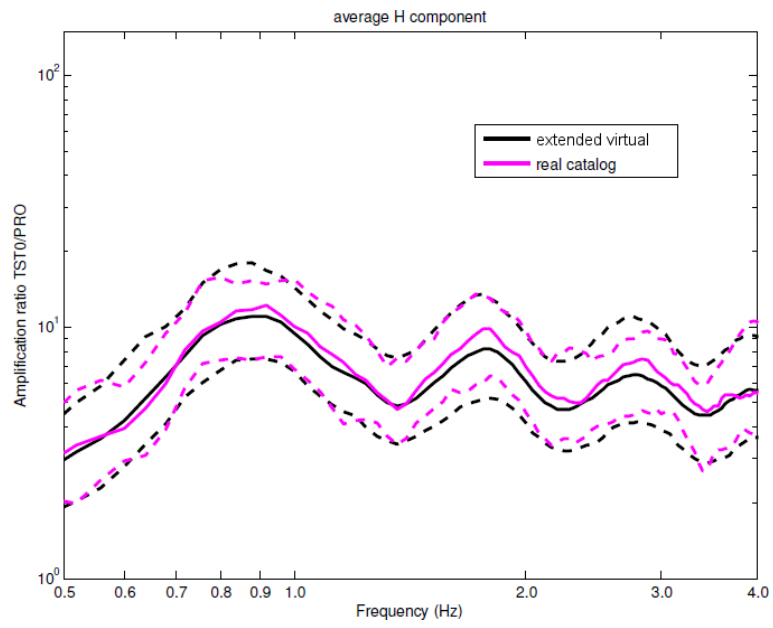
Figure 58:   Same as Figure 57 with northern rock site PRO as the reference station.

6   Comparison of observed and synthetic single-station-sigma related values

We wish to compare ground motion parameters computed through direct 3D numerical simulation of the response of the Mygdonian basin with observed values. In particular, we are interested in comparing the values of "single-station sigma" defined in the Ground Motion Prediction Equation (GMPE) community. This is a joint collaborative work within the WP2 and WP3 workpackages of the Sigma project. The observed values were provided by Olga-Joan Ktenidou and Zafeiria Roumelioti. Their work on single-station sigma measurements on the database of Euroseistest recordings can be found in Sigma deliverable `SIGMA-2012-D2/D3-132`.

For the moment, we are not able to build a synthetic GMPE because our synthetic database only contains 3 stations, so we will only compare relative mean and sigma values betweeen those stations for a set of real and virtual events.

The ground motion parameters considered here are the orientation-independent geometric mean values of the acceleration response spectra (SA) for a set of periods of interest: $T = 0$ s, 0.3 s, 0.5 s, and 1 s. Let p denote such parameter, $p = \text{GMRotD50}(SA(T))$, and $p(e, s)$ denote the value of the parameter corresponding to an event e recorded at a station s.

In the remainder, $o(e, s)$ stands for the value of the observed parameter, $p(e, s)$ for the value predicted by 3D numerical simulation and $g(e, s)$ for that predicted by a GMPE.

6.1   GMPE terminology

We want to compare our synthetic values with the output of a GMPE analysis, the terminology of which is recalled here. The reader is referred to Al Atik et al. (2010) for a comprehensive presentation of the GMPE terminology.

For an event e recorded at a station s, the observed ground parameter $o(e, s)$ is compared to its prediction by a GMPE, $g(e, s)$. Let δ_{es} denote the ratio of observed to predicted values in natural logarithmic scale:

$$\delta_{es} \;=\; \ln\left(\frac{o(e, s)}{g(e, s)}\right). \tag{6.1}$$

For each event, the ratios are roughly shifted towards unity by subtracting the mean over all stations that recorded the event. This event-by-event correction, which is denoted δB_e, is used to study the inter-event, or between-event, variability:

$$\delta B_e \;=\; \mu_s\left[\ln\left(\frac{o(e, s)}{g(e, s)}\right)\right], \tag{6.2}$$

where $\mu_s\,[\,f\,]$ stands for the arithmetic mean (over stations) of f. The remaining values, denoted δW_{es}, are used to define the within-event variability:

$$\delta W_{es} \;=\; \delta_{es} - \delta B_e = \ln\left(\frac{o(e, s)}{g(e, s)}\right) - \mu_s\left[\ln\left(\frac{o(e, s)}{g(e, s)}\right)\right]. \tag{6.3}$$

Next, a site contribution to the within-event variability, denoted d_{S2S}, is defined as the average of the δW_{es} values over all the events that were recorded at station s:

$$d_{S2S} \;=\; \mu_e\left[\delta W_{es}\right]. \tag{6.4}$$

Note that if the GPME, used to compute the g values, does not include any site correction, then the d_{S2S} are expected to be dominated by the site condition.

Subtracting the site contribution, one gets the so-called site-corrected residuals, $\delta W_{es,s}$:

$$\delta W_{es,s} \;=\; \delta W_{es} - d_{S2S}. \tag{6.5}$$

At this stage, it is useful to note that when averaging over events, the average of $\delta W_{es,s}$ is null and its standard deviation, which is called the single-station sigma and denoted $\phi_{SS,s}$, is that of δW_{es}. This writes

$$\mu_e\left[\delta W_{es,s}\right] \;=\; 0, \tag{6.6}$$
$$\phi_{SS,s} = \; \sigma_e\left[\delta W_{es,s}\right] \;=\; \sigma_e\left[\delta W_{es}\right], \tag{6.7}$$

where $\sigma_e\left[\,f\,\right]$ stands for the standard deviation from the arithmetic mean (over events) of f.

Finally, if we consider relative values between two stations s_1 and s_2, using Eq. (6.3) we have:

$$\delta W_{es}(s_1) - \delta W_{es}(s_2) \;=\; \ln\left(\frac{o(e,s_1)}{g(e,s_1)}\right) - \ln\left(\frac{o(e,s_2)}{g(e,s_2)}\right), \tag{6.8}$$
$$=\; \ln\left(\frac{o(e,s_1)}{o(e,s_2)}\right) - \ln\left(\frac{g(e,s_1)}{g(e,s_2)}\right). \tag{6.9}$$

6.2   Comparing comparable values

From the synthetic database presented in section 5, we compute the relative values of the ground motion parameters $GMRotD50(SA(T))(e,s)$ for two different pairs of stations s and different sets of real or virtual events e. The two pairs of stations are (TST_0, TST_5) and (TST_0, PRO), where TST_0 is the surface TST station, TST_5 is the downhole (at depth 198m) TST station and PRO is the surface Profitis station. Let REF stand for either TST_5 or PRO, we first compute the amplification values:

$$\ln\left(\frac{p(e,TST_0)}{p(e,REF)}\right) \tag{6.10}$$

for all the events e and then compute their mean and standard deviation:

$$\mu_e\left[\ln\left(\frac{p(e,TST_0)}{p(e,REF)}\right)\right], \tag{6.11}$$
$$\sigma_e\left[\ln\left(\frac{p(e,TST_0)}{p(e,REF)}\right)\right]. \tag{6.12}$$

The mean values are compared to the differences of the site contributions:

$$d_{S2S}(TST_0) - d_{S2S}(REF), \tag{6.13}$$

which according to Eq. (6.4) equals

$$\mu_e\left[\delta W_{es}(TST_0) - \delta W_{es}(REF)\right], \tag{6.14}$$

and the sigma values are compared to the standard deviation of the differences of the site-corrected residuals:

$$\sigma_e\left[\delta W_{es,s}(TST_0) - \delta W_{es,s}(REF)\right], \tag{6.15}$$

which, according to Eq. (6.7) equals

$$\sigma_e\left[\delta W_{es}(TST_0) - \delta W_{es}(REF)\right]. \tag{6.16}$$

Note that if the site-corrected residuals at the two stations TST_0 and REF were independent, then the square of σ_e in Eq. (6.16) would be the sum of the squares of the single-station sigmas of the two stations.

Finally, gathering Eqs (6.11, 6.12, 6.14, 6.16) and using Eq. (6.9), we are comparing:

$$\mu_e \left[\ln\left(\frac{p(e, TST_0)}{p(e, REF)} \right) \right] \quad \leftrightarrow \quad \mu_e \left[\ln\left(\frac{o(e, TST_0)}{o(e, REF)} \right) - \ln\left(\frac{g(e, TST_0)}{g(e, REF)} \right) \right], \tag{6.17}$$

$$\sigma_e \left[\ln\left(\frac{p(e, TST_0)}{p(e, REF)} \right) \right] \quad \leftrightarrow \quad \sigma_e \left[\ln\left(\frac{o(e, TST_0)}{o(e, REF)} \right) - \ln\left(\frac{g(e, TST_0)}{g(e, REF)} \right) \right]. \tag{6.18}$$

Note that although the values on the right-hand side contain a dependence on the GMPE, if the GMPE does not account for site conditions and if the distance from the TST_0 site to the reference site is small compared to the epicentral (or hypocentral) distances, then the observed and synthetic values can be compared directly.

6.3   Preliminary results

Here we show the comparison of the synthetic values (6.11 and 6.12) to their observed counterpart. The synthetic mean amplifications and the associated standard deviations were computed for a set of 52 real events that were recorded by at least 3 stations of the Euroseistest array. The location of those events is shown in Fig. 6.1, with the detail of the events that were only recorded by the pairs of stations $(TST_0 – TST_5)$ and $(TST_0 – PRO)$.
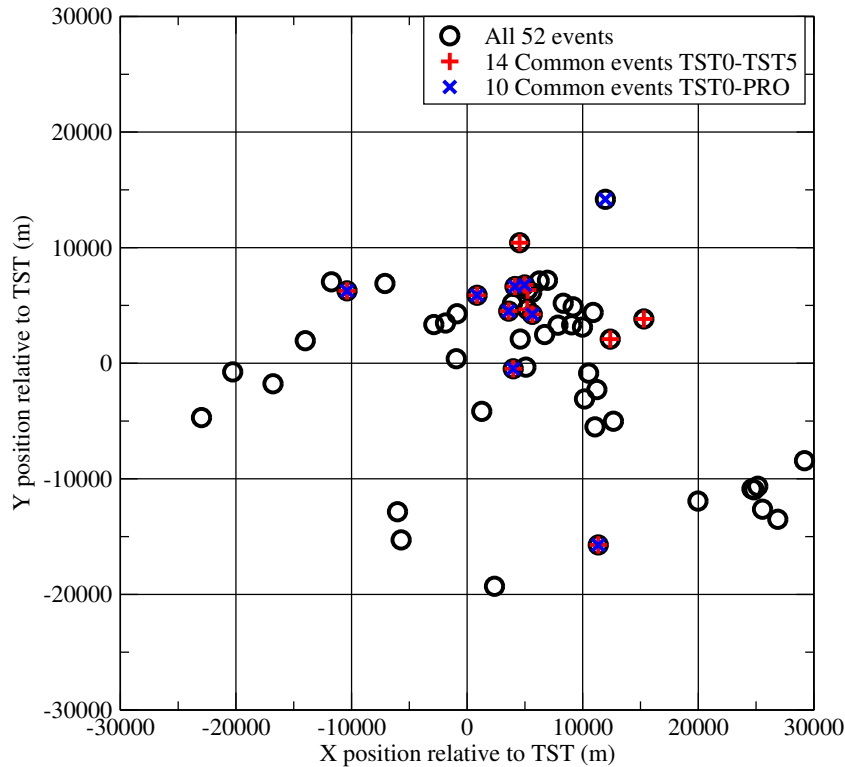
Figure 6.1 Location (relative to TST) of the seismic events used for comparing observed and synthetic values. The observed amplification between TST_0 and TST_5 (resp. PRO) were computed for events indicated by the red (resp. blue) crosses, whereas the synthetic values were computed for all the events (black circles).

The observed values were deduced from the site contributions d_{S2S} and the site-corrected residuals $\delta W_{es,s}$, both measured from a reference GMPE which did not include information

Table 1 Values of single-station sigmas ($\phi_{SS,s}$) and of site contributions (d_{S2S}) computed for the 52 events of the real catalog for the spectral accelerations at four periods. The black numbers following the $\phi_{SS,s}$ and d_{S2S} values indicate the total number of events that were used to compute the mean and standard deviation values. The number of common events that were recorded at TST_0 and PRO (resp. TST_5) are given in blue (resp. red).

T(s)	$\phi_{SS,s}(PRO)$		$d_{S2S}(PRO)$		$\phi_{SS,s}(TST_0)$		$d_{S2S}(TST_0)$		$\phi_{SS,s}(TST_5)$		$d_{S2S}(TST_5)$	
0.0	0.59	26 14	-0.38	26 14	0.23	41	0.49	41	0.20	28 28	-1.17	28 28
0.3	0.31	24 14	-0.15	24 14	0.24	41	0.47	41	0.31	26 26	-1.15	26 26
0.5	0.31	22 13	-0.30	22 13	0.30	36	0.42	36	0.34	21 21	-1.40	21 21
1.0	0.14	9 7	-0.11	9 7	0.23	30	0.43	30	0.56	10 10	-1.15	10 10

about the site conditions. As discussed in the previous section, this assumption is required to allow a direct comparison between observed and synthetic amplification values. The direct comparison should then be valid as long as the events used in the analysis are not too close from the TST and PRO stations. The global values (i.e., computed for all recorded events) of the site contributions and of the single-station sigmas are given in Table 1. In addition we computed the site-corrected residuals only for the common events that were recorded both at the TST_0 station and at the reference station (TST_5 or PRO).

As the reader will have noted, the numbers compared here are not exactly consistent because: (i) the d_{S2S} values were measured independently for each station, and their difference used even for non-common events, (ii) the $\delta W_{es,s}$ values were measured properly for the common events but their synthetic counterpart use the whole catalog of 52 events.

Despite these approximations, we show some preliminary results of the comparison in Fig. 6.2. The mean amplification values are shown in natural scale, i.e. we plot the exp of the mean values of Eq. 6.17 to ease the comparison with the results of the Standard Spectral Ratios (SSR) analysis presented in section 5.

The mean amplification between TST_0 and TST_5 is seen to be slightly overestimated in the synthetics for all periods. This observation is consistent with the results of the SSR analysis. The comparison of the amplification between TST_0 and PRO is more problematic: the observed values are smaller than the synthetic ones, by a factor comprised between 2 and 3, only. This is quite a surprising result, given the periods at which the comparison is performed. For example, the wheathered rock condition at PRO, which is known to affect the measures of PGA at high frequency, is unlikely to influence the acceleration response spectra below 4 Hz. Further work will thus be needed to understand the origin of this discrepancy, *i.e.* whether it is caused by an improper comparison methodology or related to a structural characteristic which is absent in the current model of the basin.

The comparison of the standard deviations (right part of Fig. 6.2) shows an opposite trend: the observed and synthetic deviations are of similar magnitude for the PRO reference station, and are largely underestimated in the synthetics for the TST_5 reference station.

To appreciate the influence of the catalog of events used to perform the analysis, we show in Fig. 6.3 the comparison of the observed values with the synthetic ones obtained for the full set of 1260 virtual events (see section 5). The main effect of enriching the catalog is to increase the values of the standerd deviations around the mean amplification factors, in particular when the PRO reference station is used. In this case, the synthetic deviations are even larger than the observed ones, which suggests that the number of records and the distribution of events used play a non-negligible role in the robustness of the single-station sigma measures.
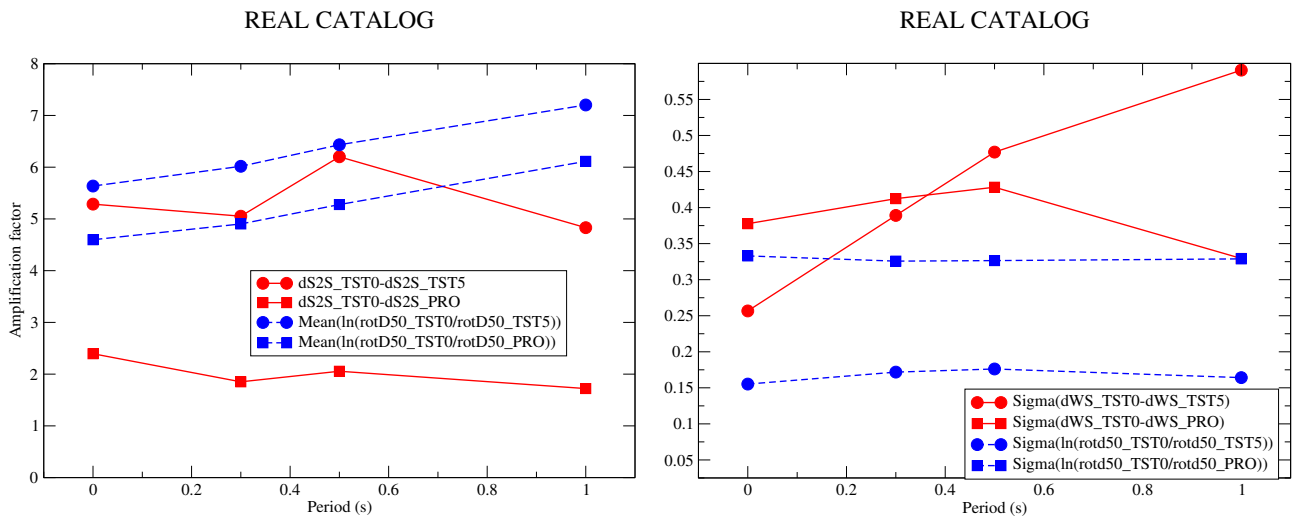
Figure 6.2 Comparison of mean (left) and standard deviation (right) of the amplification observed (red) and simulated (blue) at the TST surface station TST_0. The reference station is either the downhole TST station TST_5 (filled circles) or the Profitis surface station PRO (filled squares).
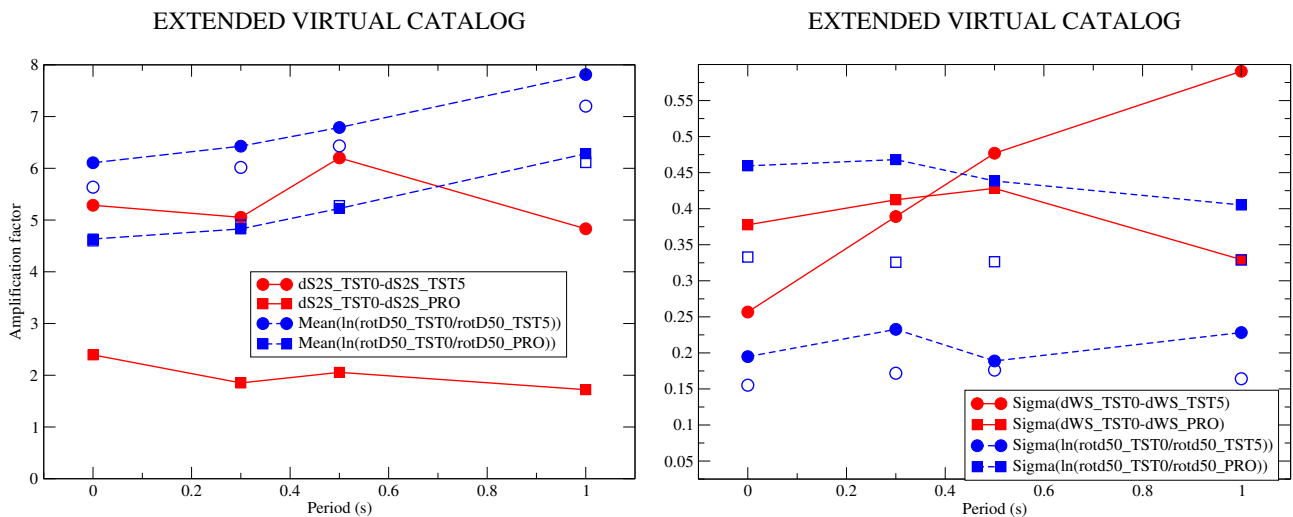
Figure 6.3 Same as Fig. 6.2 with synthetics computed for an extended catalog comprising 1260 virtual events. The synthetic values for the real events are indicated with open symbols to allow a direct comparison of the robustness of these measures to the completeness of the catalog of events used.

6.4   Conclusions and Perspectives

We have shown a proper methodology to compare the results of classical GMPE analysis of the single-station sigmas to those of direct numerical simulations of the response of the Mygdonian basin. Due to the limited size of our synthetic database (in terms of number of stations), we were able to compare the mean amplification and its associated variability at the TST station for a couple of reference stations. Our preliminary results confirm the slight overestimation of the site effect at the vertical TST array in the existing numerical simulations of the response of the basin, and point a possible discrepancy between observed and synthetic amplification relative to the PRO station. The comparison of relative values of single-station sigmas indicates that these are generally higher in the observations than in the synthetics, except when a small number of events and records is used for the measures.

The perspectives of this work are numerous and should provide some new insights to understand the variability of ground motion in sedimentary basins. In a first stage, we will complete the comparisons shown here by computing the exact same observed and synthetic values and the influence of the reference GMPE at small epicentral distance will be quantified for the set of real and of virtual events. In a second stage, we will extend the number of stations in the synthetic databases in order (i) to apply to the synthetic results the same processing that was used for observed records, and (ii) to build a synthetic local GMPE for the Mygdonian basin and investigate how the modelling assumptions (e.g. site effect proxies) or uncertainties (e.g. in the source parameters) affect the values of single-station sigmas.

7   <u>CONCLUSIONS AND PERSPECTIVES</u>

The new results of the second phase of E2VP allow drawing some conclusions and emphasizing a few issues presented hereafter.

First, the main findings of E2VP1 (as listed in Table 1) were confirmed, for both verification and validation aspects.

- The use of numerical simulation codes, even after extremely careful testing and even with the most sophisticated and up-to-date numerical schemes, can still be subject to errors (especially related to the "human factor"): careful use and cross-checking still proves to be mandatory.

- Our new results also confirm that there is no single numerical-modelling method that can be considered the best in terms of accuracy and computational efficiency for all structure-wavefield configurations.

- In addition, the very detailed investigations on canonical models, allowed identifying the origin of inaccuracies and relating them to the involved type of seismic waves and to the smoothness of the velocity model. Risks of significant code-to-code differences prove to be the largest for models with sharp velocity discontinuities, and energetic surface waves (often associated with gently-sloping sediment/bedrock interfaces). Whenever small-scale, or localized, strong variations of the material parameters have to be considered in the sediments, e.g. based on firm geological, geotechnical or geophysical evidence, an effective medium relevant for the chosen frequency range should be used; new averaging algorithms have been developed in that aim, that greatly improve the accuracy of the results without much impacting he computational cost. A strategy has also been proposed to define the effective medium with procedures of increasing complexity, depending on the degree of knowledge of the model heterogeneity and on the desired level of accuracy in the predictions. More technical details on this strategy can be found in Appendix 1.

- We thus go on with recommending that any numerical method and code that is intended to be applied for numerical prediction of earthquake ground motion should be verified through stringent models that would make it possible to test the most important aspects of accuracy. The canonical cases developed within E2VP, and made freely available to the seismological community (http://www.sismowine.org), can serve this purpose.

Most of the new work achieved during E2VP2 is related to validation. The feasibility of such a validation up to the frequency limit considered here (4 Hz) is still a real challenge, which is in the front edge of applications of numerical simulation to deterministic ground-motion prediction, for several reasons that are listed below and clearly outlined by our new results:

- The site response proves to be very sensitive to the exact position of the source – especially its depth and back azimuth – for very close events (i.e., epicentral distance less than 5 km), and for local, shallow events (epicentral distance within 20 km, depth smaller than 5 km): as it is unrealistic to obtain a precision on localization smaller than 2 km (especially for the depth), it is not recommended to select such events for validation.

- The update of the propagation model from E2VP1 to E2VP2 included two main parts: the update of the crustal structure and of the basin model.

  o The first one was based on the crustal model used for the event localization, in order to ensure an optimal consistency. The associated changes prove to induce non-negligible effects, with an increase of rock motion by a factor between 30 and 60% over the whole frequency band. There is a trend to overpredict the motion at deep rock sites (TST5), and to slightly underpredict it at one outcropping rock site (PRO) while the overall agreement is very good for the other

outcropping rock site (STE). The latter may be simply due to shallow weathering not accounted for in the numerical model, because of missing information. In any case, the presence of several rock sensors is essential in calibrating the overall amplitude level of the simulations, in order to validate the source parameters and the crustal/regional propagation.

o The second one included a large extension of the basin model to include the whole Mygdonian basin, including its western, southern and eastern edges, a modification of the velocity model with linear gradients without first order velocity discontinuities (except for the bedrock interface), and changes in the sediment thickness, especially on the eastern part. This leads in particular to less pronounced "buried pass" effects at TST site: the outward leakage of energy towards western and especially eastern parts of the basin, leads to an increased amplification at intermediate frequencies (between 0.8 and 1.5 Hz). The underestimation of site amplification within the E2VP1 model has been replaced by a slight overamplification. There are several consistent indications that this overestimation might be due to a too low attenuation within the basin (and may be also the absence of scattering in the crustal model). This emphasizes a recurrent issue which is the drastic lack of knowledge and in-situ measurement techniques for the damping (intrinsic and scattering) of elastic waves in shallow sedimentary deposits.

o Refining a geotechnical / geophysical model thus proves to be quite costly with only relatively slight improvements, at least in the present case where the initial model was already the result of an unusual set of dedicated geotechnical and geophysical surveys. In the present status of survey techniques (i.e., considering both their technical capabilities and their cost), the optimal effort in model and site characterization probably lies in between E2VP1 and E2VP2. Such an optimum should not be considered as an absolute, valid for any site; in particular, it is highly dependent on the availability or not of in-situ instrumentation: the presence of a vertical array and of nearby reference stations on outcropping rocks greatly helped in constraining the model and avoiding additional surveys.

• The distance between observations and numerical predictions remain significantly larger than the distance between carefully selected, up-to-date, and carefully implemented numerical simulation codes. However, a significant part of the uncertainties, especially for nearby events, come from uncertainties in the source parameters. Therefore, for the prediction of ground motion for future, expected events with a priori defined source characteristics, the numerical-simulation approach is fully legitimate in the toolbox for site-specific ground-motion estimation, at least in the 3D linear case and low-to-intermediate frequency range.

• In addition, the predictions-to-observations differences are significantly lower when considering only the site amplification, especially when the reference is at depth within a vertical array. The main characteristics of site amplification at TST site could be satisfactorily reproduced, in terms of spectral contents and signal duration. This emphasizes the added value of "hybrid" approaches made possible by the availability of down-hole recordings

The comprehensive sensitivity study also showed also that, beyond the deterministic prediction of ground motion for a given earthquake scenario, numerical simulation proves also to be a useful tool for investigating the structure of the aleatory variability. Up to now, it was only possible to investigate the within-event part, and more especially the single-site sigma, which is directly comparable with the SSR variability (considering jointly the δS2S terms for both the site and the reference, see section 6. The next step (already scheduled before next Summer) is to construct GMPEs directly from synthetics (with variable magnitudes and locations), and to perform a comparative analysis of the between- and within-event variabilities, for various sets of earthquake catalogs with a more-or-less complete distribution of distance and backazimuths, and well controlled levels of localization errors.

Concerning the 'single-site sigma", the high sensitivity of the site response to the source characteristics draws the attention on the potential underestimation of values derived from too sparse empirical datasets: when the available (empirical) data used for the estimation of $\Phi_{ss,s}$ do not include any close local or shallow event, and when the possibility of a significant local event should be considered in the hazard, the empirically derived single site sigma may be significantly underestimated. It is thus recommended to analyze in detail the distribution of available data in the (distance / magnitude / depth) space at every station for which single station sigma estimates are derived, and also to analyze the site variability of $\Phi_{ss,s}$ in terms of such data distribution.

Perspectives

The lessons of this verification and validation exercise have already been partially taken into account in the present version of the "operational guide to account for site effects" (Deliverable SIGMA-2014-D3-136), and will definitely be fully accounted for in the final version. One of the most important lessons is the invaluable usefulness of in-situ recordings: it seems today very difficult to predict site effects in complex geometry context with only geological, geophysical and geotechnical information. Such instrumentation should include sensors on rock and as much as possible a vertical array to allow both a control of the crustal model and hybrid modelling. Such a lesson is perfectly in line with one of the conclusions of the Pegasos project in Switzerland. In addition, another very valuable side outcome of the comprehensive numerical simulations is the insight into the structure of the aleatory variability, with special emphasis on the single-site sigma.

One must also keep in mind that this exercise deliberately focused on 3D-<u>linear</u> modeling only. The specific difficulties and uncertainties linked with NL modeling are tackled within another subproject of WP3, in the 1D case only. 3D-NL modeling should be presently considered as a –definitely needed– research topic and their application to practical design purposes as probably still premature, or at least affected by a huge epistemic uncertainty. Such models will have to be evaluated in a similar way in well controlled environments. The vertical array at Euroseistest, the vertical array to be installed soon in Argostoli (Cephalonia, Greece) within the SINAPS@ project framework, are among the very few sites that could provide opportunities to test 3D, NL codes whenever the in-situ instrumentation will have recorded a strong enough event.

A still unsolved issue common to both 3D, linear modeling and NL simulation deals with the damping in sediments, especially at large depth. The present E2VP results indicate that probably the sediment damping – estimated through the gross $Q_S=V_S/10$ rule of thumb – is probably slightly underestimated. On the opposite, the NL computations for the deep site of Grenoble (see Deliverable SIGMA-2014-D3-136) predict a very high level of damping even at large depth for highly compacted clays, that kills all 2D and 3D effects, and considerably reduces the long period amplification. Whether this is true or wrong is still completely unknown, and would certainly deserve a dedicated research project, starting with the worldwide gathering of available data from as many deep sedimentary sites as possible. As already emphasized in previous reports, the Euroseistest and its central vertical array are certainly a good candidate to improve our very poor knowledge on this issue, whenever there will be a strong enough event.

8 <u>REFERENCES</u>

Al Atik, L. A.; Abrahamson, N.; Bommer, J. J.; Scherbaum, F.; Cotton, F. & Kuehn, N. (2010), 'The Variability of Ground-Motion Prediction Models and Its Components', Seismol. Res. Lett. 81(5), 794-801.

Backus, G. E. (1962), 'Long-wave elastic anisotropy produced by horizontal layering', J. Geophys. Res. 67(11), 4427-4440.

Bard, P.-Y. (1994), Discussion session: Lessons, issues, needs and prospects. Special Theme session 5: Turkey Flat and Ashigara Valley experiments, in 'Tenth World Conference of Earthquake Engineering, Proceedings'.

Bastani, M., A. Savvaidis, L. B. Pedersen, and T. Kalscheuer (2011), CSRMT measurements in the frequency range of 1-250 kHz to map a normal fault in the Volvi basin, Greece., Journal of Applied Geophysics, 75, 180-195.

Bielak, J.; Graves, R. W.; Olsen, K. B.; Taborda, R.; Ramirez-Guzmjn, L.; Day, S. M.; Ely, G. P.; Roten, D.; Jordan, T. H.; Maechling, P. J.; Urbanic, J.; Cui, Y. & Juve, G. (2010), 'The ShakeOut earthquake scenario: Verification of three simulation sets', Geophys. J. Int. 180(1), 375-404.

Bouchon, M. & Aki, K. (1977), 'Discrete wave-number representation of seismic-source wave fields', Bull. Seismol. Soc. Am. 67(2), 259-277.

Bouchon, M. (1981), 'A simple method to calculate Green's functions for elastic layered media', Bull. Seismol. Soc. Am. 71(4), 959-971.

Bouchon, M. (2003), 'A review of the discrete wavenumber method', Pure Appl. Geophys. 160(3-4), 445-465.

Boyd, J. P. (2001), Chebyshev and Fourier spectral methods, Courier Dover Publications.

Cadet, H., and A. Savvaidis (2011), Comparative application of dispersion curve inversion strategies. Case study of noise arrays in the Euroseistest site, Greece., Near Surface Geophysics, 9, 571-583.

Capdeville, Y. & Marigo, J.-J. (2008), 'Shallow layer correction for Spectral Element like methods', Geophys. J. Int. 172(3), 1135-1150.

Capdeville, Y.; Guillot, L. & Marigo, J.-J. (2010), '1-D non-periodic homogenization for the seismic wave equation', Geophys. J. Int. 181(2), 897-910.

Capdeville, Y.; Guillot, L. & Marigo, J.-J. (2010), '2-D non-periodic homogenization to upscale elastic media for P–SV waves', Geophys. J. Int. 182(2), 903-922.

Caumon, G., P. Collon-Drouaillet, C. Le Carlier de Veslud, S. Viseur, and J. Sausse (2009), Surface-Based 3D Modelling of Geological Structures, Mathematical Geosciences, 41, 927-945.

Chaljub, E.; Cornou, C. & Bard, P.-Y. (2006), Numerical benchmark of 3D ground motion simulation in the valley of Grenoble, French Alps, in 'Third International Symposium on the Effects of Surface Geology on Seismic Motion, Proceedings'.

Chaljub, E.; Komatitsch, D.; Vilotte, J.-P.; Capdeville, Y.; Valette, B. & Festa, G. (2007), Spectral element analysis in seismology, in R.-S. WU & V. Maupin, ed., 'Advances in Wave Propagation in

Heterogeneous Media, Advances in Geophysics', Elsevier Academic Press, pp. 365-419.

Chaljub, E.; Maufroy, E.; Moczo, P.; Kristek, J.; Hollender, F.; Bard, P.-Y.; Priolo, E.; Klin, P.; De Martin, F.; Zhang, Z.; Chen, X. (2014) '3D numerical simulations of earthquake ground motion in sedimentary basins: testing accuracy through stringent models', **submitted to Geophys. J. Int. See appendix 1**.

Chaljub, E.; Moczo, P.; Tsuno, S.; Bard, P.-Y.; Kristek, J.; Kaser, M.; Stupazzini, M. & Kristekova, M. (2010), 'Quantitative comparison of four numerical predictions of 3D ground motion in the Grenoble valley, France', Bull. Seismol. Soc. Am. 100(4), 1427-1455.

Coutant, O. (1989), 'Program of numerical simulation AXITRA', Technical report, LGIT, Université Joseph Fourier, Grenoble, in French.

Cramer, C. H. (1995), 'Weak-motion observations and modeling for the Turkey Flat, U.S., Site-Effects Test Area near Parkfield, California', Bull. Seismol. Soc. Am. 85(2), 440-451.

Day, S. M.; Bielak, J.; Dreger, D.; Graves, R.; Larsen, S.; Olsen, K. B. & Pitarka, A. (2005), '3D Ground Motion Simulation in Basins: Final report for Lifelines Project 1A03', Technical report, Pacific Earthquake Engineering Research Center, 32.

Day, S. M.; Bielak, J.; Dreger, D.; Graves, R.; Larsen, S.; Olsen, K. B. & Pitarka, A. (2003), 'Tests of 3D elastodynamic codes: Final report for Lifelines Project 1A02', Technical report, Pacific Earthquake Engineering Research Center, 32.

Day, S. M.; Bielak, J.; Dreger, D.; Graves, R.; Larsen, S.; Olsen, K. B. & Pitarka, A. (2001), 'Tests of 3D elastodynamic codes: Final report for Lifelines Project 1A01', Technical report, Pacific Earthquake Engineering Research Center & Southern California Earthquake Center, 24.

De Martin, F. (2011), 'Verification of a spectral-element method code for the Southern California Earthquake Center LOH.3 viscoelastic case', Bull. Seismol. Soc. Am. 101(6), 2855-2865.

De Martin, F. (2011). Verification of a spectral-element method code for the Southern California Earthquake Center LOH.3 viscoelastic case, Bull. Seism. Soc. Am. 101.6 2855-2865.

Etienne, V.; Chaljub, E.; Virieux, J. & Glinsky, N. (2010), 'An hp–adaptive discontinuous Galerkin finite-element method for 3-D elastic wave modelling', Geophys. J. Int. 183(2), 941-962.

Faccioli, E.; Maggio, F.; Paolucci, R. & Quarteroni, A. (1997), '2D and 3D elastic wave propagation by a pseudo-spectral domain decomposition method', J. Seismol. 1(3), 237-251.

Fichtner, A. & Igel, H. (2008), 'Efficient numerical surface wave propagation through the optimization of discrete crustal modelsâ ''a technique based on non-linear dispersion curve matching (DCM)', Geophys. J. Int. 173(2), 519-533.

Fornberg, B. (1987), 'The pseudospectral method: Comparisons with finite differences for the elastic wave equation', Geophysics 52(4), 483-501.

Guillot, L.; Capdeville, Y. & Marigo, J.-J. (2010), '2-D non-periodic homogenization of the elastic wave equation: SH case', Geophys. J. Int. 182(3), 1438-1454.

Gurk, M., M. Smirnov, A. S. Savvaidis, L. B. Pedersen, and O. Ritter (2007a), A 3D magnetotelluric study of the basement structure in the Mygdonian Basin (Northern Greece). paper presented at 4th International

Symposium on Three-Dimensional Electromagnetics, September 27-30, Freiberg, Germany.

Gurk, M., M. Smirnov, A. S. Savvaidis, L. B. Pedersen, and O. Ritter (2007b), A 3D magnetotelluric study of the basement structure in the Mygdonian Basin (Northern Greece). paper presented at 4th International Symposium on Three-Dimensional Electromagnetics, Freiberg, Germany.

Gurk, M., M. Smirnov, A. S. Savvaidis, L. B. Pedersen, and O. Ritter (September 27-30, 2007), A 3D magnetotelluric study of the basement structure in the Mygdonian Basin (Northern Greece). paper presented at 4th International Symposium on Three-Dimensional Electromagnetics, Freiberg, Germany.

Hallier, S.; Chaljub, E.; Bouchon, M. & Sekiguchi, H. (2008), 'Revisiting the basin-edge effect at Kobe during the 1995 Hyogo-Ken Nanbu earthquake', Pure Appl. Geophys. 165, 1751-1760.

Hisada, Y. (1995), 'An efficient method for computing Green's functions for a layered half-space with sources and receivers at close depths (part 2)', Bull. Seismol. Soc. Am. 85(4), 1080-1093.

Hixon, R. (1998), 'Evaluation of a high-accuracy MacCormack-type scheme using benchmark problems', J. Comput. Acoust. 6(03), 291-305.

Kawase, H. & Iwata, T. (1998), A report on submitted results of the simultaneous simulation for Kobe, in Kojiro Irikura; Kazuyoshi Kudo; Hiroshi Okada & Tsutomu Sasatani, ed., 'The Effects of Surface Geology on Seismic Motion, Recent Progress and new Horizon on ESG Study', Balkema/CRC Press, .

Kawase, H. (1996), 'The Cause of the Damage Belt in Kobe: â œThe Basin-Edge Effect,â Constructive Interference of the Direct S-Wave with the Basin-Induced Diffracted/Rayleigh Waves', Seismol. Res. Lett. 67(5), 25-34.

Kempton, J.J., and J.P. Stewart (2006). Prediction equations for significant duration of earthquake ground motions considering site and near-source effects, Earthquake Spectra 22.4 985-1013.

Klin, P.; Priolo, E. & Seriani, G. (2010), 'Numerical simulation of seismic wave propagation in realistic 3-D geo-models with a Fourier pseudo-spectral method', Geophys. J. Int. 183(2), 905-922.

Komatitsch, D. & Martin, R. (2007), 'An unsplit convolutional perfectly matched layer improved at grazing incidence for the seismic wave equation', Geophysics 72(5), SM155-SM167.

Komatitsch, D. & Tromp, J. (1999), 'Introduction to the spectral-element method for 3-D seismic wave propagation', Geophys. J. Int. 139(3), 806-822.

Komatitsch, D. & Vilotte, J. P. (1998), 'The spectral-element method: an efficient tool to simulate the seismic response of 2D and 3D geological structures', Bull. Seismol. Soc. Am. 88(2), 368-392.

Komatitsch, D.; Liu, Q.; Tromp, J.; Süss, P.; Stidham, C. & Shaw, J. H. (2004), 'Simulations of Ground Motion in the Los Angeles Basin based upon the Spectral-Element Method', Bull. Seismol. Soc. Am. 94(1), 187-206.

Komatitsch, D.; Tsuboi, S. & Tromp, J. (2005), The Spectral-Element Method in Seismology, in Alan Levander & Guust Nolet, ed., 'Seismic Earth: Array Analysis of Broadband Seismograms', American Geophysical Union, Washington DC, USA, pp. 205-228.

Kristek, J.; Moczo, P. & Archuleta, R. J. (2002), 'Efficient methods to simulate planar free surface in the 3D 4th-order staggered-grid finite-difference schemes', Stud. Geophys. Geod. 46(2), 355-381.

Kristek, J.; Moczo, P. & Galis, M. (2010), 'Stable discontinuous staggered grid in the finite-difference modelling of seismic motion', Geophys. J. Int. 183(3), 1401-1407.

Kristek, J.; Moczo, P.; Chaljub, E.; De Martin, F. & Kristeková, M. (2014), 'A new discrete representation of a heterogeneous medium for the finite-difference modelling of seismic wave propagation', Geophys. J. Int..

Kristeková, M.; Kristek, J. & Moczo, P. (2009), 'Time-frequency misfit and goodness-of-fit criteria for quantitative comparison of time signals', Geophys. J. Int. 178(2), 813-825.

Ktenidou, O.-J.; Roumelioti, Z. (2014), Ground motion uncertainty (sigma) and variability at EUROSEISTEST, **Sigma deliverable SIGMA-2012-D2/D3-132.**

Lee, S. J.; Chen, H. W.; Liu, Q.; Komatitsch, D.; Huang, B. S. & Tromp, J. (2008), 'Three-Dimensional Simulations of Seismic Wave Propagation in the Taipei Basin with Realistic Topography Based upon the Spectral-Element Method', Bull. Seismol. Soc. Am. 98(1), 253-264.

Lee, S. J.; Komatitsch, D.; Huang, B. S. & Tromp, J. (2009), 'Effects of topography on seismic wave propagation: An example from northern Taiwan', Bull. Seismol. Soc. Am. 99(1), 314-325.

Madariaga, R. (1976), 'Dynamics of an expanding circular fault', Bull. Seismol. Soc. Am. 66(3), 639-666.

Mallet, J. L. (2002), Geomodelling, Oxford University Press, 666.

Manakou, M. (2007), 'Contribution to the determination of a 3D soil model for site response analysis. The case of the Mygdonian basin', PhD thesis, Ph D Thesis (in Greek with English abstract), Department of Civil Engineering, Aristotle University of Thessaloniki..

Manakou, M. (2007), Contribution to the determination of a 3D soil model for site response analysis. The case of the Mygdonian basin., 239 pp, Aristotle University of Thessaloniki.

Manakou, M., D. Raptakis, F. J. Chávez-García, P. I. Apostolidis, and K. Pitilakis (2010), 3D soil structure o he Mygdonian basin for site response analysis., Soil Dynamics and Earthquake Engineering, 30, 1198-1211.

Manakou, M.; Raptakis, D.; Chavez-Garcia, F.; Apostolidis, P. & Pitilakis, K. (2010), '3D soil structure of the Mygdonian basin for site response analysis', Soil. Dyn. Earthq. Eng. 30(11), 1198-1211.

Maufroy E., Chaljub E., Bard P.-Y., Hollender F., (2012), Evaluation of the relevance of the numerical simulation approach for site effect estimation: lessons of the Euroseistest Verification and Validation Project (E2VP) - phase 1 and perspectives for phase 2. **Sigma deliverable SIGMA-2012-D3-38.**

Maufroy, E., E. Chaljub, F. Hollender, J. Kristek, P. Moczo, P. Klin, E. Priolo, A. Iwaki, T. Iwata, V. Etienne, F. De Martin, N. P. Theodoulidis, M. Manakou, C. Guyonnet-Benaize, K. Pitilakis, and P.-Y. Bard (2014). Earthquake ground motion in the Mygdonian basin, Greece: the E2VP verification and validation of 3D numerical simulation up to 4 Hz, **submitted to Bull. Seism. Soc. Am. See appendix 2**.

Maufroy, E., V. M. Cruz-Atienza, F. Cotton, and S. Gaffet (2014). Frequency-scaled curvature as a proxy for topographic site-effect amplification and ground-motion variability, accepted in Bull. Seism. Soc. Am.

Moczo, P. & Kristek, J. (2005), 'On the rheological models used for time-domain methods of seismic wave propagation', Geophys. Res. Lett. 32(1).

Moczo, P.; Kristek, J. & Gális, M. (2004), 'Simulation of the planar free surface with near-surface lateral discontinuities in the finite-difference modeling of seismic motion', Bull. Seismol. Soc. Am. 94(2), 760-768.

Moczo, P.; Kristek, J. & Gális, M. (2014), The Finite-Difference Modelling of Earthquake Motions: Waves and Ruptures, Cambridge University Press.

Moczo, P.; Kristek, J.; Galis, M.; Chaljub, E. & Etienne, V. (2011), '3-D finite-difference, finite-element, discontinuous-Galerkin and spectral-element schemes analysed for their accuracy with respect to P-wave to S-wave speed ratio', Geophys. J. Int. 187(3), 1645-1667.

Moczo, P.; Kristek, J.; Vavrycuk, V.; Archuleta, R. J. & Halada, L. (2002), '3D heterogeneous staggered-grid finite-difference modeling of seismic motion with volume harmonic and arithmetic averaging of elastic moduli and densities', Bull. Seismol. Soc. Am. 92(8), 3042-3066.

Moundrakis, D., et al. (1995), Neotectonic map of Greece, Langadas Sheet, scale 1/100.000, Tectonic Committee of the Geological Society of Greece.

Novotný, O., J. Zahradník, and G.-A. Tselentis (2001). Northwestern Turkey earthquakes and the crustal structure inferred from surface waves observed in western Greece, Bull. Seism. Soc. Am. 91.4 875-879.

Ozdenvar, T. & McMechan, G. A. (1996), 'Causes and reduction of numerical artifacts in pseudo-spectral wavefield extrapolation ', Geophys. J. Int. 126 , 819-828 .

Papazachos, C. B. (1998), 'Crustal P- and S-velocity structure of the Serbomacedonian massif (northern Greece) obtained by non-linear inversion of traveltimes', Geophys. J. Int. 134, 25-39.

Papazachos, C.B. (1998). Crustal P- and S-velocity structure of the Serbomacedonian Massif (Northern Greece) obtained by non-linear inversion of traveltimes, Geophys. J. Int. 134.1 25-39.

Peter, D.; Komatitsch, D.; Luo, Y.; Martin, R.; Goff, N. L.; Casarotti, E.; Loher, P. L.; Magnoni, F.; Liu, Q.; Blitz, C.; Nissen-Meyer, T.; Basini, P. & Tromp, J. (2011), 'Forward and adjoint simulations of seismic wave propagation on fully unstructured hexahedral meshes', Geophys. J. Int. 186(2), 721-739.

Pitilakis, K., D. Raptakis, K. Lontzetidis, T. Tika-Vassilikou, and D. Jongmans (1999), Geotechnical and geophysical description of EUROSEISTEST, using field, laboratory tests and moderate strong motion recordings., Journal of Earthquake Engineering, 3, 381-409.

Priolo, E.; Carcione, J. M. & Seriani, G. (1994), 'Numerical simulation of interface waves by high-order spectral modeling techniques', J. Acoust. Soc. Am. 95(2), 681-693.

Psilovikos, A. (1977), Paleogeographic devlopment of he basi and lake of Mygdonian (Lagada - Volvi area, Greece). Aristotle University of Thessaloniki.

Raptakis, D., F. J. Chávez-García, K. Makra, and K. Pitilakis (2000), Site effects at Euroseistest-I. Determination of the valley structure and confrontation of observations with 1D analysis., Soil Dynamics and Earthquake Engineering, 19, 1-22.

Raptakis, D., M. Manakou, F. J. Chávez-García, K. Makra, and K. Pitilakis (2005), 3D configuration of Mygdonian basin and preliminary estimate of its site response., Soil Dynamics and Earthquake Engineering, 25, 871-887.

Riepl, J., P.-Y. Bard, D. Hatzfeld, C. Papaioannou, and S. Nechtschein (1998). Detailed evaluation of site response estimation methods across and along the sedimentary valley of Volvi (EURO-SEISTEST), Bull.Seism. Soc. Am. 88.2 488-502.

Seriani, G. & Priolo, E. (1994), 'A spectral element method for acoustic wave simulation in heterogeneous media', Finite Elem. Anal. Des. 16, 337-348.

Sotiriadis, L., A. Psiolovikos, E. Vavliakis, and G. Syrides (1983), Some Tertiary and Quaternary Basins of Macedonia / Greece. Formation and Evolution., Clausthaler Geologische Abhandlungen, pp. 21.

Soufleris, C.; Jackson, J. A.; King, G. C. P.; Spencer, C. A. & Scholz, C. H. (1982), 'The 1978 earthquake sequence near Thessaloniki (northern Greece)', Geophys. J. Int. 68(2), 429-458.

Souriau, A.; Chaljub, E.; Cornou, C.; Margerin, L.; Calvet, M.; Maury, J.; Wathelet, M.; Grimaud, F.; Ponsolles, C.; Pequegnat, C.; Langlais, M. & Gueguen, P. (2011), 'Multimethod characterization of the French-Pyrenean valley of Bagneres-de-Bigorre for seismic-hazard evaluation: observations and models', Bull. Seismol. Soc. Am. 101(4), 1912-1937.

Tam, C. K. & Webb, J. C. (1993), 'Dispersion-Relation-Preserving Finite Difference Schemes for Computational Acoustics', J. Comput. Phys. 107(2), 262-281.

Theodulidis, N.; Roumelioti, Z.; Panou, A.; Savvaidis, A.; Kiratzi, A.; Grigoriadis, V.; Dimitriu, P. & Chatzigogos, T. (2006), 'Retrospective Prediction of Macroseismic Intensities Using Strong Ground Motion Simulation: The Case of the 1978 Thessaloniki (Greece) Earthquake (M6.5)', Bull. Earthq. Eng. 4(2), 101-130.

Trifunac, M.D., and A.G. Brady (1975). On the correlation of seismic intensity scales with the peaks of recorded strong ground motion, Bull. Seism. Soc. Am. 65.1 139-162.

Virieux, J. (1984), 'SH-wave propagation in heterogeneous media: Velocity-stress finite-difference method', Geophysics 49(11), 1933-1942.

Virieux, J. (1986), 'P-SV wave propagation in heterogeneous media: Velocity-stress finite-difference method', Geophysics 51(4), 889-901.

Zhang, W. & Chen, X. (2006), 'Traction image method for irregular free surface boundaries in finite difference seismic wave simulation', Geophys. J. Int. 167(1), 337-353.

Zhang, W. & Shen, Y. (2010), 'Unsplit complex frequency-shifted PML implementation using auxiliary differential equations for seismic wave modeling', Geophysics 75(4), T141-T154.

Zhang, W.; Zhang, Z. & Chen, X. (2012), 'Three-dimensional elastic wave numerical modelling in the presence of surface topography by a collocated-grid finite-difference method on curvilinear grids', Geophys. J. Int. 190(1), 358-378.

Zhang, Z.; Zhang, W. & Chen, X. (2014), 'Complex frequency-shifted multi-axial perfectly matched layer for elastic wave modelling on curvilinear grids', Geophys. J. Int., ggu124.